Brine Availability Test in Salt (BATS) FY23 Update

Spent Fuel and Waste Disposition

Prepared for:
US Department of Energy
Office of Nuclear Energy
Office of Spent Fuel and Waste Disposition
Office of Spent Fuel and Waste Science and Technology

Prepared by:

Sandia National Laboratories
Kristopher Kuhlman, Melissa Mills, Richard Jayne, Edward Matteo, Courtney Herrick, Martin Nemer, Yongliang Xiong, Charles Choens, Matthew Paul, Christine Downs

Los Alamos National Laboratory
Philip Stauffer, Hakim Boukhalfa, Eric Guiltinan, Thom Rahn, Shawn Otto, Jon Davis, Daniel Eldridge, Aidan Stansberry

Lawrence Berkeley National Laboratory
Jonny Rutqvist, Yuxin Wu, Hafssa Tounsi, Mengsu Hu, Sebastian Uhlemann, Jiannan Wang

August 2023 • M2SF-23SN010303052 • SAND2023-08820R

Sandia National Laboratories is a multimission laboratory managed and operated by National Technology & Engineering Solutions of Sandia, LLC, a wholly owned subsidiary of Honeywell International Inc., for the U.S. Department of Energy's National Nuclear Security Administration under contract DE-NA0003525.

EXECUTIVE SUMMARY

This report summarizes the fiscal year 2023 (FY23) status of the second phase of a series of borehole heater tests in salt at the Waste Isolation Pilot Plant (WIPP) funded by the Disposal Research and Development (R&D) program of the Spent Fuel & Waste Science and Technology (SFWST) office at the US Department of Energy's Office of Nuclear Energy's (DOE-NE) Office in the Spent Fuel and Waste Disposition (SFWD) program.

High-level purpose: The Brine Availability Test in Salt (BATS) field test campaign intends to understand brine occurrence (i.e., where, and how much) and migration (i.e., how easily it moves) in salt through the damaged region surrounding excavations. These field tests are the part of a wider systematic multi-year field investigation campaign to improve the post-closure repository safety case for disposal of heat-generating radioactive waste in a generic salt repository. BATS seeks to better understand and ultimately predict how much brine can flow into both ambient and heated excavations (e.g., boreholes or rooms) in salt. This work is helping to train a new generation of repository scientist on both the design and execution of field tests, as well as the modeling and understanding of the coupled processes in salt via the BATS data used as part of DECOVALEX Task E.

Brine availability is important in a salt repository because:

1. brine can corrode metallic and glass waste forms or waste packages;
2. brine can facilitate transport of radionuclides off-site;
3. water is needed for gas generation (e.g., steel corrosion or water radiolysis), which can increase gas pressure, providing a driving force for migration away from the repository;
4. chlorine and borate in brine absorb neutrons, thereby reducing in-package nuclear criticality hazards; and
5. accumulated brine in an excavation undergoing creep closure provides back-pressure that may resist ultimate creep closure and sealing of a repository excavation.

The ongoing BATS field test activities and data collection are associated with a pair of similar heated and unheated arrays of horizontal boreholes in the underground experimental area at WIPP, southeastern New Mexico. BATS shakedown tests began in 2018 and BATS phase 1 (BATS 1) began in January 2020. BATS 1 included one heater test in January to March 2020 and continued with multiple gas and liquid tracer tests in 2021 (including a heated tracer test). BATS phase 2 (BATS 2) began testing July 2022 and continued into 2023 to examine the effects heating has on the response of the salt under a range of thermal loads.

FY23 Accomplishments: The main Disposal Research Salt R&D achievements during this fiscal year include the following two BATS-related activities:

- Executing four three-week heater tests in the BATS 2 array, while monitoring a suite of physical and geophysical response of the salt to different levels of heating (Figure E-1). These four steps were each at a hotter temperature than the previous step (from 90 °C [194 °F]) up to 145 °C [293 °F]), to observe the incremental effects of increasing temperature on brine availability (Section 4)
- Modeling to support interpretation of BATS 2 field data summarized in LANL and LBNL FY23 level-3 reports (Guiltinan et al., 2023; Rutqvist et al., 2023), and international collaborative modeling efforts (e.g., DECOVALEX-2023 task E; see Kuhlman et al., 2023)

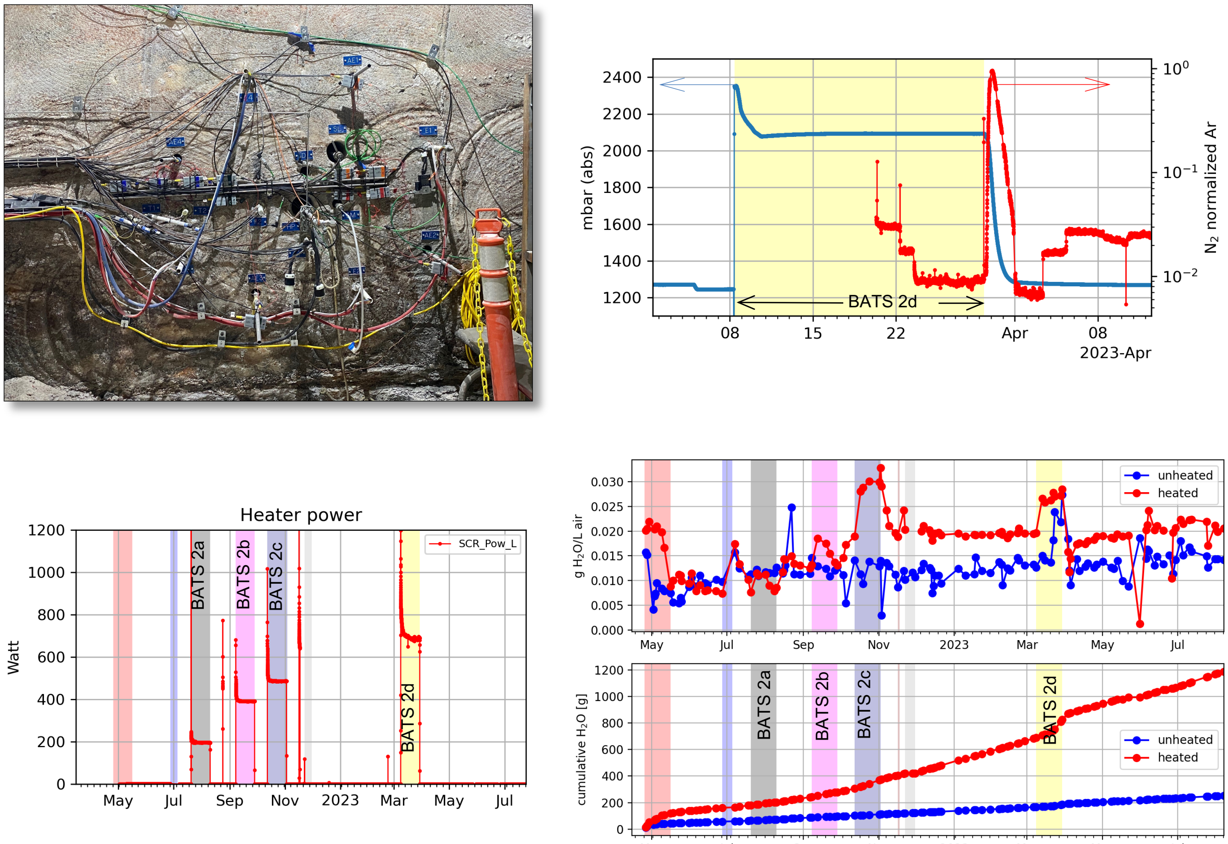

Figure ES-1. Photo of BATS 2 heated array (upper left), power applied in each BATS 2 heater event (lower left), water production in BATS 2 (lower right), and breakthrough of argon gas at end of BATS 2d heater event (upper right).

FY23 Key Finding: The fundamental observation in BATS 2 is seeing multiple lines of evidence that an accumulation of damage occurs in the salt associated with both heating and cooling. The BATS tests included:

- thermal (changes in temperature due to a range of heat setpoints);
- hydrological (water production in HP borehole and gas tracer tests between D and HP boreholes using argon);
- mechanical (closure observations in HP and SL boreholes and damage observations through monitoring acoustic emissions);
- chemical (water isotope observations through time in HP borehole and brine chemistry observations through time in SM borehole); and
- indirect geophysical responses (electrical resistivity tomography and distributed fiber optic strain and temperature measurements).

Each of these responses were characteristic of a system changing through damage and brine migration.

These diverse data support the key finding that heated salt is a complex dynamical system as based on the following features or behaviors of the system:

1) opening and closing of fractures that may be interconnected for flow fluid or not at different times;
2) nonlinear and hysteretic two-phase flow of air and brine through discrete fracture networks; and
3) evolving water isotopes and fluid chemistry (Figure ES-2) in response to mechanical damage, fluid migration, and potentially evaporation or other processes.

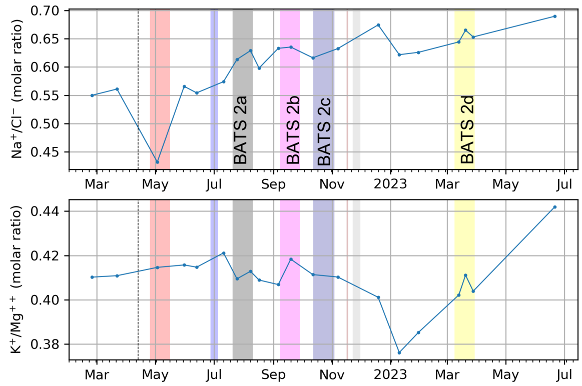

Figure ES-2. Changes in Brine Chemistry observed in SM borehole during BATS 2.

Next Stages of Work:

The current three-to-five-year plan for BATS (Kuhlman et al., 2021a) and the longer-term strategy document for testing in salt (Stauffer et al., 2015) list the overall project's longer-term plans. In the next fiscal year plans include:

- Continuing additional BATS 2 heater tests in FY24, with heater events that include:
  - at hotter temperatures with higher N_2 flowrates (to prevent condensation in the flowlines, as was observed in BATS 2d), which will help us to better understand and the response of the salt at elevated temperatures.
  - ramping up and ramping down temperatures over the course of hours to days (rather than a step change on or off), to explore the association of observed responses and damage accumulation with the time rate of change in heating.
- Continuation of laboratory tests, numerical modeling, and international collaborations in FY24 required to further interpret and explore the data that have already been and continue to be collected as part of BATS.
- Planning the next field-testing phase (BATS 3), including an update the 5-year BATS plan document in FY24. As part of this update, we will give more detail about BATS 3, which is envisioned as a series of smaller, more focused tests in the Salt Disposal Investigation (SDI) experimental area of WIPP. These uncoupled tests will allow more detailed monitoring of individual processes relevant to long-term performance of salt repositories, rather than focusing on coordination (and interference) between many simultaneous geophysical measurements.
- Use BATS 3 to re-start WIPP's role as an internationally relevant underground research laboratory in salt.

VERSION INFO

This report is an annual update of a series of BATS status reports. The FY20 BATS report details the construction of the BATS 1 arrays and the first round of heating (SAND2020–9034R). The FY21 report details further data collection during periods without active heating and results of gas tracer tests conducted between boreholes (SAND2021–10962R). The FY22 report detailed decommissioning of the BATS 1 heated array and construction of the BATS 2 heated array (SAND2022–12142R). This report describes the continued data collection in the new BATS 2 heated array and the original unheated array from BATS 1.

Date	Version
Aug 29, 2023	DOE-NE review (SNL sensitivity review: 1720173)
Sep 5, 2023	Final version approved for external release (SAND2023-08820R)

ACKNOWLEDGMENTS

The project is financially supported by the Disposal R&D program of DOE-NE's SFWST office. We acknowledge key assistance from the following groups: the Salado Isolation Mining Contractors (SIMCO, which was formerly the Nuclear Waste Partnership); Waste Isolation Pilot Plant (WIPP) underground facilities personnel, who provide underground access, power infrastructure, and drilling support; and the DOE Office of Environmental Management (DOE-EM) Carlsbad Field Office (CBFO) chief scientist, George Basabilvazo, for whom Shawn Otto and Jon Davis of the WIPP Test Coordination Office (TCO) work for. The authors thank Jason Heath of Sandia National Laboratories (SNL) for providing a detailed technical review of the entire document.

CONTENTS

LIST OF FIGURES

LIST OF TABLES

ACRONYMS

2D, 3D	two- or three-dimensional
AE	acoustic emissions (also BATS boreholes)
BATS	Brine Availability Test in Salt
CBFO	Carlsbad Field Office
CRDS	cavity ring-down spectrometer
DOE	Department of Energy
DOE-EM	DOE Office of Environmental Management
DOE-NE	DOE Office of Nuclear Energy
DRZ	disturbed rock zone
DSS	distributed strain sensing
DTS	distributed temperature sensing
EDZ	excavation damaged zone
EdZ	excavation disturbed zone
ERT	electrical resistivity tomography
FY	fiscal year (October-September)
HP	BATS central heater/packer borehole
IPI	Inflatable Packers International
LANL	Los Alamos National Laboratory
LBNL	Lawrence Berkeley National Laboratory
LVDT	linear variable differential transformer
MB-139	marker bed 139 (also MB-140)
MPFM	multiparameter flowmeter
MU-0	map unit 0; also MU-1 to MU-5
NETL	National Energy Technology Laboratory
PA	performance assessment
PEEK	polyether ether ketone
PVC	polyvinyl chloride
R&D	research and development
RH	relative humidity
RTD	resistance temperature detector
SDI	Salt Disposal Investigations
SFWD	Spent Fuel & Waste Disposition
SFWST	Spent Fuel & Waste Science and Technology
SIMCO	Salado Isolation Mining Contractors
SL	BATS seal borehole
SN	serial number
SNL	Sandia National Laboratories
SRS	Stanford Research Systems
TC	thermocouple
TCO	WIPP Test Coordination Office
THMC	thermal-hydrological-mechanical-chemical
UHP	ultra-high purity (99.999%)
US	United States
VPG	Vishay Precision Group
WIPP	Waste Isolation Pilot Plant

BRINE AVAILABILITY TEST IN SALT FY23 UPDATE

This fiscal year 2023 (FY23) report presents data collected in phase 2 of the Brine Availability Test in Salt (BATS 2) in a new heated borehole array. The test is funded by the US Department of Energy's Office of Nuclear Energy (DOE-NE) Spent Fuel and Waste Disposition Program, under the Disposal Research and Development (R&D) program of the Office of Spent Fuel & Waste Science and Technology (SFWST). The test is located underground at the Waste Isolation Pilot Plant (WIPP), southeastern New Mexico, which is a DOE Office of Environmental Management (DOE-EM) site managed by the Carlsbad Field Office (CBFO).

A high-level test plan by Stauffer et al. (2015) places BATS in the context of a multi-year testing strategy, which involves testing a range of processes at multiple scales, eventually culminating in a drift-scale disposal demonstration. The organization of the current phases of the BATS field test is outlined in *"Project Plan: Salt In-Situ Heater Test"* (SNL et al., 2020), and a three-to-five year plan is presented in *"Brine Availability Test in Salt (BATS) Extended Plan for Experiments at the Waste Isolation Pilot Plant (WIPP)"* (Kuhlman et al., 2021a).

An early conceptual design of the BATS field test was laid out in Kuhlman et al. (2017), which includes appendices with references to historic heated salt field tests. This summary provides context, historical examples, and motivation for the individual test components of BATS. This level-2 milestone report presents data collected with new boreholes drilled in FY22, which constitutes BATS 2. More details on the as-built state of the BATS phase 1 (BATS 1) experiment can be found in the FY20 milestone report "*FY20 Update on Brine Availability Test in Salt"* (Kuhlman et al., 2020). An unheated array of boreholes, which has been monitored during both BATS 1 and 2, is described in the FY20 and FY21 reports and this current FY22 report. The FY21 milestone report "*Brine Availability Test in Salt (BATS) FY21 Update*" (Kuhlman et al., 2021b) presented a summary of 2020–2021 data, including several gas tracer tests conducted between boreholes. The FY22 milestone report "*Brine Availability Test in Salt (BATS) FY22 Update*" (Kuhlman et al., 2022) presented a description of the decommissioning activities for the BATS 1 heated array and a description of the construction of the new BATS 2 heated array. This report presents data collected during the first four heating phases in BATS 2 (a-d), and new FY23 data from the unheated array as a comparison to the BATS 2 heated data.

This level-2 milestone report incorporates input from level-3 milestone reports recently completed as part of Salt Disposal Research R&D by Los Alamos National Laboratory (LANL; Guiltinan et al., 2023) and Lawrence Berkeley National Laboratory (LBNL; Rutqvist et al., 2023). The team preparing, designing, implementing, debugging, and interpreting the BATS results includes members from multiple national laboratories, namely Sandia National Laboratories (SNL), LANL, and LBNL. The tight integration of our DOE-NE Salt R&D team over several years has helped make the ongoing field experiment possible. The work presented here would not be possible without the DOE-EM WIPP Test Coordination Office (TCO), who is onsite and underground at WIPP every week.

1. Background and Test Overview

1.1 Motivation for BATS

The focus of the BATS field test campaign is brine availability in geologic salt. These field tests are the first part of a wider systematic multi-year field investigation campaign to improve the existing long-term repository safety case for disposal of heat-generating radioactive waste in a generic salt repository. BATS seeks to improve current understanding for predictions of how much brine can flow into both ambient and heated excavations (e.g., boreholes or rooms) in salt. Brine availability is important to the long-term repository safety case for radioactive waste disposal in salt (Kuhlman & Sevougian, 2013) because of the following:

1) brine can corrode metallic and glass waste forms or waste packages;

2) brine can facilitate transport of radionuclides off-site;

3) water is needed for gas generation (e.g., steel corrosion or water radiolysis), which can increase gas pressure, providing a driving force for migration away from the repository;

4) chlorine and borate in brine absorb neutrons, thereby reducing in-package nuclear criticality hazards; and

5) accumulated brine in an excavation undergoing creep closure provides back-pressure that may resist ultimate creep closure and sealing of a repository excavation.

Future different field tests under the wider field campaign will explore other performance aspects of the long-term repository safety case that are separate from the brine availability focus of the current BATS 2 field test.

In a generic salt repository for "hot" radioactive waste (i.e., above brine boiling temperature at the waste package surface), an area around the waste packages will dry out once water vapor is driven away. Additional water associated with clays and water bound up in hydrous evaporite minerals may become mobile upon heating, and thermal expansion of the solid matrix and intergranular brine located away from the excavation in the host salt leads to thermal pressurization, driving brine towards lower pressure excavations. If conditions are right, a small-scale heat pipe convection process can set up in a high-permeability excavation damaged zone or granular salt regions around waste (Olivella et al., 2011; Jordan et al., 2015). The heat pipe includes salt precipitation near the waste package and salt dissolution where steam condenses as fresh water away from the heat source. The conceptual model is that creep closure eventually reconsolidates any granular salt backfill, closes gaps around waste packages, and heals the Excavation Damaged Zone (EDZ) or Excavated disturbed Zone (EdZ; both EDZ and EdZ are discussed below) associated with access drifts to create a relatively dry, low-porosity, low-permeability zone around the waste packages (Blanco-Martín et al., 2018). Knowledge of brine availability facilitates understanding the following key performance aspects of the repository system: the amount and distribution of brine that flows to an excavation, as well as the long-term behavior of brine around waste packages that affects transport (e.g., brine-radionuclide interactions); and the resistance to creep closure from accumulated brine that does not flow away from the repository excavation. The interplay of brine availability and the complex coupled thermal-hydrological-mechanical-chemical (THMC) processes controls the extent and timing of ultimate drift closure.

In undisturbed geologic salt systems, the ultra-low permeability and porosity of salt (Beauheim & Roberts, 2002) provides the primary natural barrier to contain radioactive waste over performance assessment (PA) relevant time scales (10^4 to 10^6 years). However, near-field conditions (e.g., fluid pressures, liquid saturation, and chemical composition) and processes (e.g., brine and gas flow, waste package corrosion, precipitation and dissolution of salt, thermal expansion and contraction of salt and brine, and salt creep) can impact releases in disturbed scenarios (i.e., off-normal scenarios like inadvertent human intrusion) and are the initial conditions for long-term PA simulations. BATS is focused on understanding processes necessary to quantify inflow rates and brine composition in the near-field (i.e., at scales of cm to m from the heat source) with the aim to improve:

1) our understanding of coupled THMC processes affecting prediction of near-field conditions;

2) conceptual models of near-field behavior that inform the safety case; and

3) the numerical models, constitutive relationships, and parameterizations that are implemented in process models and PA models.

Brine availability in a salt repository depends on both the distribution of water in the host salt geologic formation and the flow and transport properties of the EDZ or EdZ surrounding an excavation (Kuhlman & Malama, 2013; Kuhlman, 2019). Note that we may use the generic term "water" to refer to the aqueous liquid that may range in total dissolved solids from fresh water to brine, as heating processes and condensation may alter the salinity of the aqueous liquid, and we may also use "water" to refer to the molecule itself—the specific context should make the usage clear. The EDZ is a region surrounding excavations where the salt is damaged, and both its material properties (i.e., porosity and permeability) and state or potential energy (i.e., pressure, stress, or temperature) have changed—note that the EDZ is often equivalently called the disturbed rock zone (DRZ). The EdZ is a larger region surrounding the EDZ, where only the state variables are disturbed from their far-field values, while rock material properties are unchanged (Davies & Bernier, 2005). The distribution of water in the system includes the following: bound water that is both liquid or structural in the salt formation (i.e., brine in clay, intragranular brine, intergranular brine, and hydrous minerals; Roedder, 1984); and water in both the liquid and gas phases before and during emplacement of heat-generating radioactive waste, which is affected by heating processes, evaporation, and condensation. The primary EDZ property of interest for the BATS field test is the distribution and evolution of mechanical damage and coupled hydrologic properties (i.e., porosity, permeability, and the nature of induced fractures) around the access drift and test boreholes, which provides the primary path for flow around the access drifts and test boreholes.

1.2 BATS Phases

The preliminary BATS "shakedown" test location was in WIPP drift E-140 (Figure 1), utilizing existing boreholes. Referred to as BATS 1s, it was performed June 2018 through April 2019 (Boukhalfa et al., 2019; Guiltinan et al., 2020).

Figure 1. WIPP underground map. BATS phases 1 and 2 location indicated with red circle. BATS 1s shakedown test location indicated with blue star.

BATS phase 1a began with two nearly identical new horizontal borehole arrays (heated and unheated) drilled in the Salt Disposal Investigation (SDI) area of WIPP (on the south side of N-940 west of E-540; see Figure 2). BATS phase 1a refers to testing that occurred from January to March 2020 and involved data collection from both the heated and unheated arrays. BATS phase 1b was conducted from January to June 2021 and involved addition of gas tracers to the D boreholes in both the heated and unheated arrays. BATS phase 1c was conducted July to August 2021 and involved adding liquid tracers in the same heated and unheated D boreholes (Kuhlman et al., 2021b). Here, the references to the “BATS 1” boreholes mean the boreholes used in phases 1a through 1c, not the 1s shakedown test boreholes in drift E-140.

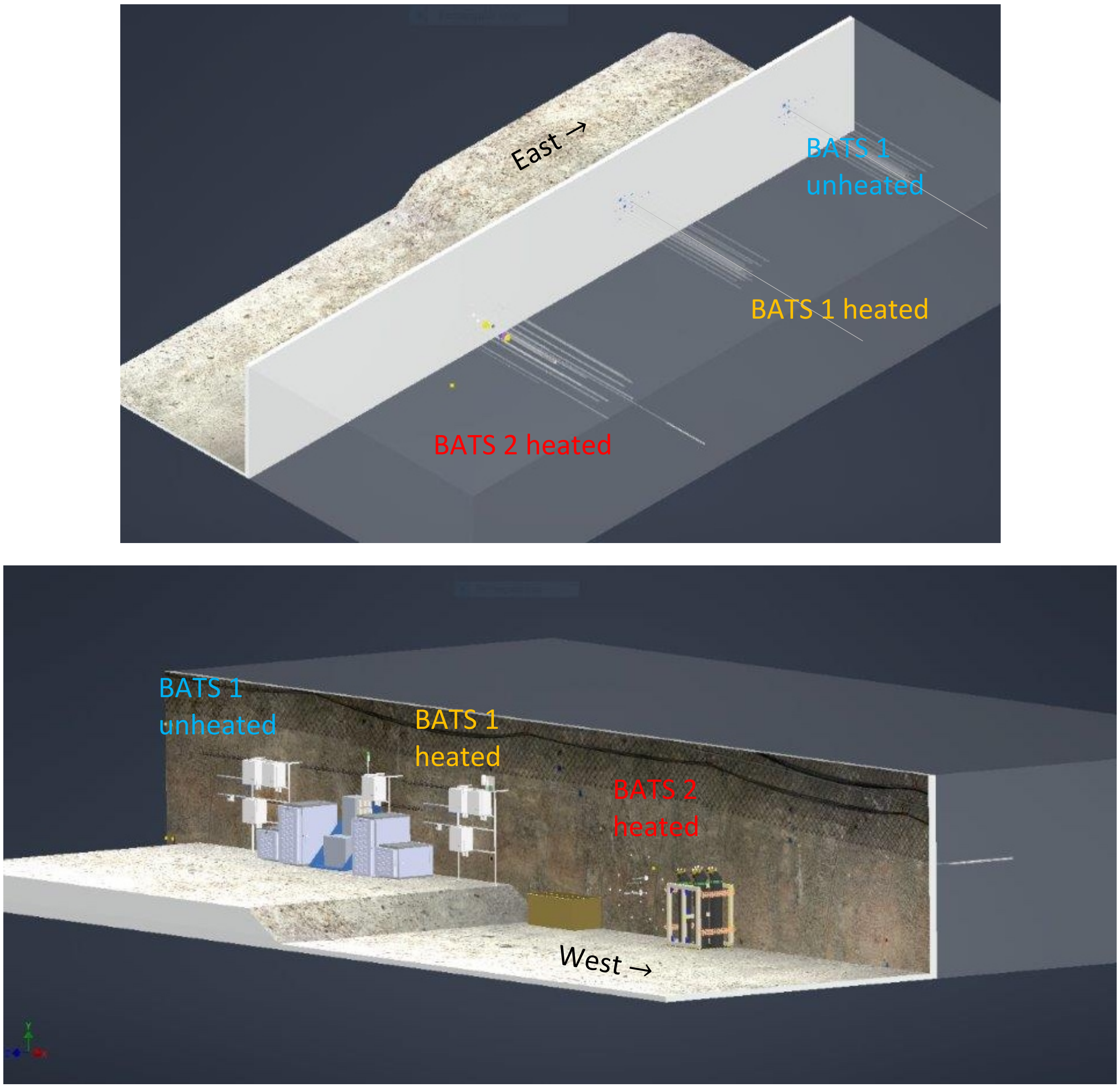

Figure 2. Layout of borehole arrays and in-drift equipment in N-940 showing relation between BATS 1 and BATS 2. Boreholes are on the south side of drift; the unheated array is east of the heated arrays. Upper panel shows orientation of boreholes.

BATS 2 boreholes were drilled October 2021 and January through February 2022 in the N-940 drift at WIPP, approximately 20 feet [6.1 m] west of the BATS 1 heated arrays. Four heater testing events have occurred so far in BATS 2 (July 2022 through March 2023) named BATS 2a, 2b, 2c, and 2d, with follow-on heater tests planned to continue in 2023 and possibly into 2024. The BATS 2 heater tests are being conducted in a newly constructed (October 2021 through February 2022) heated borehole array, while reusing the BATS 1 unheated array (constructed in 2019).

1.3 BATS Field Test Components

The western test array of BATS 2 is heated by the heater in the central HP borehole, and the eastern array is the unheated array from BATS 1 (see Kuhlman et al., 2020, for detailed info on the unheated array). Figure 2 shows the location of the adjacent BATS 1 and BATS 2 arrays in the N-940 drift. Table A-1 lists the sequence boreholes drilled as part of BATS 1 decommissioning and BATS 2 setup. Appendix A includes several lists of tabular data important for documentation of BATS 2, such as the sequence of BATS 2 borehole drilling and coring, as-built coordinates of BATS 2 boreholes, various measurement or sensor names and locations, and other similar information. The HP boreholes in the two BATS 1 arrays were 6.9 m apart horizontally and at the same level vertically, while the BATS 2 heated array is 13 m west and 1 m lower vertically than the unheated array (distance between HP boreholes).

The heated BATS 2 array is configured with several types of instruments in the central HP borehole and surrounding satellite boreholes. See Table 1 for a listing of information on the various boreholes, Figure 3 for borehole locations projected on an image of the drift, and Figure 4 for views of the boreholes and temperature sensor locations from three different viewpoints. Table A-2 lists the planned and as-built coordinates for the boreholes, and Table A-3 lists the locations of temperature measures, both of which were used to plot Figure 4. There are some minor differences apparent between as-built and planned locations in Figure 3 and Figure 4, mostly visible in the boreholes furthest from the center. This is likely due to image warping issues with the application used to create Figure 3; Figure 4 is more accurate, and is based on survey data.

Compared to BATS 1 (including the unheated array, which is still partially monitored), there are additional AE and E boreholes (four in BATS 2 heated array compared to three in each array for BATS 1a), and the SL, AE, and E boreholes are all longer. The narrowest boreholes in BATS 1 were 1.75 inches [4.4 cm] diameter, while the narrowest boreholes in BATS 2 are 2.1 inches [5.3 cm] diameter. Temperature distribution, strain, and brine movement are monitored with thermocouples, fiber-optic distributed strain sensing (DSS) and temperature sensing (DTS), acoustic emissions (AE) monitoring, and electrical resistivity tomography (ERT).

Table 1. Summary of BATS 2 heated array boreholes.

Type	Purpose	Boreholes per array	Diameter [in]	Length [ft]	Isolation Device
HP	Heater, packer, borehole closure, N_2 circulation, gas sampling, gas permeability testing	1	4.8	12	Inflatable packer
D	Tracer source, gas permeability testing	1	2.1	15	Inflatable packer
SM	Liquid sampling	1	2.1	15	Mechanical packer
F	Fiber-optic temperature and strain	2	2.1*	18 & 30	Grouted
E	Electrical resistivity tomography (ERT) electrodes	4*	2.1*	19*	Grouted
AE	Acoustic emissions (AE) and ultrasonic travel-time tomography sensors	4*	2.1	11*	Sensors on borehole wall with de-centralizer
T	Thermocouples	2	2.1*	18	Grouted
SL	Cement seals behind mechanical packers with embedded strain gauges and thermistors	1	4.8	11.5*	Mechanical packer

* The given number or size is different between BATS 1 and BATS 2

Inflatable packers are used in the HP and D boreholes to isolate the region behind the packer from the drift air (Table 1). This is to prevent dry-out of the salt, loss of moisture, and contamination of samples. The rubber bladder is inflated to approximately 80 psi [5 bars] pressure above atmospheric pressure. The HP borehole packer has multiple pass-through tubes or pipes, to allow sensors and power to reach the isolated part of the borehole. These pass-throughs are sealed with wire compression nuts, made by Conax Technologies. The D borehole packer has a port for application of gas pressure behind the inflated packer but does not have wire pass-throughs. Mechanical packers are also used in the SM and SL boreholes to isolate the rear part of the borehole from the drift environment. The mechanical packers use mechanical compression of a rubber sleeve by tightening nuts on a threaded rod to isolate the rear of the borehole. The wires to the sensors behind the packer are sealed against the inside of the threaded pipe with plumber's putty.

2. Test Design Details

The following testing methods relate to the setup and initial monitoring of the BATS 2 heated array. For the as-built details of the BATS unheated array boreholes and more information on BATS 1 in general, see previous milestone reports by Kuhlman et al. (2020; 2021b).

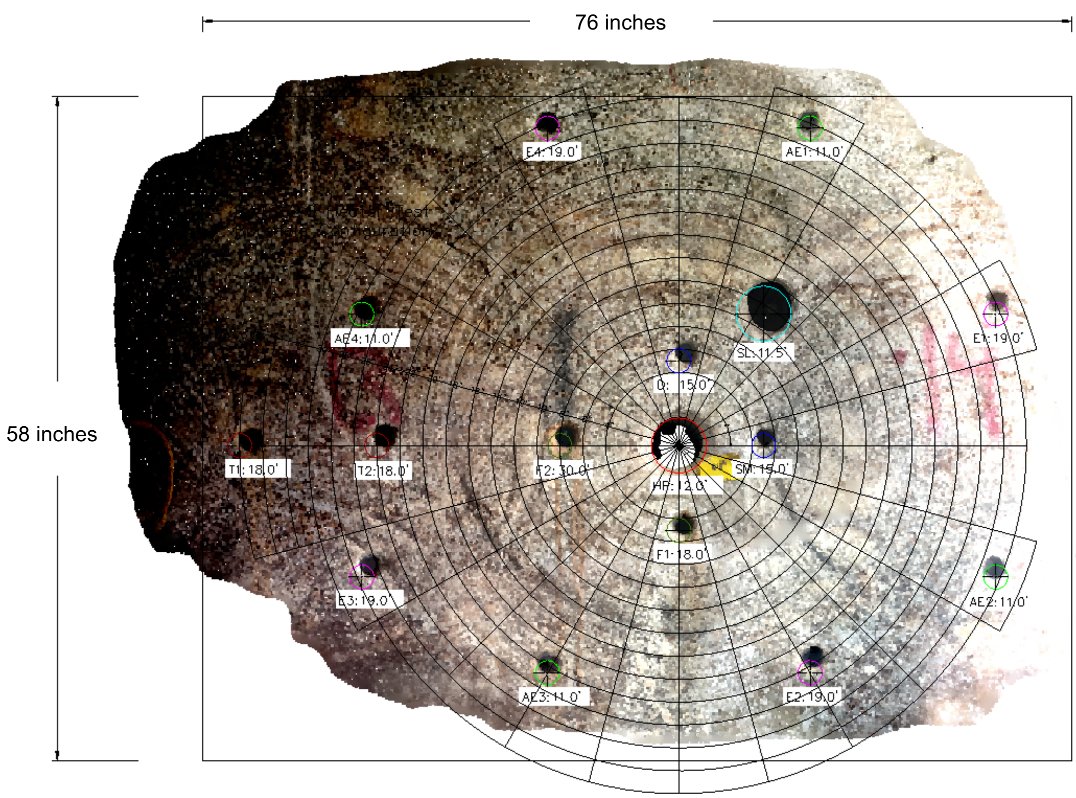

Figure 3. Planned (overlay) and as-drilled (image) locations of boreholes in BATS 2 array. Borehole lengths given in feet.

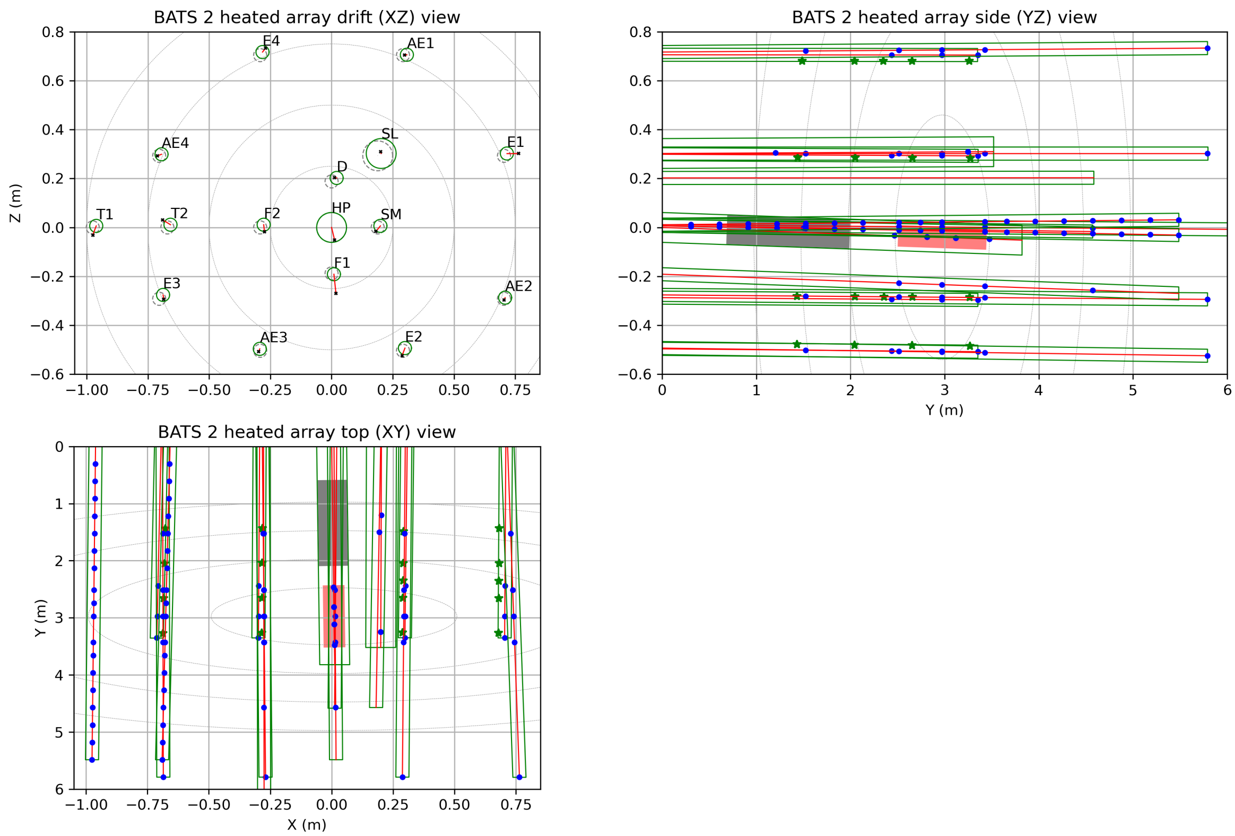

Figure 4. Drift, side, and top views of BATS 2 boreholes. Drift view shows proposed (gray dashed) and as-built (green) borehole positions in drift; red line is axis of boreholes with "×" labeling end of boreholes. Side and top views show thermocouple and resistance temperature detector (RTD) locations (blue dots), AE sensor locations (green stars), HP heater (filled red box), and HP packer (filled gray box). Gray contours indicate distance from center of heated interval.

2.1 BATS 2 Testing Phases

To date, four heater tests have been conducted in BATS 2, each for three weeks of heating. The tests have consisted of a three-week heating phase, followed by at least two weeks of cool down period. The fourth heater test (BATS 2d) was initially aborted after approximately one day, due to an error configuring the heater controller. After removing the packer and troubleshooting all the components of the system, the controller was re-programmed. The BATS 2d was eventually run in March 2023, after some delays due to instrumentation being repaired or replaced (i.e., for the Picarro cavity ringdown spectrometer and Standard Research Systems (SRS) gas analyzer).

The full-length heater test periods are referred to as BATS 2a, BATS 2b, BATS 2c, and BATS 2d. The setpoints, achieved power, and temperatures observed are discussed in detail in Section 4.1.6.

3. Configurations of BATS 2 Boreholes and Measurements

The following subsections describe the arrangement of boreholes and measurement equipment in the new BATS 2 heated array. The boreholes in the unheated array were completed as part of BATS 1, and they are described in Kuhlman et al. (2020).

3.1 HP (Heater and Packer) Borehole

There is one central 12.54-ft [3.82 m] long and 4.8-inch [12.2 cm] diameter HP borehole. The 1250-watt quartz lamp heater (BATS 1 used a 750 W heater of the same physical size) and centralized borehole-closure gauge are mounted behind the 4.5-inch [11.4 cm] diameter 4.2-ft [1.3 m] long inflatable packer, which is built around a 0.5-inch [12.5 mm] stainless steel pipe. The HP borehole in BATS 2 is like the configuration used in BATS 1, but a longer packer is employed to provide better isolation of the heated interval (Figure 5).

The BATS 2 packer was manufactured by Inflatable Packers International (IPI) and is 4.49 inches [11.4 cm] maximum outer diameter and 4.27 ft [1.3 m] long (from shoulder to shoulder), with the inflatable portion (i.e., the black nitrile rubber portion) of the packer being 3.25 ft [1 m] long. The BATS 2 heater was placed at the same depth into the borehole as the BATS 1 heater to improve comparison between tests, but the BATS 2 packer covers a longer interval than the BATS 1 packer (Figure 5).

Figure 5. Comparison of BATS 1 Aardvark HP packer after removal (right, in pipe) with BATS 2 IPI packer before installation (left, in box).

The heater/packer assembly is placed almost to the back of the borehole (Table 2), with only a 6.49-inch 16.5-cm [6.49-inch] gap behind the back of the heater/packer assembly (because the borehole ended up being 16.5 cm longer than initially planned). Approximately 69 cm of heater/packer assembly extends out of the borehole into the drift. The packer sealing element is inflated with N_2 to approximately 80 psi [5.5 bar] gauge pressure (i.e., above atmospheric pressure) to isolate the heater and gas circulation from the drift. The packer inflation is valved off from the N_2 bottle after filling, and the inflation pressure is monitored.

There are two 0.25-inch [6.4 mm] pass-through tubes allowing gas flow to and from the interval behind the packer: one tube is connected to ultra-high purity (UHP > 99.999%) bottled N_2 (inflow) and the other is connected to the downstream gas instrumentation (outflow). The inflow gas tube extends to the rear of the heater/packer assembly (near the back of the borehole; Figure 8), while the gas outflow tube ends at the back of the packer (the front of the isolated interval, closer to the drift). The thermocouples exit the borehole through two 0.38-inch [9.5 mm] pass-through tubes and are sealed with Conax Technologies fittings near the drift side of the packer (which are inside the borehole when the packer is installed). The heater power and a linear variable differential transform (LVDT) data cable pass through the 0.5-inch [12.7 mm] pipe, which is sealed with Conax Technologies fittings at the end of the 0.5-inch pipe, visible in the drift.

Table 2. BATS 2 HP heater/packer assembly component distances.

HP Packer Component		From front of assembly [m]	From drift face [m]	From rear of assembly [m]
Drift end	end assembly	0.000	-0.686	4.343
Packer	drift-side steel shoulder	1.372	0.686	2.972
	drift-side edge of rubber	1.527	0.841	2.816
	heater-side edge of rubber	2.521	1.835	1.822
	heater-side steel shoulder (N_2 out)	2.667	1.981	1.676
LVDT	center of centralizer	3.124	2.438	1.219
Heater	shallow reflector	3.302	2.616	1.041
	shallower TC	3.505	2.819	0.838
	center	3.658	2.972	0.686
	Deeper TC	3.810	3.124	0.533
	deeper reflector	4.013	3.327	0.330
Support	center of centralizer	4.191	3.505	0.152
Far end	back of assembly (N_2 in)	4.343	3.658	0.000
Behind	back of HP borehole	4.508	3.822	-0.165

3.1.1 Routing and analysis of gas streams

Upstream of the HP borehole, a bottle of UHP N_2 gas flows at a constant mass flowrate maintained via a programmable Omega flow controller (FMA-2605A-V2). BATS 2 is mostly run at a constant flowrate, 75 std mL/min (i.e., mass flowrate at standard temperature and pressure), while the unheated array is mostly maintained at 25 std mL/min. When the gas flow was first turned on (25 April 2022), both the heated and unheated arrays were set at a higher flowrate to more quickly remove any standing brine in the boreholes (Section 4.1.1). We wish to prevent standing water in the borehole (for water isotopes), but there is also a concern regarding having too much dry air circulating through the borehole, which might dry out the salt surrounding the borehole (changing the flow regime from single to two-phase around the borehole).

Later in BATS 2d the gas flowrate was also increased in the heated array because there was evidence of condensation in the tubing. The flowrate of N_2 is otherwise set to maintain a minimum humidity of the gas stream, based on the calibration range (> 10,000 ppm by volume of H_2O) for the Picarro cavity ring-down spectrometer (CRDS). Omega (FMA6708-12V) multiparameter flowmeters (MPFM) are located downstream of the packers to monitor the air temperature, pressure, and flowrate, with data recorded on a Campbell Scientific datalogger.

The Picarro CRDS and the SRS QMS-200 gas analyzer are shared between the heated and unheated arrays. The gas plumbing changes which branch the Picarro/SRS are on periodically (2 hours on unheated array, 10 hours on heated array, repeating twice daily) via solenoid-actuated three-way valves (Figure 6). The Picarro analyzer reports the concentration of water isotopologues in the gas stream (three stable oxygen and two stable hydrogen isotopes). The system is designed to keep the water as a vapor, to prevent condensation and evaporation in the tubing, which could lead to fractionation of isotopes. A dedicated LI-COR analyzer on each branch of the plumbing (upstream of the switching) measures mmol H_2O and μmol CO_2 per mol gas. On 6 September 2022, the LI-COR systems were switched out because the systems were not properly calibrated (data reported for the LI-COR systems in Kuhlman et al., 2022 were not accurate). The analog outputs from the LI-COR are connected to a Campbell Scientific CR1000X datalogger, while the Picarro and SRS gas analyzers each have their own logging computers.

The SRS QMS-200 gas analyzer is a quadrupole mass spectrometer operating in a vacuum chamber evacuated with a turbomolecular pump. The unit splits the sample, directing most of it to the backing vacuum pump, which permits the unit to directly sample gases at atmospheric pressure.

The output streams from the gas analyzers go through another pair of plumbing tees and three-way solenoid-actuated valves before passing through a pair of air temperature and relative humidity (RH) probes (labeled as TRH probes in Figure 6) and a pair of canisters of desiccant, with subsequent TRH probes at the outflow. The TRH probes before and after the desiccant are used to confirm the RH of the gas stream, and to confirm the desiccant is removing all the moisture from the gas stream. These final set of switching valves ensures that one set of desiccant canisters is associated with the heated array and the other associated with the unheated array, even though the intervening gas analyzers are switching between arrays.

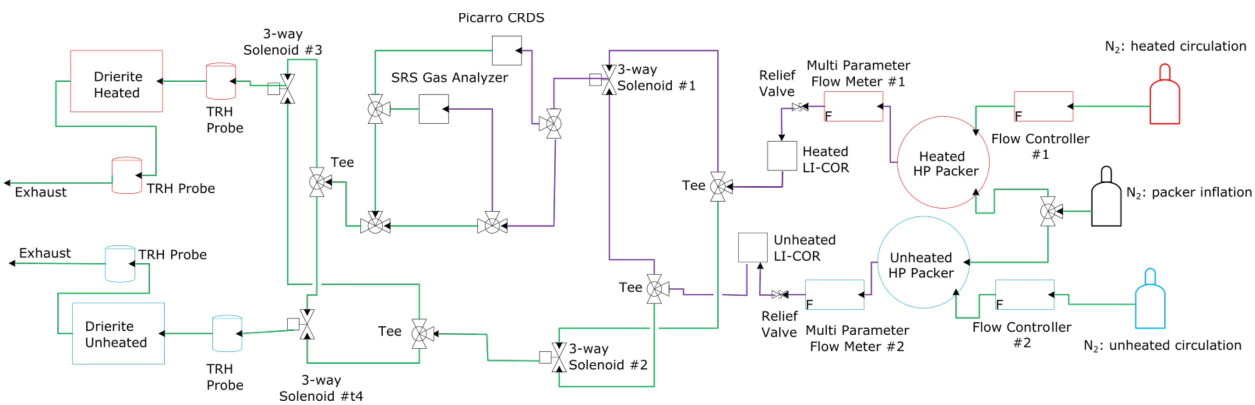

Figure 6. Plumbing of BATS 2 gas flow from HP boreholes (right) through Picarro, Stanford Research System (SRS), and LI-COR gas analyzers to exhaust (left). Green lines are 0.25-inch [6.4 mm] polyethylene tubing, purple lines are 0.25-inch stainless steel tubing, red items are only for the heated array, and blue items are only for the unheated array, gray items switch between the heated and unheated arrays. TRH means temperature and relative humidity.

3.1.2 Applied heater power

The 1250-watt, 208-volt Tempco Gemini Medium Wave quartz twin-bore infrared heater is mounted on a 1-inch [2.5 cm] steel pipe with perpendicular disc-shaped reflectors (4-inch [10.2 cm] outer diameter) installed on either end of the heater to confine the radiative energy to an approximately 28-inch [71 cm] long interval of the borehole wall. Four thermocouples are installed to measure the temperature of the borehole wall (extending radially from stainless steel guide tubes) between the two reflectors (Figure 7).

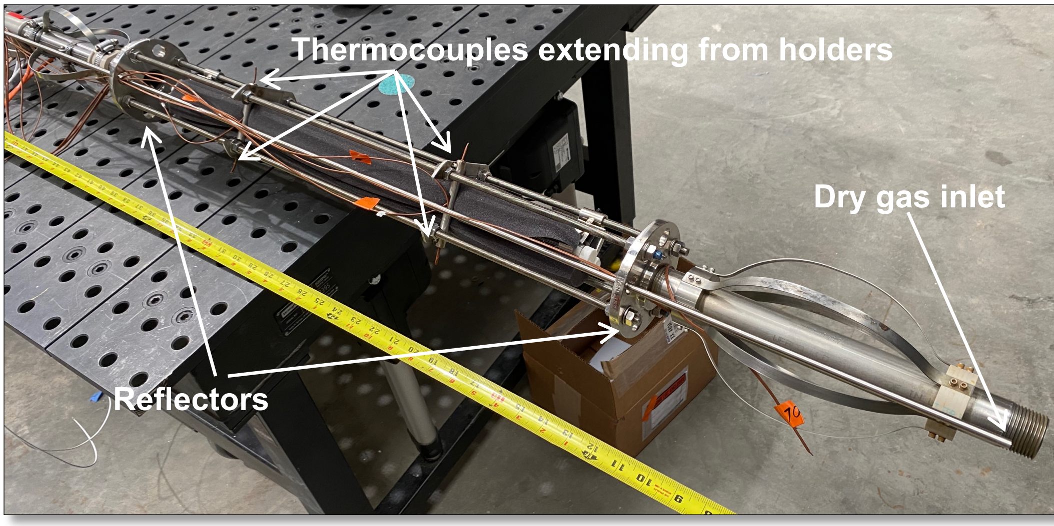

Figure 7. Borehole closure gauge (left), heater, thermocouples, rear centralizer, and gas inlet tubing (right) for heater HP packer assembly in BATS 2.

The heater is controlled to maintain the setpoint thermocouple at constant temperature (which is pressed against the borehole wall), while a second thermocouple pressed against the wall is used as an emergency over-limit check, shutting down heater power in case a malfunction with the primary controlling thermocouple leads to overheating. In the aborted BATS 2d test, the limit thermocouple functioned as designed (the issue was it was set too low at 145 ºC) and shut the test down. The Watlow F4T controller output (applied power, current, voltage, resistance, and duty through time—along with several other system diagnostics) is transmitted to a Campbell Scientific CR1000X datalogger. The hot and neutral power wires for the heater pass through the packer via the 0.5-inch [12.7 mm] pipe and are sealed via a Conax Technologies fitting at the drift, while the 0.5-inch pass-through pipe is used for grounding.

On the heater side of the packer, the 0.5-inch [12.7 mm] pipe goes through a union (to allow breaking and easier transport of the assembled packer), a reducer (to convert between 1 and 0.5 inch pipe), and a plumbing "T" (to let the thermocouples and LVDT wires out of the tube before reaching the heated interval) before the borehole closure gauge (Figure 8 and Figure 9).

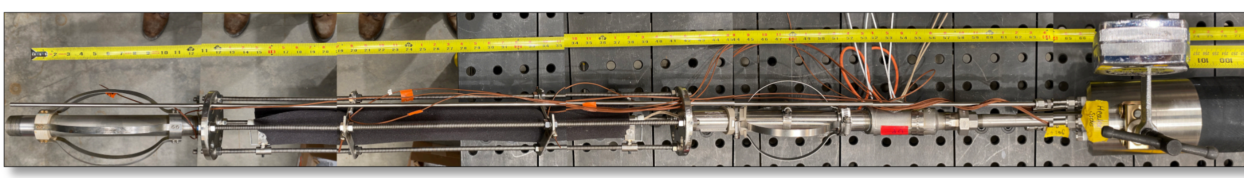

Figure 8. Packer (right), borehole closure gauge and LVDT, heater (covered with black foam), 0.25-inch [6.4 mm] gas line to back of borehole, and rear centralizer (left) used in BATS 2 during assembly. Measuring tape (in feet and inches) zeroed at end of packer assembly.

3.1.3 Borehole closure

The borehole closure gauge is made of a four-arm spring steel centralizer fixed to the 1-inch [2.5 cm] pipe on one end, with the other end connected to a polyether ether ketone (PEEK) bushing, which slides on a key over the 1-inch pipe (Figure 9). The bushing connects to an axial LVDT, which measures displacement of the bushing. The axial measurement was found to be more robust than a radial LVDT measurement with the gauge pressed against the borehole wall. Displacement can be related linearly to borehole circumference. The response of the LVDT at different borehole radii was calibrated against standard-diameter calibration rings. The LVDT is equipped with an in-line signal conditioner and is connected to a Campbell Scientific CR1000X datalogger.

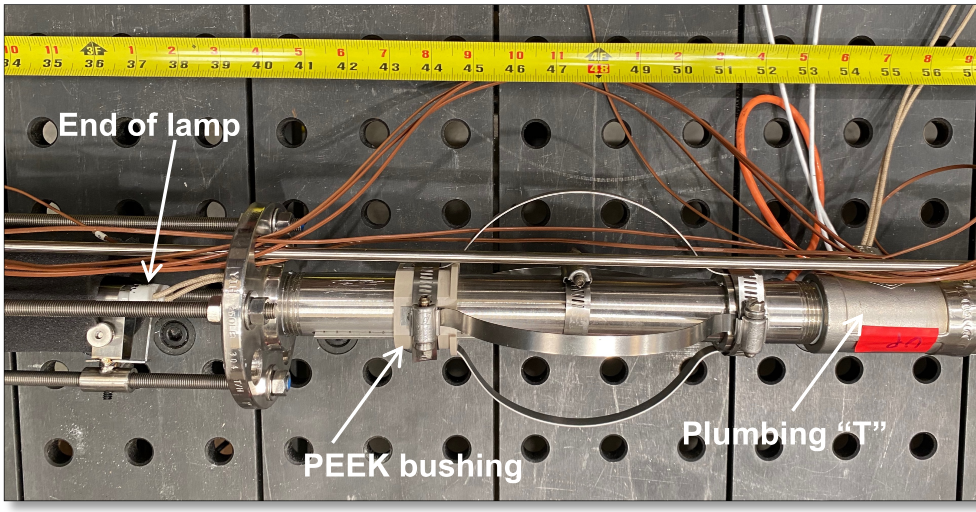

Figure 9. Closeup of borehole closure gauge (heater to left, packer to right – out of photo); distance from far end of packer/heater assembly indicated (in inches and feet) with measuring tape. LVDT (connected to orange wire, held to pipe with hose clamp) is not visible behind central pipe.

3.2 AE (Acoustic Emission) Boreholes

There are four 11-ft [3.35 m] long (2.1-inch [5.3 cm] diameter) AE boreholes with multiple piezoelectric sensors, namely Physical Acoustics Nano30 AE sensors, in each borehole. The AE boreholes are not grouted. There are two Mistras Micro-II Express data acquisition systems (one for each array) used to listen passively to piezoelectric sensors (8 channels unheated array, 16 channels heated array). The unheated array is monitored to measure AE associated with the unheated boreholes (i.e., background effects), while the heated array is used to monitor AE generated during heat-up and cool-down. Eight more channels are used in the heated array than in the unheated array, to better characterize the distribution of AE events spatially around the heater. There are also three thermocouples in each AE borehole (12 total in BATS 2 heated array) between the decentralized piezoelectric sensors (Table A-3). The four AE boreholes are arranged in a rough square surrounding the heated borehole (Figure 3).

The same sensor type and mounting method as BATS 1 were used for the BATS 2 installation. AE boreholes were moved to a further radial distance out from the central borehole. Four AE Boreholes were also drilled to a greater depth than previously, that is, to 3.05 m as opposed to 2.75 m, to have a larger interrogation volume of rock and get closer to the heater. Four sensors are mounted in each borehole for a total of 16 sensors, with two extra sensors installed as spares, to allow switching out damaged or noisy sensors. Small form factor inline preamps were used on the deepest sensor in each borehole, but were eventually abandoned due to unacceptable noise levels, otherwise the 2/4/6 preamps from BATS 1 were reused to amplify the millivolt signals coming from the sensors at a gain value of 40 dB. The Mistras system from the previous system was redeployed for BATS 2, and acquisition parameters were set to a 28 dB threshold and a 100 to 700 kHz bandpass filter. The sensors from BATS 1 were reused in BATS 2 after disassembly, cleaning, testing, and re-assembly on new longer hollow-tube conveyance pipes.

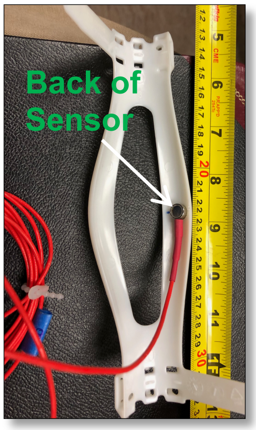

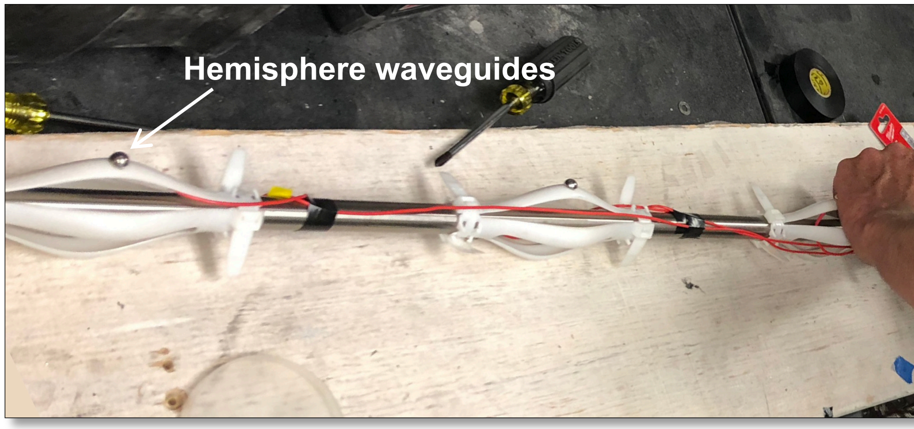

Figure 10. AE sensors and inside of centralizers (left); sensors and hemisphere waveguides installed on 0.75-inch [19.1 mm] stainless-steel conveyance rod with centralizers.

The AE sensors are installed through the arms of kwik-ZIP centralizers (made of polyoxymethylene thermoplastic) mounted on the outside of a 0.75-inch [19.1 mm] stainless-steel hollow-tube conveyance pipes (Figure 10). One end of each centralizer is screwed to the stainless-steel tube to fix a given sensor's position, while the other is fastened around the conveyance, but is free to slide along the tube. The flat circular faces of the piezoelectric transducers have 304 stainless steel hemispheres epoxied to them. The hemispheres act as wave guides to improve contact between the flat face of the transducers and the curved borehole walls. The piezoelectric transducers are all located on the sides of the AE boreholes that are closest to the HP borehole to optimize detection of the first arrival (i.e., P-wave) of acoustic emissions from the heated borehole (see sensor Figure 10). The Mistras system automatically picks AE events based on a magnitude threshold to record events and waveforms.

The piezoelectric sensors have 9.8-ft [3 m] leads, which are connected to an in-line signal preamplifier box at the drift face, which prevents them being installed more deeply into the boreholes. The cable from the preamplifier to the Mistras control computer does not have the same cable-length constraints. The Mistras logging systems with either eight or 16 channels are computers with internal data acquisition boards connected to a keyboard and mouse, which are rack-mounted inside an enclosure.

Electrical interference from the ERT system has been problematic for the heated array AE measurements, especially the channels associated with the inline preamps. To address this, a front-end filter was placed on the incoming signals where the Mistras systems automatically discards any hit that has a duration less than 10 counts. This solution works well for the channels using the 2/4/6 preamps, but channels on the inline preamps still show excessive electrical noise from the ERT system. These channels were disabled to allow heater tests to proceed. Existing data was filtered to this duration minimum and channel arrangement.

The unheated array from BATS 1 was left in place and is still active for the current and future phases of testing. Eight sensors are installed into three AE boreholes.

3.3 T (Thermocouple) Boreholes

There are two 19-ft [5.5 m] long (2.1-inch [5.3 cm] diameter) T boreholes (Figure 3) with 18 thermocouples in each (grouted outside 0.75-inch [19.1 mm] polyvinyl chloride (PVC) conveyance pipe; Table A-3). One of the boreholes is at 2-ft [61 cm] radial distance away from the edge of the heated borehole (T2), and the other at 3-ft [91 cm] radial distance (T1). Thermocouples are also located in other measurement boreholes to increase the density of observations and help correct other observations for local temperatures (Figure 4). The 10-minute averages of thermocouple temperatures are read on

Campbell Scientific CR1000X loggers through Campbell Scientific AM25T thermocouple multiplexers. The T1 and T2 boreholes in the BATS 2 array are in the same relative configuration to the central HP borehole as the BATS 1 array.

3.4 E (Electrical Resistivity Tomography) Boreholes

There are four 18-ft [5.79 m] (2.1-inch [5.3 cm] diameter) E boreholes with 16 ERT electrodes on the outside of each 0.75-inch [19.1 mm] PVC conveyance pipe (12-inch [30 cm] spacing between adjacent electrodes, starting from the far end of the borehole), with grout installed in the space inside and outside the PVC. Like the AE boreholes, the BATS 2 ERT electrodes are spread across four boreholes (compared to three boreholes in BATS 1), which are now 1 ft [30.5 cm] deeper and approximately 1 ft [30.5 cm] radially further from the HP borehole to increase the volume of interrogated rock. The electrodes are 1-inch [2.5 cm] wide copper foil rings installed on the outside of the conveyance pipes with jacketed wires running down the inside of the pipes. The electrodes are driven by Multi-Phase Technologies ERT controller (MPT DAS-1), located in an enclosure in the drift. In the heated array, the four ERT boreholes have a total of 64 electrodes. The ERT electrodes in the unheated array are no longer monitored.

The thermocouples used in the BATS 1 ERT boreholes were replaced in BATS 2 with RTDs (Table A-3) as an attempt to combat the anomalous non-physical temperatures that were measured in BATS 1 during ERT surveys (i.e., when applying current to ERT electrodes, from approximately 1:00 AM to 6:00 AM daily). The RTDs still record some anomalous readings during ERT surveys, but the RTD data are much less noisy than thermocouple data were in BATS 1. A complete ERT survey takes approximately one hour to perform at each frequency. A suite of ERT tests was scheduled to run at several frequencies nightly (9 PM to midnight each night, during BATS 2) to estimate the temporal evolution of the apparent resistivity distribution.

3.5 F (Fiber Optic Distributed Sensing) Boreholes

There is one 18-ft [5.5 m] (2.1-inch [5.3 cm] diameter) F1 borehole and a second 30-ft [9.1 m] F2 borehole (Figure 3, same diameter), both with grouted distributed fiber-optic sensors. The F1 and F2 boreholes in BATS 2 have the same relative orientation and distance to the HP borehole as in BATS 1. Each F borehole has four fibers: one for DTS and three others for DSS. Both types of fibers are protected with a braided steel sheath and polymer coatings to improve their durability during the experiment. The DTS fibers are inside a gel-filled tube to reduce sensitivity to strains. All fibers are attached to the outside of a 0.75-inch [19.1 mm] PVC conveyance pipe and grouted into the borehole. Efforts were made to arrange the strain fibers at 0-, 90-, and 180-degree circumferential positions clockwise from vertically up (Figure 11). Additional thermocouples (four in borehole F1 and eight in F2) were grouted in with the fibers for calibration and verification of DTS data (Table A-3). After grouting, the fiber optic sensors were well-coupled with the salt formation. The straight DSS fiber measures longitudinal strain along its length. The DTS measurements can be validated or calibrated against thermocouple observations in the same borehole. The fibers are connected to an eight-channel Luna fiber interrogator (ODiSi 6108) that reads the fibers hourly, located in an enclosure in the drift. The thermocouples are read at 10-minute averages using a Campbell Scientific CR1000X datalogger.

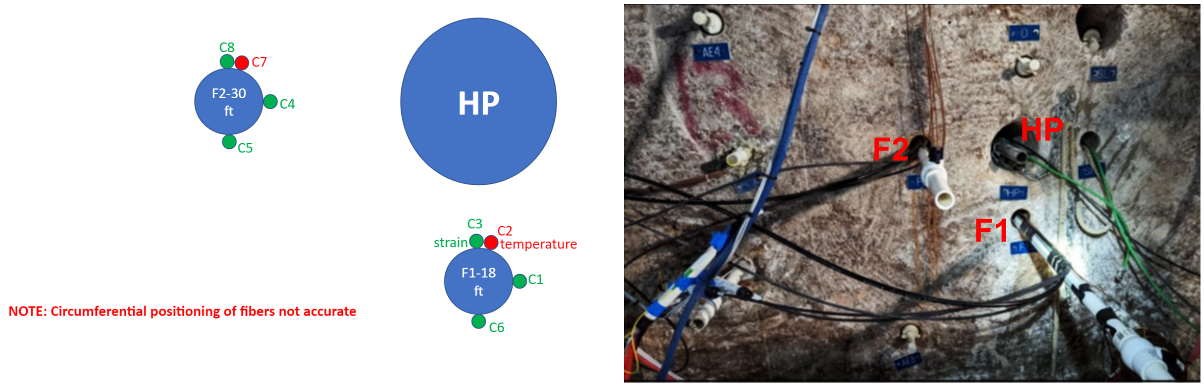

Figure 11. Fiber installation details in F1 and F2 boreholes of BATS 2 heated array. Green circles are DSS fibers; red circles are DTS fibers (Rutqvist et al., 2023).

3.6 D (Tracer Source) Borehole

There is one 15-ft [4.6 m] (2.1-inch [5.3 cm] diameter) D borehole (Figure 3) with a 2.1-foot [64 cm] long 1.9-inch [4.8 cm] diameter IPI packer inflated in the borehole (with the back of the packer set at 1.53 m depth). The packer sealing element is inflated to 80 psi [5.5 bar] above atmospheric pressure when in use. The BATS 2 D borehole has the same relative orientation and distance to the central HP borehole as in BATS 1. The BATS 2 D tracer borehole has been used for permeability testing to date, using UHP argon to pressurize behind the borehole. Gas tracer tests with other tracers are planned during later phases of BATS 2.

3.7 SM (Liquid Sample) Borehole

A 15-ft [4.6 m] long and 2.1-inch [5.3 cm] diameter liquid sampling borehole (SM; see Figure 3) is plugged with a mechanical packer beyond major fractures near the drift wall (the back of the packer is set at 1.35 m depth). The mechanical packer has a Campbell Scientific EE181-L air temperature and RH probe (TRH) behind it to confirm equilibrium of the air in the borehole with formation brine behind the plug. An RH in the range 70% to 75% indicates there is not significant mine ventilation (typically <50% RH) reaching the interval behind the packer, which would remove liquid water and impact the brine composition and water isotopes. The TRH probes are logged using a Campbell Scientific CR1000X datalogger.

Through the pass-through in the plug, a 0.25-inch [6.4 mm] stainless steel tube extends to the back of the borehole, which is the lowest elevation point in the borehole. The tube is sealed into the plug pass-through with plumber's putty. When not being sampled, the sampling tube is valved off at the drift face.

Approximately weekly, the valve on the 0.25-inch [6.4 mm] stainless-steel tube is opened to attempt to collect a liquid-phase sample from the tube that extends to the back of the borehole. A Nalgene polypropylene fluid-transfer closure is used to connect a portable vacuum pump to the permanent 0.25-inch stainless steel tube. The closure is connected to a larger (1 L) Nalgene sample collection bottle. This larger sample collection bottle is used to fill smaller sample bottles for delivery to the SNL and LANL geochemistry labs for analysis. The total volume of brine collected is estimated via graduated cylinder and recorded.

3.8 SL (Seal) Borehole

The 11.5-ft [3.5 m] deep SL borehole has a pair of composite lab-constructed cement seals emplaced and sealed behind a mechanical packer (the back of the packer is set at 1.05 m depth). The BATS 2 heated SL borehole is deeper than the SL borehole was in BATS 1, but it is at the same position and distance relative to the central HP borehole as was in BATS 1. The borehole was deepened from a length of 8 ft [2.44 m] in BATS 1, to get the seal emplaced closer to the heater. The composite seal was constructed in a single cylindrical cardboard tube mold of 4.6-inch [11.7 cm] diameter in the laboratory. First the salt concrete seal was constructed at the bottom of the mold, with the sorel cement seal emplaced on top of it after the salt concrete had cured for 28 days (Figure 12). Salt concrete and sorel cement seals were emplaced, with plans to eventually over-core and remove them for comparison of the two seals' relative reactions to hot brine exposure and mechanical loading due to creep closure.

Figure 12. BATS 2 lab-constructed composite seal emplaced in SL borehole. Salt concrete (left) and sorel cement (right) were constructed in a single mold. Thermocouple (red) and strain gauge (gray) wires are visible coming out of the drift-side of the plug on the right. Ruler marked in inches.

The sorel cement used a slightly different recipe than in BATS 1 (less salt aggregate and different MgO; Kuhlman et al., 2022), mostly because of a change in MgO source material. The salt concrete recipe used was the same as in BATS 1. The order of the two seals in the borehole was also switched (salt concrete in back, sorel cement in front) relative to the order in BATS 1 because of delays associated with procuring MgO.

The cement seals each have a Vishay Precision Group (VPG) concrete embedment (EGP-5-12 or "waffle") gauge estimating strain (Figure 13) with thermocouples embedded in the cement near the strain gauges. These sensors were embedded into the cement seals in the laboratory, and the seal was installed in the SL borehole to respond when the salt eventually closes in around it. The laboratory-made seals fit in the horizontal SL boreholes with a 0.25-inch [6.4 mm] or smaller gap. The seals were pushed back into the borehole to make contact with the back of the seal borehole, and a 4-foot [1.2 m] mechanical packer with a pass-through for wires was used to seal the borehole near the drift from mine ventilation. A TRH probe (Campbell Scientific EE181-L) was installed behind the mechanical packer to monitor the RH and air temperature between the packer and seal, confirming the isolation of the interval from mine ventilation (i.e., maintenance of near 75% RH). The sensor wires pass through the mechanical packer and the remaining gap between the wires was sealed with plumber's putty.

The strain gauges in the cement plugs serve two purposes. First, they should provide an indication of when the borehole creeps closed around the cement plug, causing the cement plug to deform. Secondly, once the salt has made contact and loaded with the plug, the strain in the cement plug provides some information on the stress state in the rock (i.e., the stress-strain behavior of the cement plug is assumed to be relatively well-known). The strain gauges, thermocouples, and hygrometer are monitored with a Campbell Scientific CR1000X datalogger.

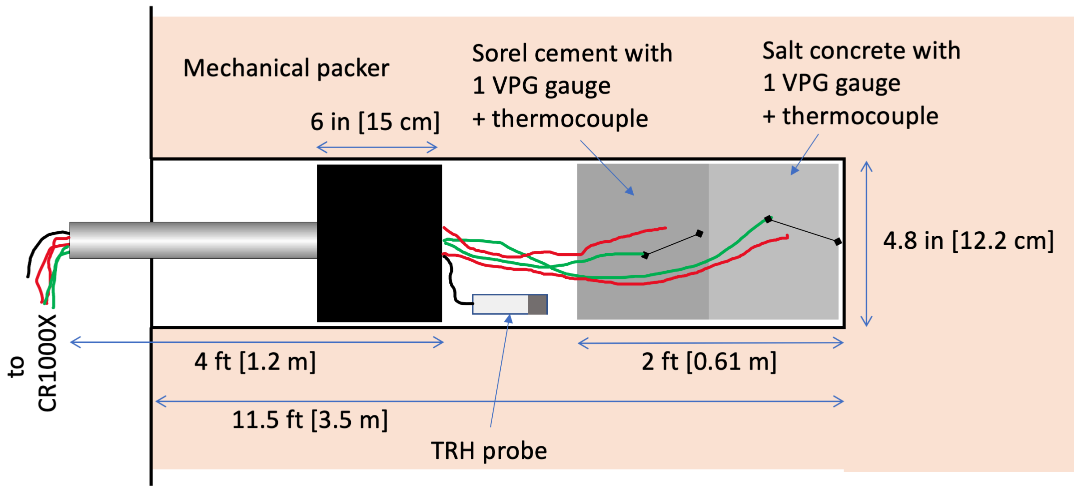

Figure 13. Cross-sectional of BATS 2 SL borehole showing relative positions of plugs, strain gauges (green), thermocouples (red), TRH probe (black), and mechanical packer.

3.9 In-Drift Observations

Ambient drift air pressure, air temperature, ventilation (i.e., "wind") speed, and RH are monitored in the drift between the BATS 1 unheated and BATS 2 heated arrays. Temperature is also monitored on the drift wall to provide information on how the heat from the tests interacts with the ambient drift air. Barometric pressure fluctuations can impact migration of gases during permeability and tracer tests. The weather station and drift thermocouples are monitored by a Campbell Scientific CR1000X datalogger.

4. BATS 2 Borehole Observations

Previous BATS 1 reports (Kuhlman et al., 2020; 2021b) focused on data collected January 2020 to August 2021, which include several heater tests and tracer tests. In this section, we mostly present BATS 2 data from the BATS 2a heating period (July to August 2022) until summer 2023. Additional BATS 1 and 2 data will be presented in subsequent reports and journal manuscripts after analyses are complete.

4.1 Data from Central Heater/Packer Boreholes

Dry UHP N_2 gas is circulated through the interval isolated behind the HP packer. The gas inflow location is at the back of the borehole (i.e., the inlet gas is directed to the area behind both heater reflectors through a 0.25-inch [6.4 mm] stainless steel tube), and the gas outflow location is on the back of the packer (Table 2). The mass flowrate of gas into the interval behind the packer is controlled by an Omega flow controller between the N_2 gas bottle regulator (set to approximately 20 psi [1,379 mbar] gauge pressure) and the packer. The flowrate of gas out of the packer-isolated interval is measured immediately downstream of the packer with an Omega MPFM, which measures mass flowrate, temperature, and pressure.

4.1.1 HP: Gas stream pressure and flowrate time series

Figure 14 shows the time series of gas stream mass flowrate (the active flow controller upstream and the passive mass flowmeter downstream of the packer for both heated and unheated arrays) averaged every 10 minutes by Campbell CR1000X dataloggers. The legends and titles in Figure 14 and subsequent figures use the naming convention of variables in the data spreadsheets used by the WIPP TCO. In these variables, heated or unheated array are indicated by a starting letter "H" or "U". The next letters relate to the borehole (in this case "HP"), and "GQUp" and "GQDown" refer to gas "G" flowrate "Q" up and downstream of the HP packer (see Figure 14).

In the time series plots, the minor tick-marks indicate weeks (each Monday). The colored dots indicate individual 10-minute average values, while lines of the same color are used to connect dots but may not be representative of the value between averages. The colored vertical stripes are common across all time-series figures and are associated with key testing events listed in

Table 3. The pink bar indicates when gas flow started (at a higher flowrate to remove excess water, “Q”), the blue bar indicates a planned WIPP power maintenance activity (all data collection and gas flow stopped, “W”). The gray bar is the BATS 2a (first) heating event, “a”, the magenta bar is the BATS 2b (second) heating event, “b”, the dark blue bar is the BATS 2c (third) heating event, “c”, and the yellow bar is the BATS 2d (fourth) heating event, “d”. The lighter gray bar is the period when the HP packer was out of the borehole, “p”. These events are labeled with letters in Figure 14 for clarity of explanation but are not labeled with letters on subsequent figures.

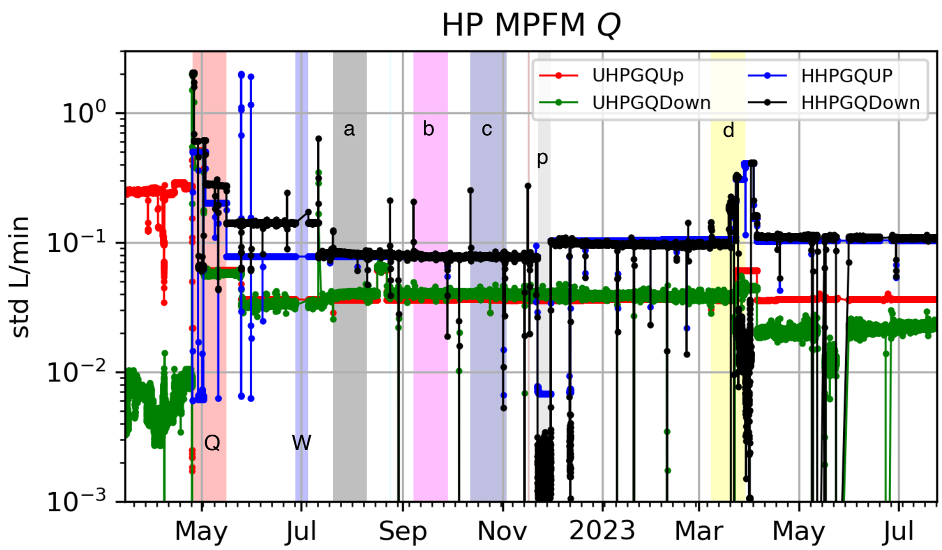

Figure 14. Gas stream mass flowrates (GQ) up- and down-stream of HP packer for heated (H) and unheated (U) arrays.

In Figure 14 the mass flowrates of gas upstream and downstream of the packers are close to the same (red vs. green for unheated and black vs. blue for heated) during most of the data record. Before the BATS 2a heating event (“a”) the downstream flowrate (black) is slightly higher than the upstream rate (blue) in the heated array, for unknown reasons. During BATS 2d the downstream gas flowrate in the heated array is erroneously low (~0.02 std L/min), likely due to water condensation on the MPFM instrument caused by the high water-production rate during the hottest heater test event. After BATS 2d the downstream flowrate is slightly lower than the upstream flowrate in the unheated array, which is not as expected (the unheated array should not be impacted by the heater test in the adjacent array).

Differences can be observed between the upstream and downstream mass flowrate (standard liters per minute, with standard temperature for Omega equipment being 21 °C) and a non-zero flowrate was reported when gas was not being flowed (before 25 April 2022). Values at or below ~0.01 std L/min likely correspond to zero flow.

Table 3. BATS 2 events associated with colored bars in timeseries figures.

Event	Color	Begin	End
Higher gas flowrate to initially dry out HP boreholes	Pink	25 Apr 2022 12:30	16 May 2022 09:00
WIPP power maintenance	Blue	27 Jun 2022 08:30	05 Jul 2022 10:15
BATS 2a heater test (90 °C)	Black	20 Jul 2022 08:29	10 Aug 2022 07:38
Aborted BATS 2b heater test (<1 hour)	Cyan	24 Aug 2022 07:53	24 Aug 2022 08:45
BATS 2b heater test (115 °C setpoint)	Magenta	07 Sep 2022 14:52	28 Sep 2022 08:02
BATS 2c heater test (130 °C setpoint)	Dark Blue	12 Oct 2022 10:01	02 Nov 2022 11:43
Aborted BATS 2d heater test (~1.5 days)	Maroon	16 Nov 2022 07:30	17 Nov 2022 17:02
HP Packer out of borehole	Gray	22 Nov 2022 09:45	30 Nov 2022 08:05
BATS 2d heater test (140 °C setpoint)	Yellow	8 Mar 2023 09:20	29 Mar 2023 09:36

Figure 15 shows the time series of air pressure in the tubing between the packer and the switching solenoids for the heated and unheated arrays measured at the MPFM and averaged every 10 minutes on the Campbell dataloggers. Figure 16 shows the time series of air temperature in the tubing upstream and downstream of the HP borehole packer (upstream of the switching solenoids), measured at the MPFM and averaged every 10 minutes on the Campbell dataloggers. Gas pressure rose above nominal levels when the gas flowrate was highest at the beginning of gas flow (late April into early May 2022) and during BATS 2d. Gas stream temperatures show effect of changes in ambient temperature, with few additional fluctuations visible.

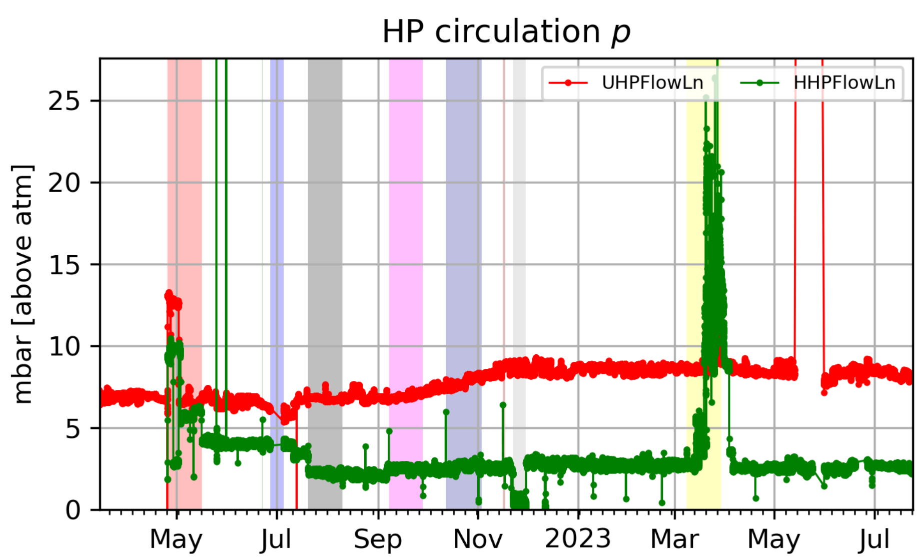

Figure 15. Gas stream pressure downstream of HP packers; "FlowLn" indicates flowline.

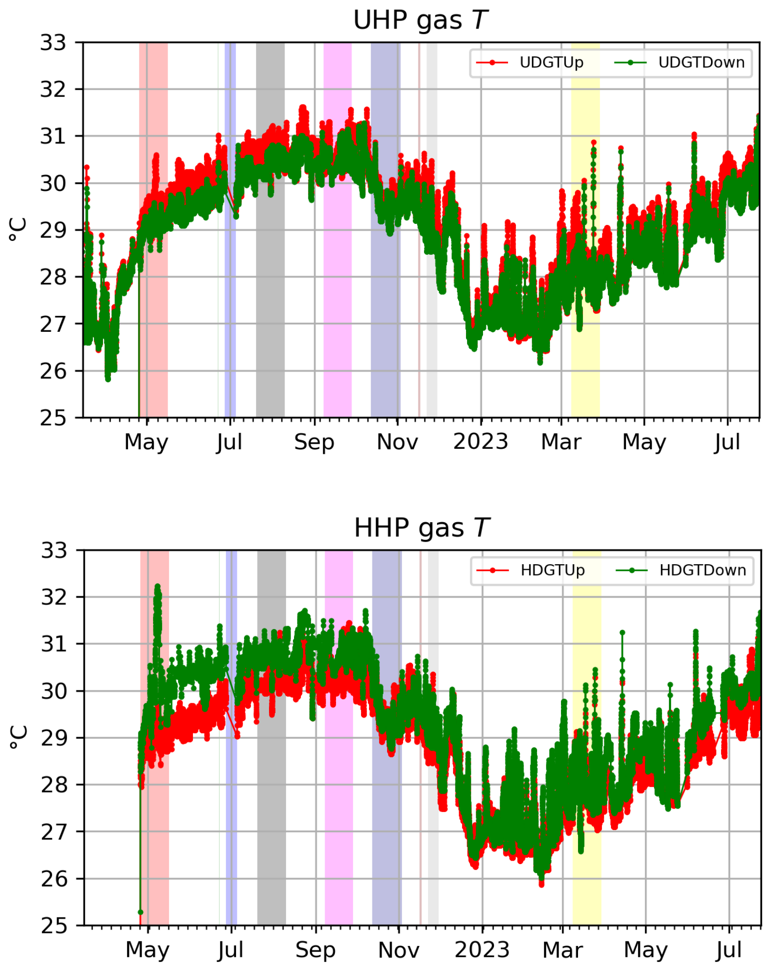

Figure 16. Gas temperature up- (red) and down-stream (green) of HP packers (unheated array top, heated array bottom).

4.1.2 HP: Water content time series

Water content is measured at multiple locations downstream of the HP packers. The gas flowing into the packer-isolated interval is assumed dry (UHP N_2). The flowrate of water recovered from behind the packer is determined using a combination of the gas mass flowrate and the concentration of water in the gas measured by two LI-COR 850 instruments (both heated and unheated) recording data at 10-minute averages (Figure 17 and Figure 18). The concentration of water is also measured by the Picarro CRDS (data at approximately 2-minute intervals), depending on the state of the three-way solenoidal switching valves (Figure 21). Finally, both branches of the gas system have Campbell EE181-L TRH probes measuring in-line air temperature and RH at 10-minute average (Figure 19) before and after pairs of heated stream and unheated stream desiccant canisters on each branch, which are weighed once or twice weekly (Figure 20) as an independent check on the calculation of the total mass of water leaving the borehole system from the high-frequency flowrate data.

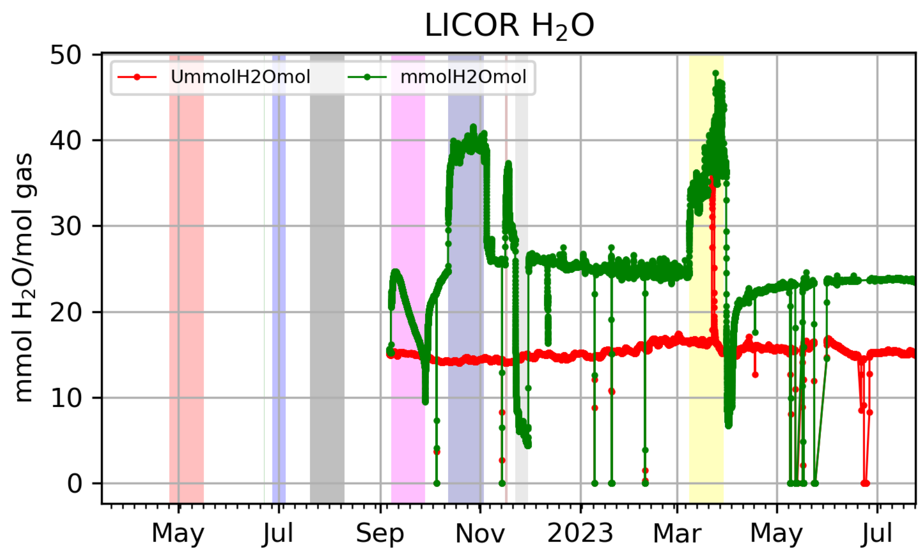

Figure 17. LI-COR water concentrations. Red is unheated array green is heated array. No initial capital letter is heated array, leading "U" is unheated.

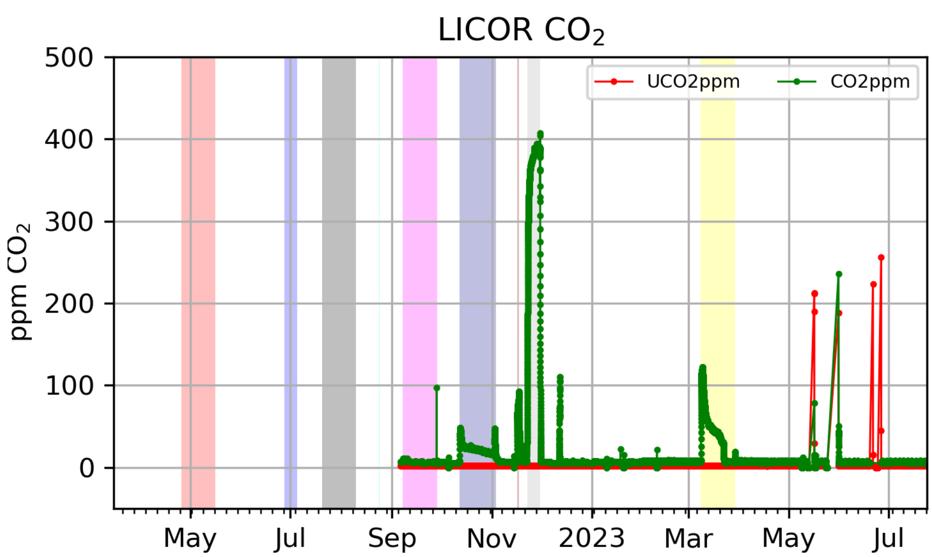

Figure 18. LI-COR CO_2 concentrations. Red is unheated array green is heated array. No initial capital letter is heated array, leading "U" is unheated.

The LI-COR data reported in the FY22 report (Kuhlman et al., 2022) were erroneous (until 6 September 2022) and are left out Figure 17 and Figure 18. The instruments were far out of calibration and required servicing by the manufacturer.

The water concentrations reported by the LI-COR (Figure 17) show increasing water concentration during the BATS 2b through BATS 2d heater tests. The LI-COR shows a spike in water concentration at the beginning of the BATS 2b heater test, with declining concentration during the remaining 3 weeks of the heater test. During BATS 2c and BATS 2d, the water concentration was consistently higher during the entire heating event.

During BATS 2d, the LI-COR on the unheated array showed a brief spike in water concentrations up to those experienced in the heated array. This spike corresponded to the replacement of a MPFM on the unheated array, opening the array to the drift air briefly. The drop in water concentration after BATS 2d is partially due to the increase in gas flowrate used to dry out the system after water had apparently condensed in the tubing, leading to erroneous MPFM pressure readings. The LI-COR reported lower water concentrations during the period the packer was out of the heated HP borehole, which is consistent with the relative humidity of the drift air.

The spikes in the LI-COR output in May and June 2023 are due to power outages in the experimental area underground at WIPP. During extended outages, the gas flow stops since the flow controllers are electrically powered, and they default to the off position (no flow) when they are not supplied power.

The LI-COR also measures CO_2 concentrations (Figure 18), which were at approximately atmospheric levels while the heated HP packer was out of the borehole (400 ppm), as expected. During BATS 2b, there was a minimal change in the CO_2 concentration, but there was a small spike and subsequent decay at the beginning of the third heating event, and a larger spike and decay at the beginning of BATS 2d. These spikes and decays likely are caused by CO_2 desorbing from the borehole wall or exsolving from brine at elevated temperatures.

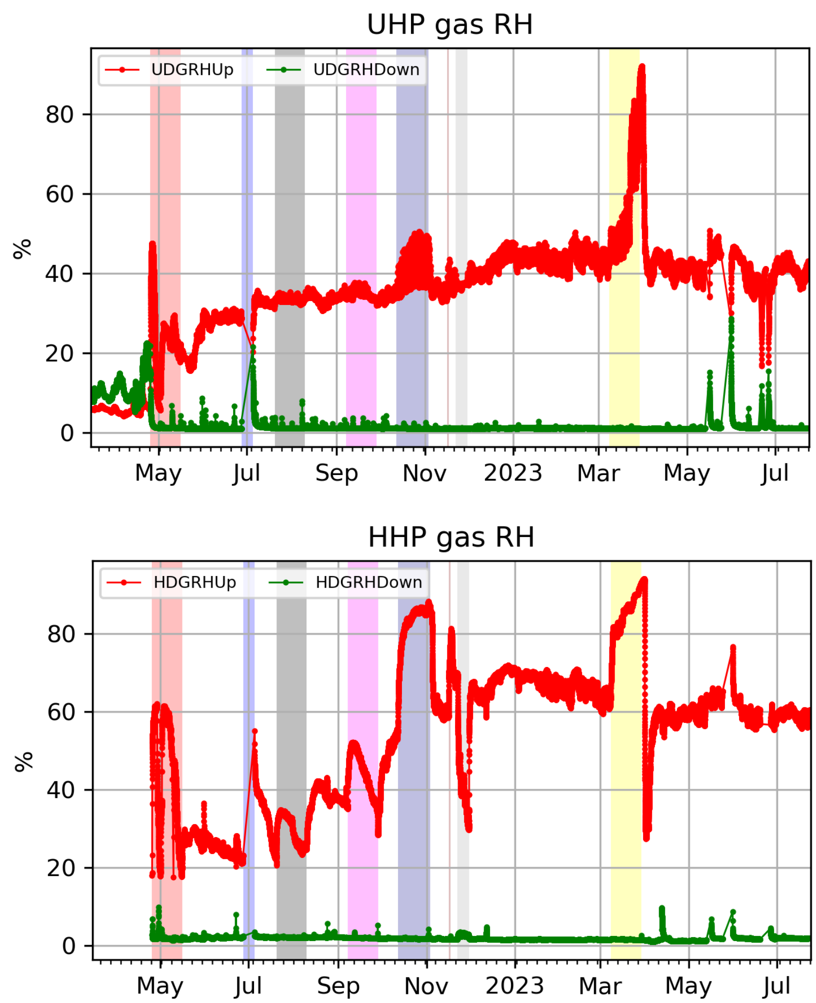

Figure 19. RH up- (red) and down-stream (green) of the unheated array (top) and heated array (bottom) desiccant.

Relative humidity (RH) time series are measured both upstream and downstream of the Drierite desiccant canisters (Figure 19). These RH sensors are downstream of the second set of solenoid valves (Figure 6).

The upstream RH in the unheated array was elevated at the end of BATS 2d (and to a lesser degree during BATS 2c), which supports the spike reported by the LI-COR. The upstream RH measurements are in the portion of the gas plumbing that switches between heated and unheated (gray lines in Figure 6), and they show more significant cross-contamination than the LI-COR, which is upstream of the switching. The downstream RH is mostly ≤ 1% (green curves), except when the gas is not flowing (before 25 April) and briefly after the power outage in June to July 2022 or May to June 2023, especially for the unheated array.

The desiccant water production data is listed in Table A-10 (heated array) and Table A-11 (unheated array) and presented graphically in Figure 20. After the early high flowrate period (pink shaded area) and before BATS 2b (magenta shaded area), the unheated array produced similar amounts of brine to the heated array. At early times the newly drilled BATS 2 heated array was producing more brine because the borehole was fresh. After BATS 2b (and even more between BATS 2c and 2d) brine production likely increased due to induced damage from heating and cooling cycles.

Both arrays show a spike in water production after the power outage in June to July 2022 and May to June 2023, when gas flow stopped. This is likely due to an accumulation of a small amount of standing water in the boreholes during the stoppage of gas flow. The unheated array showed a spike in water production during BATS 2d, which is like the data seen in the RH sensors and LI-COR during this period. This supports the hypothesis that some of the large amount of water produced during this test went into the unheated array tubing. Water concentration in the unheated array rose to levels in the heated array (~0.025 g H_2O/L air) near the end of the heating period.

Notably, there was not a significant inflow of brine observed in the heated array after the shutdown of the heater during the BATS 2 heater tests.

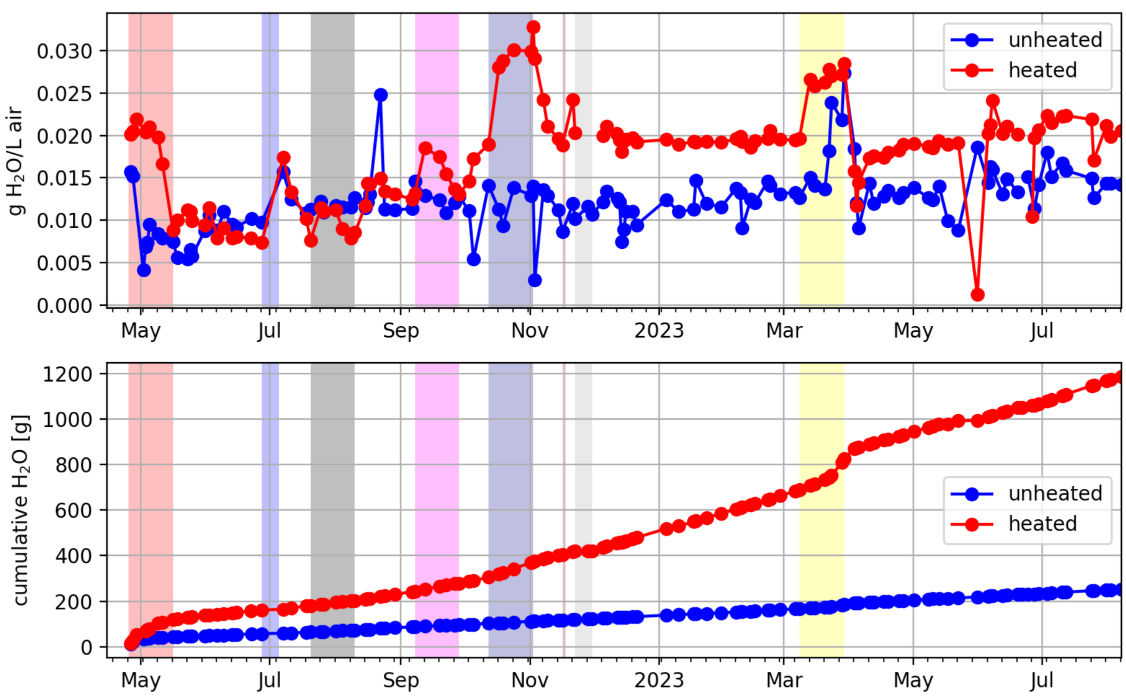

Figure 20. Desiccant water production concentration (top) and cumulative water mass (bottom) data.

4.1.3 HP: Water isotopic composition time series

The Picarro CRDS measures concentration of different isotopes of water vapor in the N_2 stream (i.e., oxygen and hydrogen isotopes) at approximately two-minute intervals. The raw Picarro time series

(Figure 21) shows similar trends as the LI-COR 850 data (Figure 17). More detailed analysis of field-collected brine samples, fluid inclusions, and field water isotope data can be found in the 2023 LANL M3 report (Guiltinan et al., 2023).

Figure 21 clearly shows the change in reported isotopes with changing Picarro CRDS instruments. At the end of BATS 2dt, the water concentration values measured by the Picarro were well above the calibration range; therefore, the gas flowrate was increased to dilute the water vapor with dry N_2. By the time this was observed, there was likely already water condensed in the tubing. In future tests, the gas flow rate will be increased before testing at high temperatures to help prevent condensation from happening.

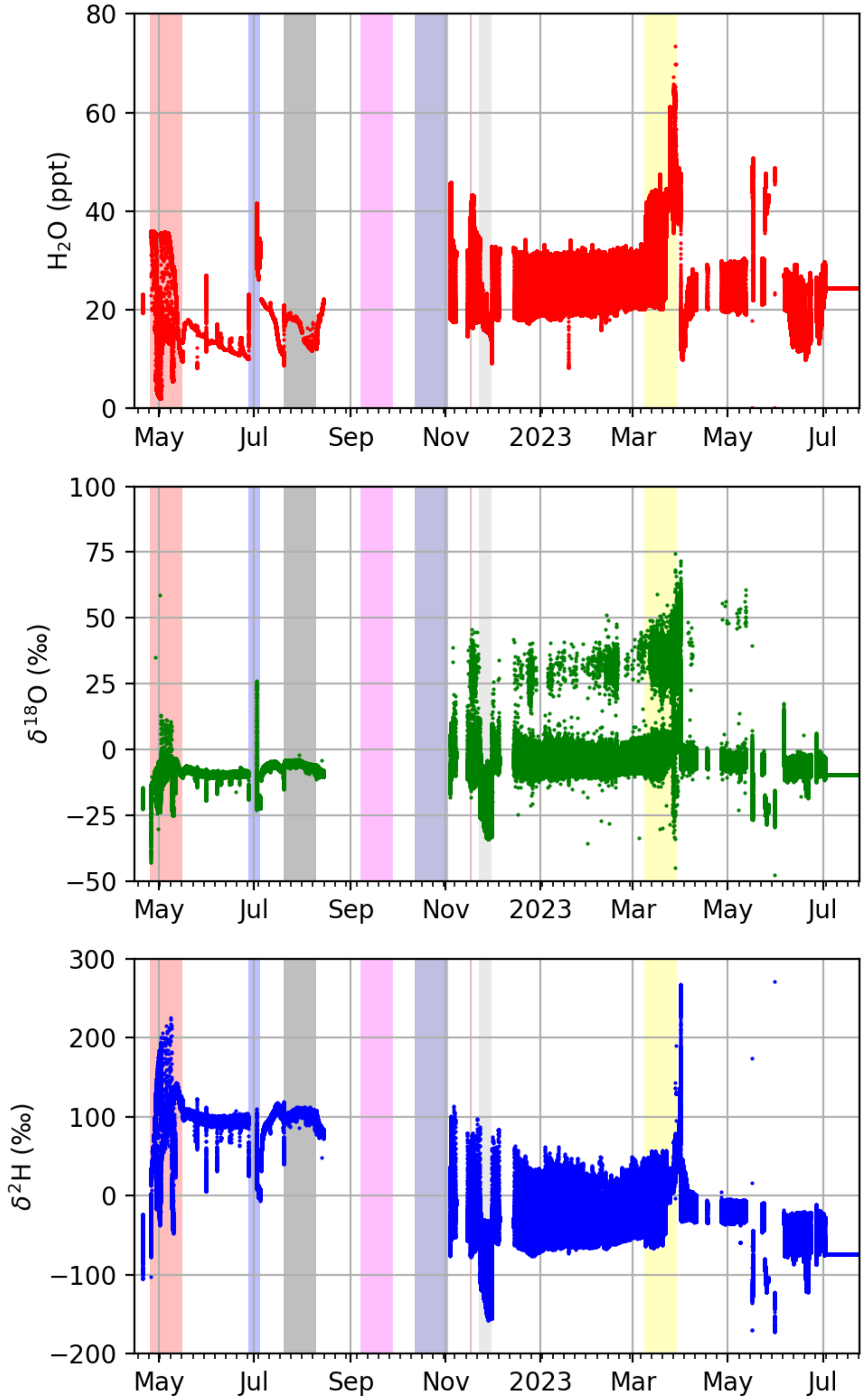

Figure 21. Picarro CRDS raw data on water concentration (top), oxygen isotopes (middle), and hydrogen isotopes (bottom). Data included from both heated and unheated arrays (data stream switches 2× per day). Data before September from original Picarro instrument, data after November 2022 from new Picarro instrument.

Using laboratory measurements of water isotopes in fluid inclusions taken from BATS core (discussed in detail in Guiltinan et al., 2023), some estimates were made of the fraction of the brine flowing into the BATS 2 heated HP borehole, based upon the isotopic signature (Figure 22). Less than 30% of the total brine could be attributed to fluid inclusions, using the mixing model illustrated in Figure 22a. Some evaporation models were used to predict that amount of evaporation needed to explain the observed isotopic data from BATS 2 (Figure 22b), showing the data could be explained by physically realistic evaporation models.

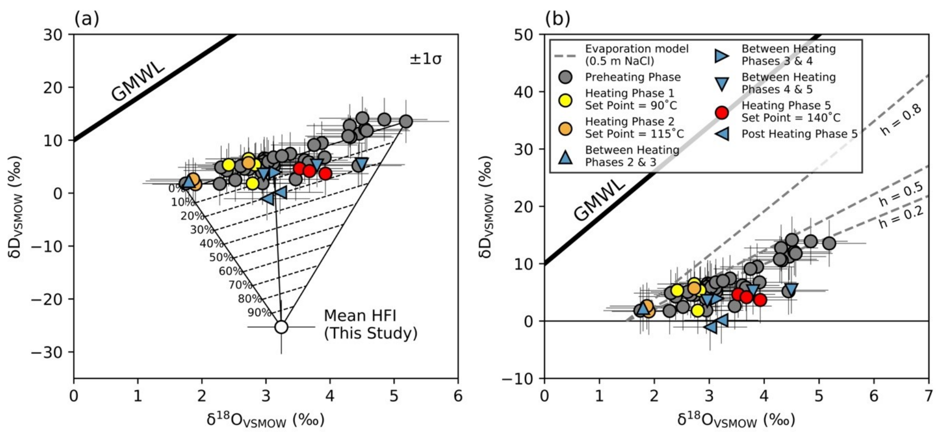

Figure 22. Isotopic variation of water composition in BATS 2 brines related to (a) fraction of fluid inclusion contribution and (b) evaporation models (Guiltinan et al., 2023). In this figure, “Phase 4” corresponds to the aborted BATS 4d heating event (Nov 2022), and “Phase 5” corresponds to full BATS 4d heating event (Mar 2023).

4.1.4 HP: Gas composition time series

The gas stream from the Picarro CRDS flows into an SRS QMS-200 Gas Analyzer, which analyzed the gas stream for compositional changes with time. The gas analyzer is operating in “P vs. T” mode, which monitors the partial pressure of several gases, using an electron multiplier. Figure 23 shows the relative reported ion current for three key gases, normalized by the ion current reported for N_2 (to adjust for differences in pressure of the input gas stream).

The gas analyzer was sent back to the manufacturer for repairs from December 2022 through January 2023. The dynamic range of the instrument was expanded significantly after replacing the electron multiplier and the ionizer. Significant breakthrough of argon was observed at the end of BATS 2d (using the repaired gas analyzer, Figure 24). No significant breakthrough of argon was observed associated with the other heating events, but the dynamic range of the SRS gas analyzer was significantly lower. No significant release of helium associated with BATS 2d was seen (none was seen in the other heating events, but similarly the instrument did not have the expected dynamic range, either during the first three heating events – BATS 2a-c). Most of the observed spikes and decays in CO_2 data are likely representative of CO_2 sorbing to metal inside the instrument vacuum chamber, rather than CO_2 being released from the salt (i.e., compare to LI-COR CO_2 values, Figure 18). The step increase in CO_2 concentration reported at the beginning of BATS 2d may correspond to the step observed using the LI-COR, while other spikes and decays can be related to restarts of the instrument and its turbomolecular pump after a power outage.

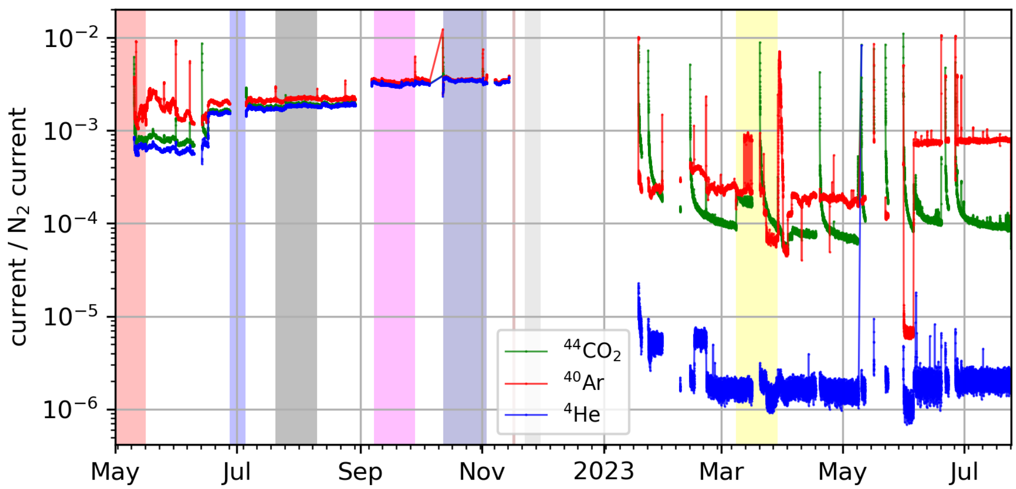

Figure 23. SRS Gas Analyzer observations from HP gas stream. Plot clearly shows difference in data before (2022) and after (2023) repairs. Only heated array data shown.

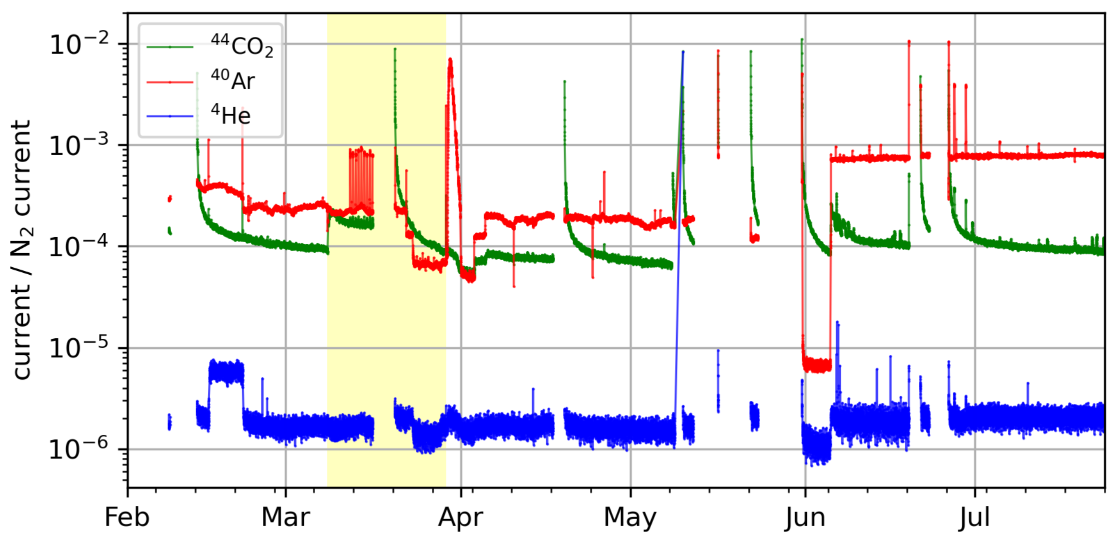

Figure 24. SRS gas analyzer data since February 2023 (after repairs). Heated array data shown.

4.1.5 HP: Borehole closure gauge time series

A linear variable differential transformer (LVDT) was used to measure the diameter of both heated and unheated HP boreholes through time. Figure 25 shows the change in borehole diameter since the beginning of BATS 2. The unheated array shows steady borehole closure (green), while borehole closure gauge in the heated array (red) shows small step changes and change associated with heating and cooling during the BATS 2a heating event. The LVDT on the unheated array stopped working in December 2022.

The jumps in the heated LVDT data may be due to the PEEK bushing sticking against the 1-inch [2.54 cm] steel pipe, when the pipe heats up and expands. This sticking effect was also observed in BATS 1. Some effort was made during BATS 2 construction to lubricate the bushing with high-temperature grease and increase the clearance between these elements to reduce sticking, but this effort was apparently not successful.

When the packer was removed from the heated HP borehole (light gray bar in November 2022), a 0.5 mm reduction in borehole diameter occurred, possibly representing borehole closure occurring once the inflated packer was removed. The packer (inflated to 80 psi gauge, only 45 cm from the borehole closure instrument; see Table 2) likely slows down the closure of the borehole compared to an open borehole.

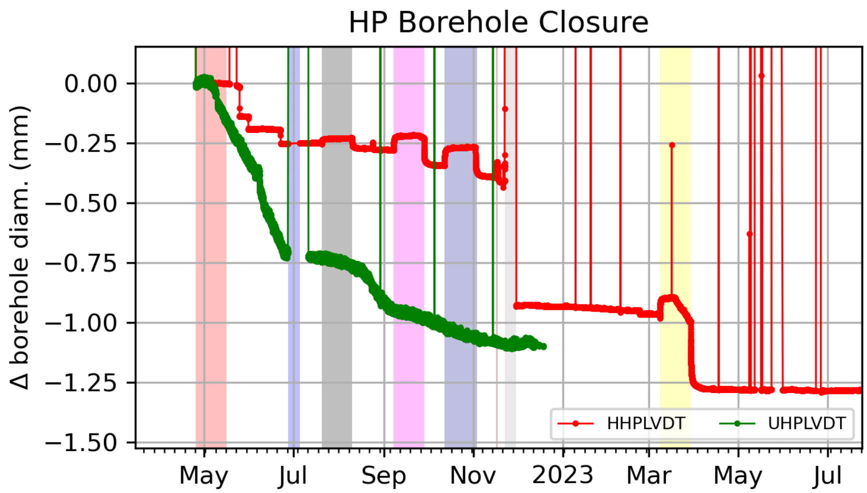

Figure 25. Change in diameter of HP boreholes measured by LVDT.

4.1.6 HP: Heater power and temperature time series

The heater controller reports applied current and voltage, apparent heater resistance, and power for the heater, which are critical to characterizing the applied thermal boundary condition (Figure 26). The controller also reports the temperature at thermocouples inside the borehole used to control and provide a high temperature safety limit for the heater. In the upper-left panel 4TC_C_SP_Max (green) gives the temperature observed on the setpoint thermocouple, while 4TC_C_SP (red) gives the setpoint; they only differ when the borehole is hotter than the heater (i.e., during cooling). These data are used in thermal-hydrological-mechanical models to drive the thermal response of the entire system. Only the heated array HP borehole is collecting this time series.

The power measured by the heater controller can be confirmed by using either $P = VI$ (power from potential and current) or $P = I^2R$ (power from current and resistance). Both checks give similar values to those reported directly by the controller, providing some confidence in the internal consistency of the measurements. The heater element resistance increases slightly (33.5 to 34.75 ohm) with each heater test episode, which is a sign the heating element is healthy but aging. Most of the heater controller parameters (aside from thermocouples) are only reported or make sense when the heater is on.

The BATS 1a heater test, which had a setpoint of 120 ºC, had an average power of approximately 520 W (after applying a correction to the reported power). Table 4 lists the setpoint and controller limit temperatures, steady-state applied power, and temperature in the nearest observation to the heater that is not in the HP borehole (19.3 cm from the center of the heater or 13.2 cm from the HP borehole wall, Table A-4), for each of the four tests comprising BATS 2 so far.

BATS 2a only applied approximately 200 W to the salt, while BATS 2b applied approximately double that. BATS 2c was similar power levels BATS 1a, at approximately 500 W. BATS 2d applied approximately 700 W to the salt. Some of the data in Table 4 are plotted in Figure 27. This plot shows BATS 2d appears to be slightly different from the previous three heating events (between the setpoint thermocouple and the applied power or limit thermocouple temperatures).

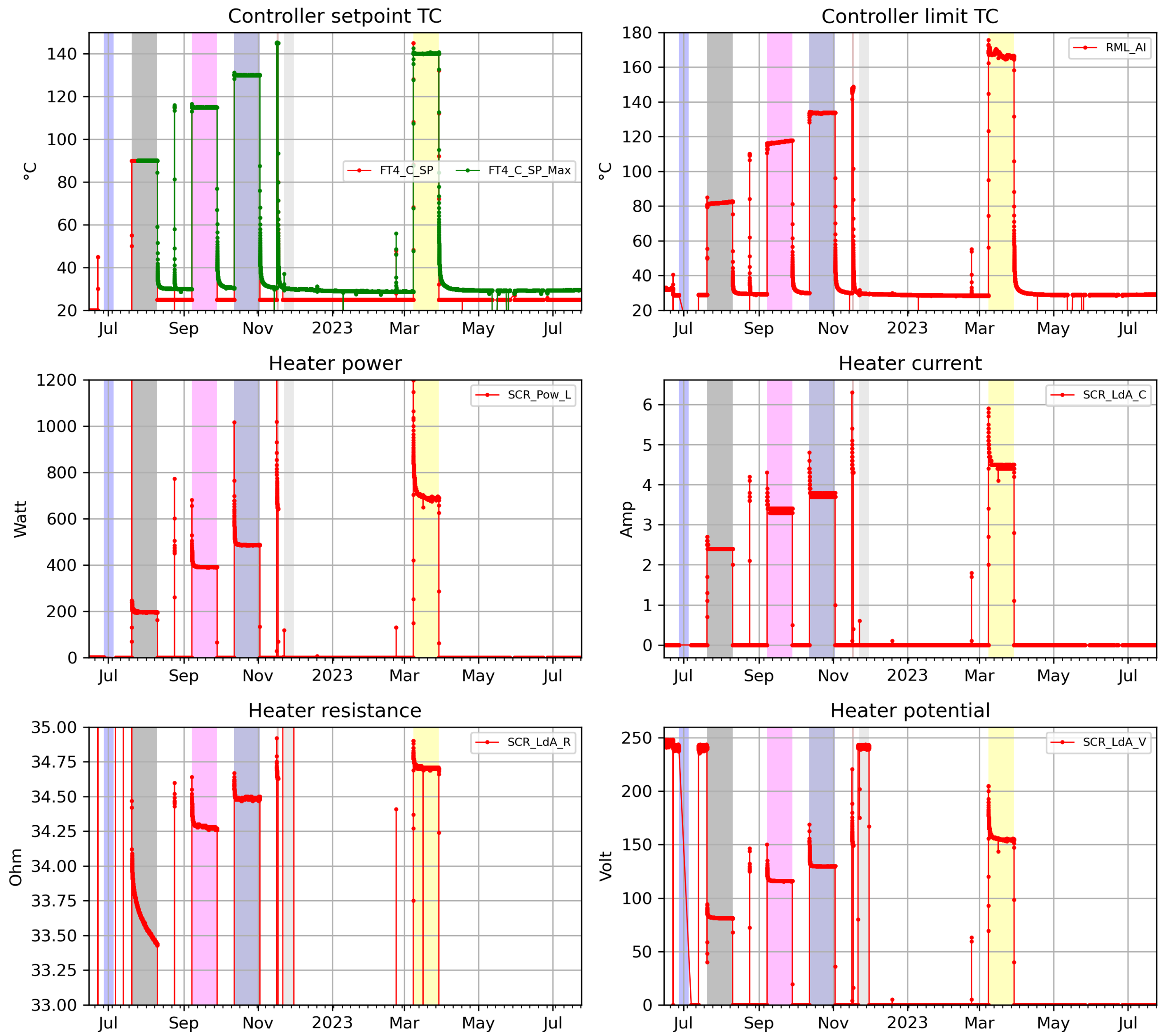

Figure 26. Heater controller parameters.

This difference may be from removing the heated HP packer from the borehole between BATS 2c and BATS 2d, which may have changed how the thermocouple contacts the borehole wall. During the removal and replacement of the heater in November 2022, the controller setpoint and limit thermocouples (see them in Figure 7) may have cause a change in their contact with the salt, or whether the heater lamp shines on them directly.

Table 4. Summary of BATS 2 heating events.

Heating Event	Beginning	Ending	Setpoint TC temperature [ºC]	Applied power* [W]	Limit TC temperature* [ºC]	HF1TC2 temperature* [ºC]
A	20 Jul 2022 08:29	10 Aug 2022 07:38	90	195	82.5	41
B	07 Sep 2022 14:52	28 Sep 2022 08:02	115	391	117.8	56
C	12 Oct 2022 10:01	02 Nov 2022 11:43	130	487	133.8	63
D-aborted	16 Nov 2022 07:30	17 Nov 2022 17:02	145	650	148.9	69
D	8 Mar 2023 09:20	29 Mar 2023 09:36	140	690	166.3	79

*At end of each heating event (aborted D heating event was 1.5 days, others were ~3 weeks)

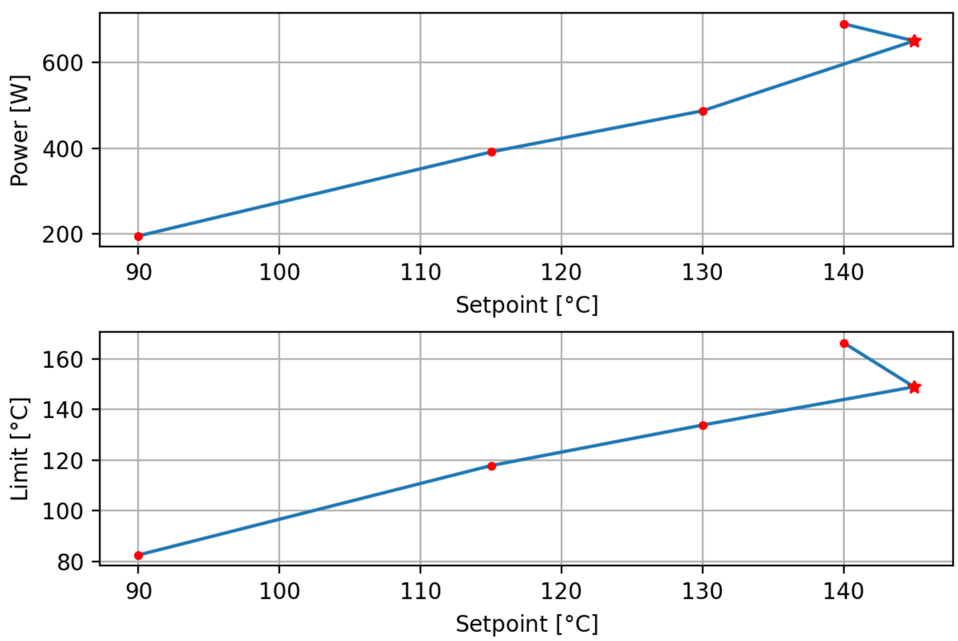

Figure 27. Comparison of setpoint to applied power and limit thermocouple reading. Day-long aborted BATS 2d test is indicated with a star.

4.2 D: Continuous Pressure Testing

The interval behind the inflatable IPI packer in the D borehole was pressurized to 20 psi [1.4 bar] above atmospheric pressure and closed in (i.e., disconnected from the inflation tank). The packer inflation pressure (roughly 80 psi [5.5 bar] above atmospheric) and the pressure of gas in the interval behind the packer are both monitored. Figure 28 shows the gas pressure behind the packer in the D borehole through time.

Initially the interval was pressurized with UHP N_2 (May and July 2022). The drop in pressure just before BATS 2a heater test (20 July) is when N_2-filled interval was depressurized and re-pressurized with UHP Ar to the same pressure. Argon was used to get tracer travel information from the gas permeability tests, when the argon was observed breaking through by the gas analyzer in the HP borehole.

The slow decrease in pressure behind the D borehole between heating events (Figure 28) can be used to constrain the interval relative gas permeability, which appears to increase (i.e., steeper declines) after each successive test. Interpretation of these data is more complex than interpreting single-phase pressure decline since this is movement of gas through a variably brine-saturated fracture system. Gas pressure decline is sensitive to the gas relative permeability of the interval. The relative permeability might change due to fractures opening and closing (i.e., changes in absolute permeability) or due to changes in brine content in fractures (i.e., changes in relative permeability).

The rise in pressure during the BATS 2 a, b, and c heater tests (Figure 28; dark gray, magenta, and dark blue stripes) can be explained by the pressure rise expected due to heating a closed container (i.e., permeability is low enough to prevent significant gas leakage).

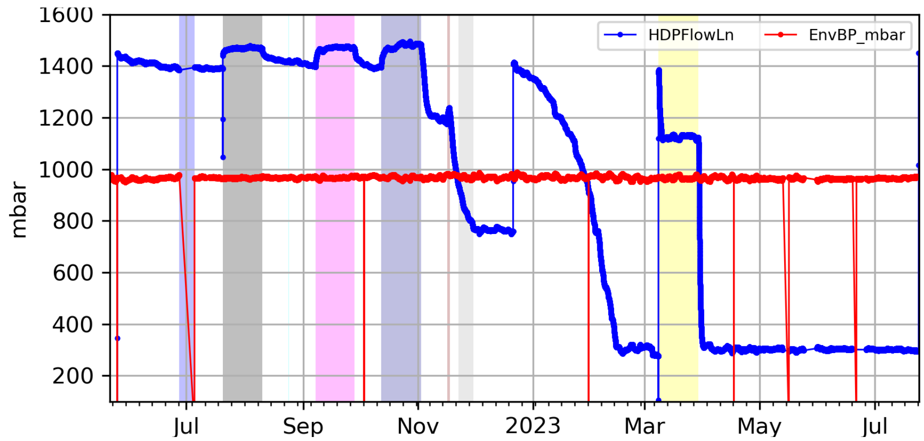

Figure 28. Interval gas pressure (above atmospheric) for heated D borehole.

Adding the atmospheric pressure measured in the drift (red line in Figure 28) to the gauge gas pressure measurement behind the packer in the heated D borehole (blue line in Figure 28) produces the absolute pressure (Figure 29), where most of the high-frequency daily fluctuations are now canceled out. Fluctuations of the same magnitude and opposite direction occur in the atmospheric pressure data and the heated D borehole pressure data.

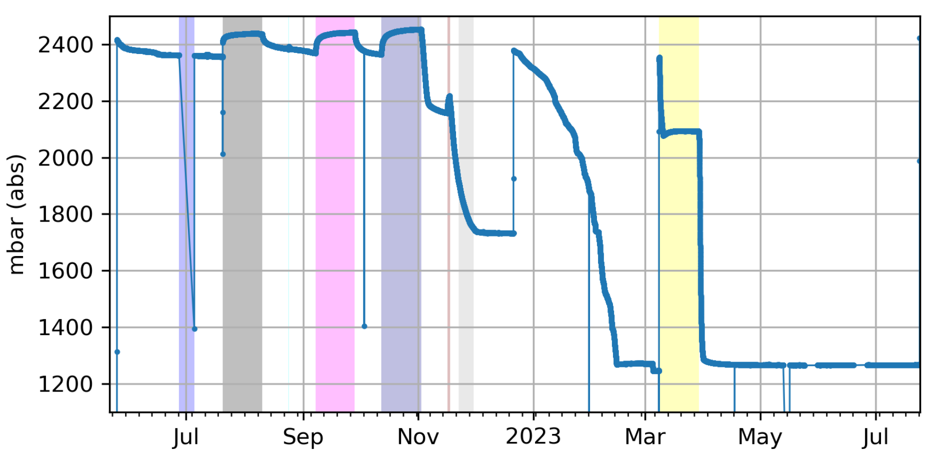

Figure 29. Interval gas pressure (absolute) for heated D borehole.

The pressure response in the heated D borehole between December 2022 and February 2023 had an atypical "concave down" curvature. A pressure decay through a non-deforming, single-phase porous medium should be a concave-up exponential. LANL has recently investigated this response using two-phase flow models (Figure 30) to try to re-create this atypical response. This figure illustrates the different curvature the data have (blue line), compared to a range of simulations with different material properties and starting liquid saturations (many orange curves). This difference indicates the effective gas permeability of the medium must be changing with time, driven by some process other than gas pressure in the D borehole. Either the solid part of the medium is changing (e.g., fractures opening or closing) and/or brine that was initially blocking gas flow is moving out of the way as flow continues. Additional modeling of this response with discrete fracture networks is also underway (Guiltinan et al., 2023).

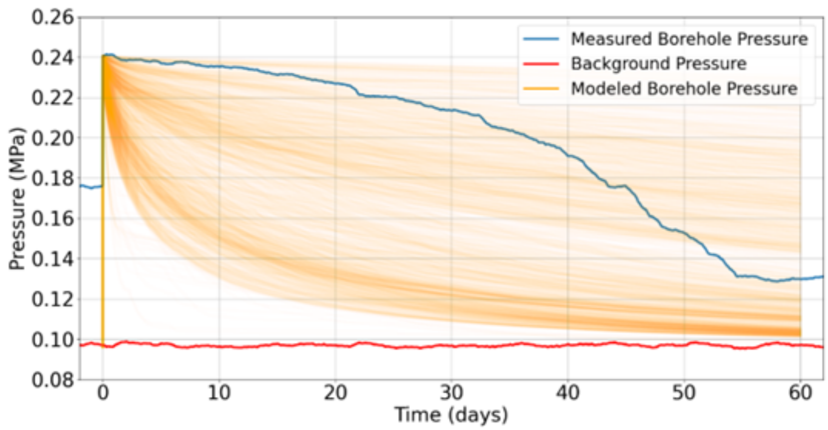

Figure 30. LANL modeling study to investigate "concave down" pressure response in the heated D borehole December 2022 through February 2023 (Guiltinan et al., 2023).

Argon was used to pressurize the heated D borehole since the start of the BATS 2a heater test, but no significant Ar was observed breaking through to the heated HP borehole until the BATS 2d heating event in 2023 (but also the dynamic range of the SRS gas analyzer has improved in 2023). Zooming in on BATS 2d, Figure 31 shows the D borehole pressure and the Ar response in the heated HP borehole. The yellow shaded interval is the period the heater was at the 140 ºC setpoint. An hour before turning on the heater, the D packer interval was depressurized, then repressurized to 20 psi gauge [1,379 mbar] pressure (~2,350 mbar absolute pressure) with UHP Ar. The pressure in the heated D interval declined initially as the salt heated up. After approximately three days, the pressure leveled off in the heated D interval, and it held steady until the end of the heating period (with a very slight rise likely due to thermal expansion of the gas as the now-sealed borehole continued to heat).

Immediately after turning off the heater, the gas pressure in the heated D interval fell to a similar pressure it was before the BATS 2d heater test (~1.2 bar absolute pressure), and the normalized Ar-40 signal on the SRS gas analyzer in the heated HP borehole rose 100× above background (despite the 5× increase in N_2 flowrate in the heated HP borehole to remove water, which further dilutes the Ar signal), clearly showing Ar was flowing from the D borehole to the HP borehole in the heated array in response to shutting off the heater. This change may reflect a change in aperture of fractures and effective permeability due to thermal expansion and contraction of the salt.

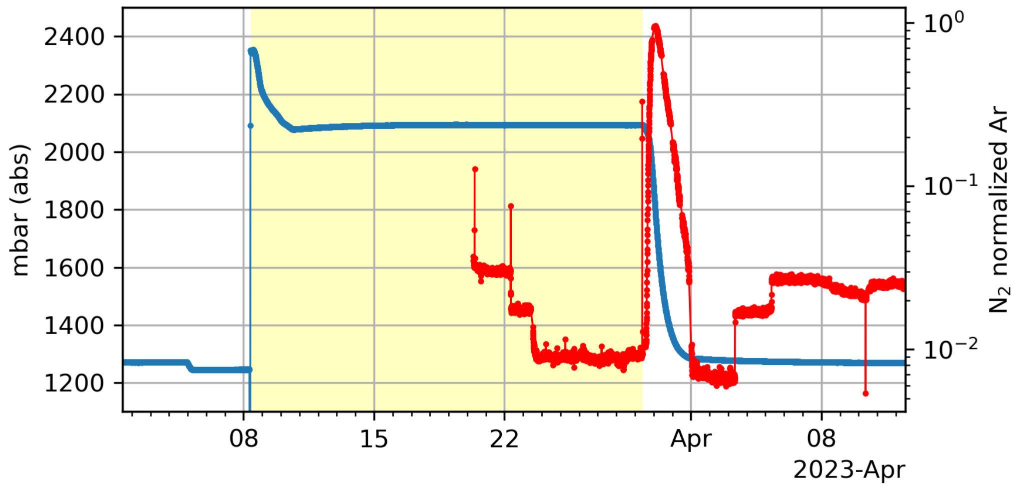

Figure 31. Absolute pressure in heated D borehole (blue) shown with normalized Ar response in HP borehole measured with SRS gas analyzer (red).

4.3 AE Data from BATS 2 AE Boreholes

This section discusses cumulative AE data recorded in the heated BATS 2 array from July 2022 to June 2023. Orange intervals in the figures indicate the extent of heater tests. AE activity increases at the onset of heating, and further increases after heated intervals when the borehole intervals started cooling. Increase in AE activity outside of heated or cooling intervals are believed to be associated with mine activity, like drilling boreholes, vehicles using the N940 drift, and blasting the new utility shaft. Broader responses in energy and frequency are observed during times of increased AE activity. The breaks in the data collection (due to power outages or issues with data due to noisy sensors producing extremely large data files) can also be seen in Figure 32.

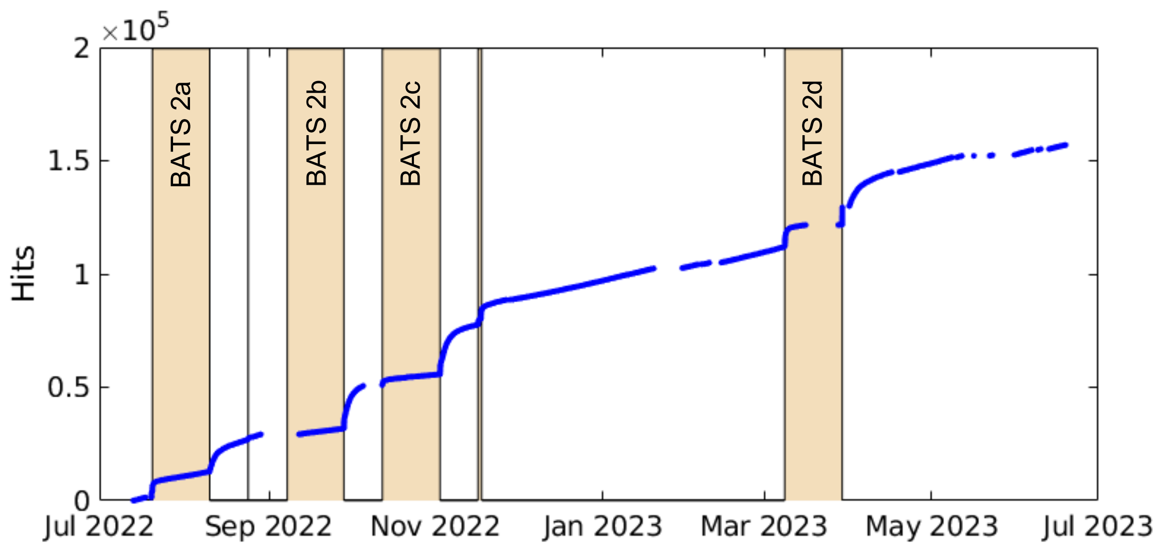

Figure 32. Cumulative AE hits over time for BATS 2 heating events. Heated periods marked in orange and labeled. Breaks indicate missing data.

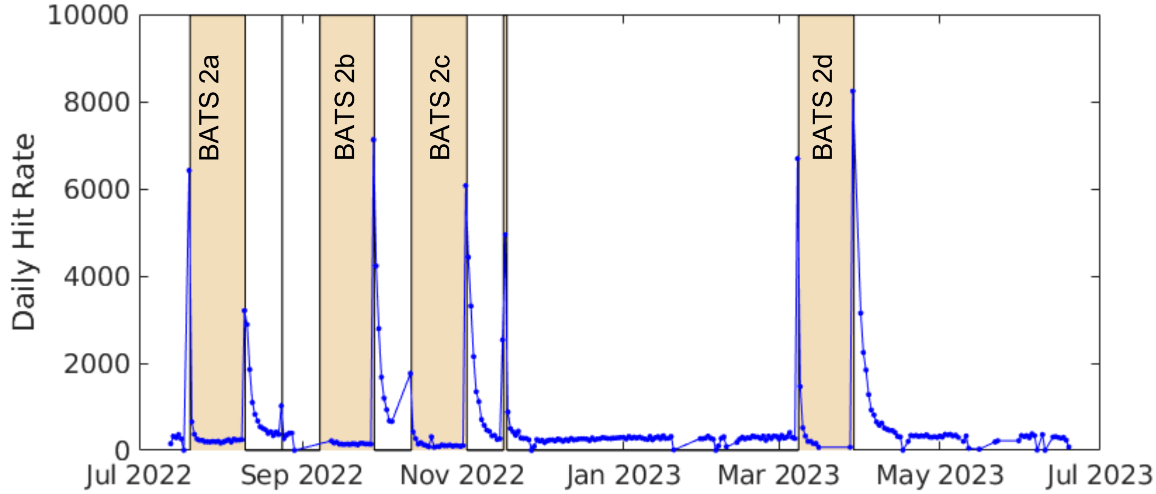

Figure 33. Daily AE hit rate for BATS 2 heating events. Heated periods marked in orange and labeled. Gaps in data more apparent in other AE figures.

Most of the days with large hit counts are seen to line up with the beginning or ending of heating periods (Figure 33). There is an elevated background level since approximately November 2022. The reason for this elevated background level is not fully understood, but it appears to be some type of interference or noise on the sensors.

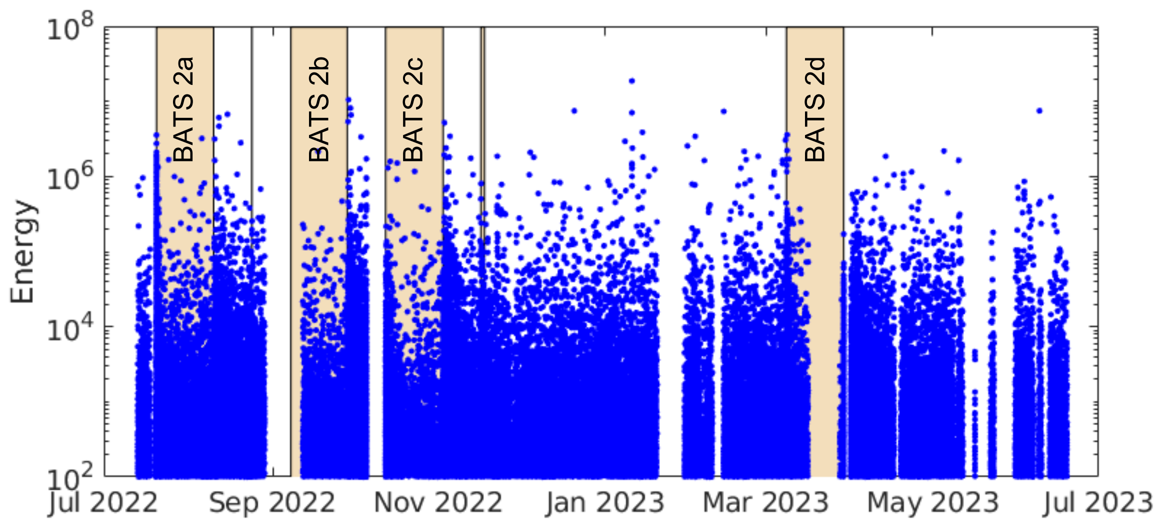

Figure 34. AE energy (µvolt-sec/count) for BATS 2 heating events. Heated periods marked in orange and labeled. Gaps indicate missing data.

The plot of energy through time (Figure 34) shows most periods with higher energy (10^4 to 10^5 µvolt-sec/count) correspond to beginning or ending of heating periods. Low-energy hits were screened out of the dataset, as they corresponded to noise and were unrelated to events related to heating and cooling.

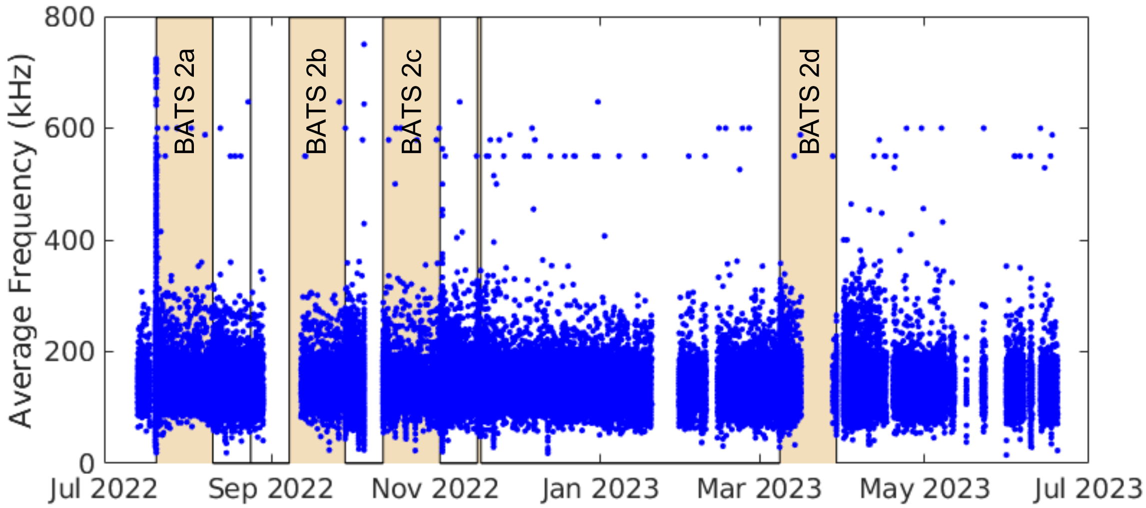

Figure 35. AE frequency for BATS 2 heating events. Heated periods marked in orange and labeled. Gaps indicate missing data.

Figure 35 shows most events have frequencies in the range 100 to 200 kHz, with excursions up to 300 kHz during events associated with the beginning of heating and cooling. The very high frequencies >400 kHz may be noise.

Located events from the BATS 2a heater test show that activity is concentrated in the array, and most located events are within the receiver borehole array. Timing of events are associated with the heater intervals. There is an initial surge of activity when a heating event starts, which falls to a lower level for the duration of the heater test. Events surge again after the heater is turned off and the borehole intervals begins to cool.

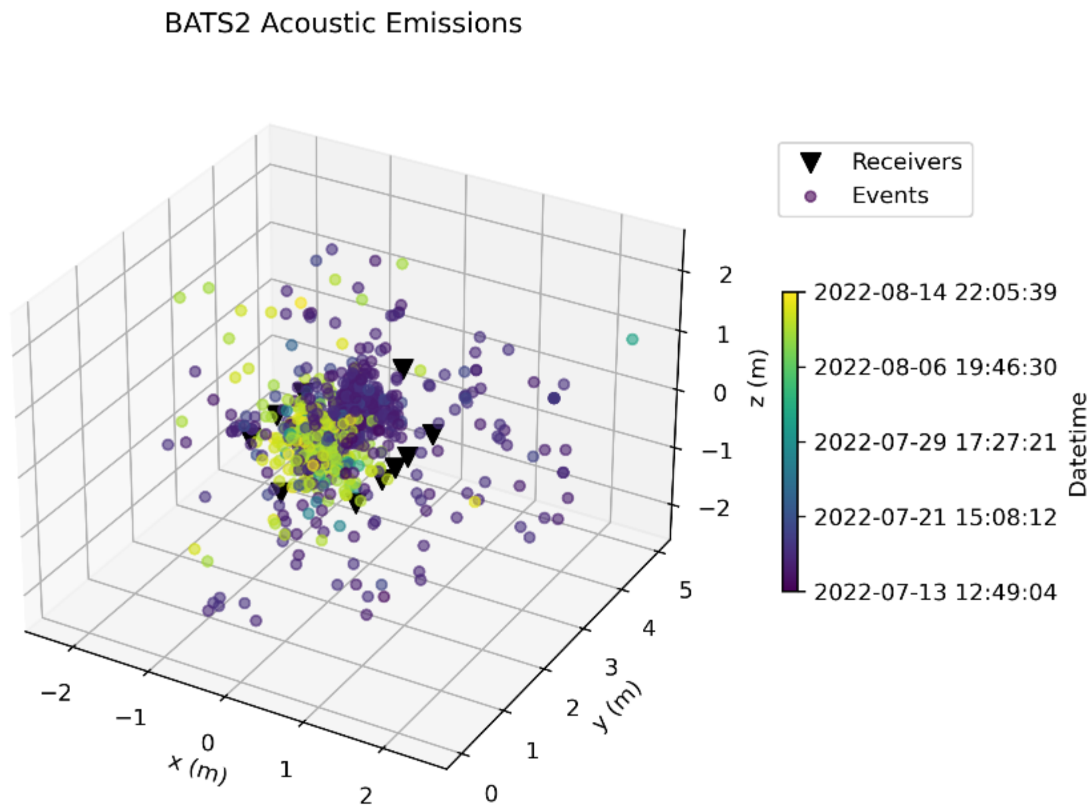

Figure 36. Located events from the BATS 2a heating event. Depth into the drift is increasing on the y axis. Black triangles are the locations of the receivers, and circles are the locations of identified events. Color scale on the events show the occurrence date.

4.4 T: Temperature Time Series

Thirty-six sealed Type-K thermocouples are grouted into the two T boreholes, and more thermocouples are co-located with other observations in other boreholes (e.g., AE, F, and SL). RTDs are used in place of thermocouples in the ERT boreholes (E1 through E4). Temperature measurement locations are tabulated in Table A-3.

The unheated array (Figure 37) now shows regional fluctuations of temperature in the salt, as ERT testing is no longer being conducted in the unheated array. Most of the thermocouples in the ERT boreholes in the unheated array have failed since they were installed in 2019. The BATS 2 heated array is further away from the BATS 1 unheated array than the BATS 1 heated array was (Figure 2), so the effects of the BATS 2 heating events are not observed in the unheated array, as they were in BATS 1. The unheated T1 borehole shows the variation of ambient temperature with depth varies with seasons (an unexplained shift appears to impact the deepest two thermocouples in the UT2 borehole). In the summer, the drift air is warmer than the salt and in the winter the salt is warmer than the drift air. A maximum of 1 ºC difference is observed between TC1 and TC16 in the summer, and approximately 0.75 ºC difference is observed between these thermocouples in the winter. The annual variation in the shallowest thermocouple is approximately 2 ºC, and the annual variation in the deepest thermocouple is only 0.7 ºC.

An average "deep" salt temperature of 27.88 ºC [82.18 ºF] is inferred from the average UT1TC16 temperature over a twelve-month period. This is consistent with what has been observed previously at WIPP, but it is clearer in the unheated array data now than it was previously (fewer man-made impacts).

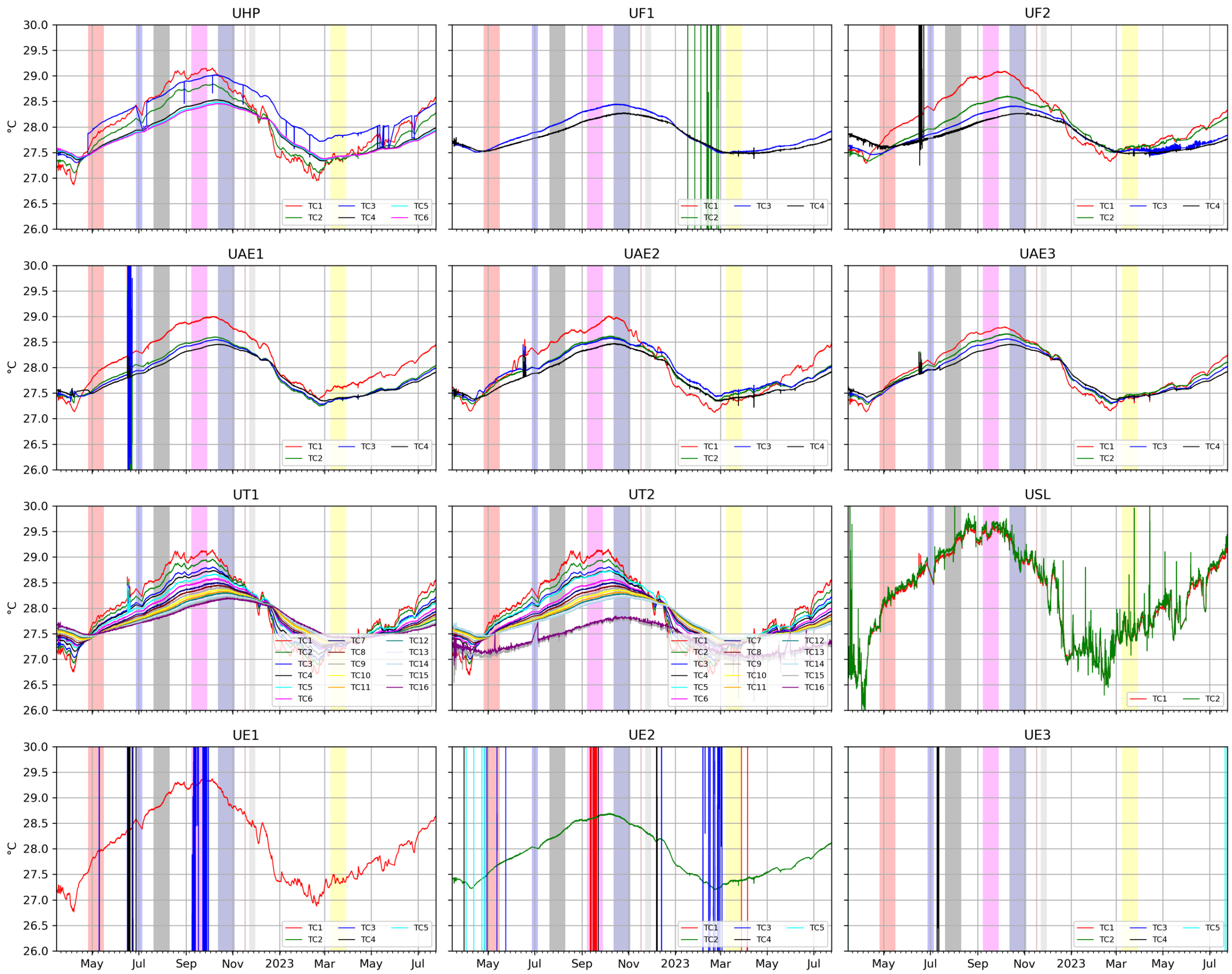

Figure 37. Thermocouple data from unheated array.

Figure 38 shows temperature data observed in the BATS 2 heated array. Each panel in the plot is a different borehole; curves within each panel show data from different thermocouples. In each borehole thermocouple “TC1” is closest to the drift, “TC2” is deeper in the borehole, etc. Thermocouple and RTD data collected during ERT surveys are not deleted from the BATS 2 dataset (some noise is still observed in the data during ERT surveys each night), as was done in BATS 1.

RTD5 in the BATS 2 heated array AE3 borehole is quite noisy since BATS 2a began, so it was plotted without lines connecting the dots.

The temperature rise observed in TC2 of the heated F1 borehole is the largest temperature rise observed outside the heated HP borehole (approximately 53 ºC rise). This thermocouple is 19.3 cm from the center of the HP heater (13.2 cm from the HP borehole wall).

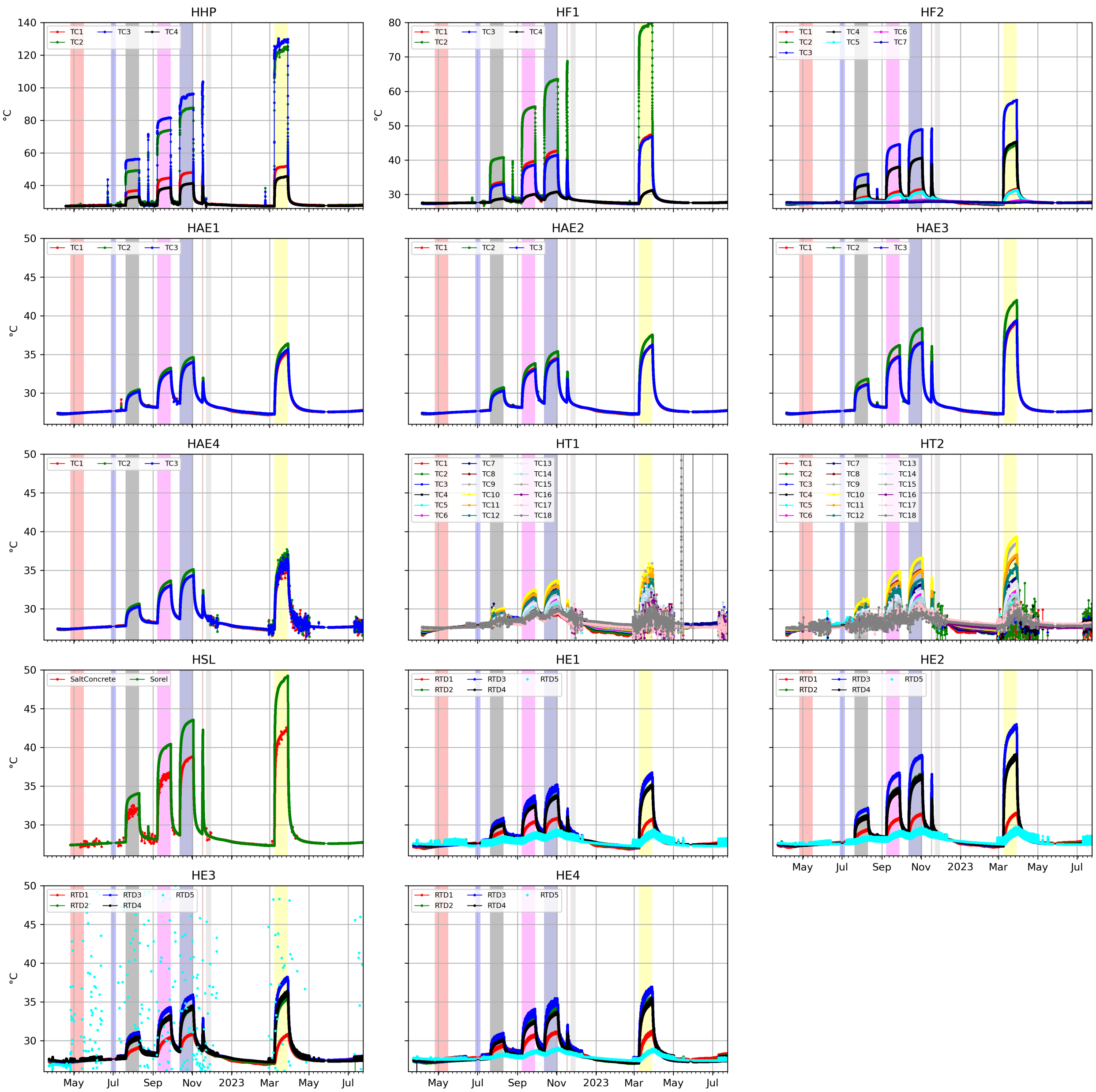

Figure 38. Background temperature data from heated array. Each subplot shows the thermocouples or RTDs from a single borehole.

4.5 E: Electrical Resistivity Tomography (ERT) Data

Rutqvist et al. (2023) provide a detailed summary of data collection, inversion, and preliminary analysis of BATS 2 ERT data. Primarily, improvements were made to the model used to invert the data, and there are more electrodes across more boreholes in BATS 2 as compared to BATS 1.

ERT surveys were nominally conducted nightly, but they were not conducted during power outages or periods when there were equipment issues (see surveys on days with asterisks in Figure 39). Only presenting the days that have ERT surveys, the raw resistance and the percent change in resistance are shown against time in Figure 40.

In the raw resistance data (Figure 40c), the intra-borehole measurements (<100 ohm) are clearly delineated from the inter-borehole measurements (>100 ohm).

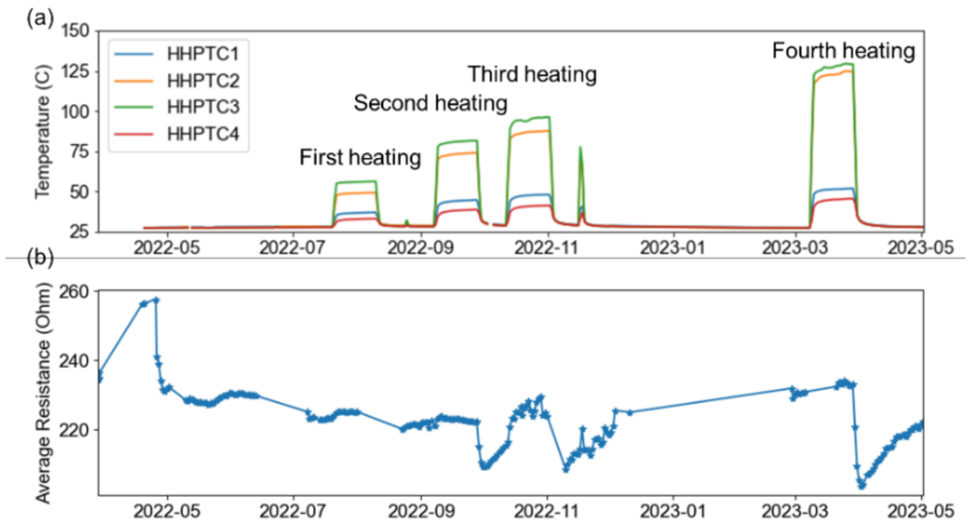

Figure 39. Time-series of temperatures and average resistance during BATS 2. (a) Temperatures in the HP borehole. (b) Average measured resistance, with ERT survey dates indicated using asterisks (Rutqvist et al., 2023).

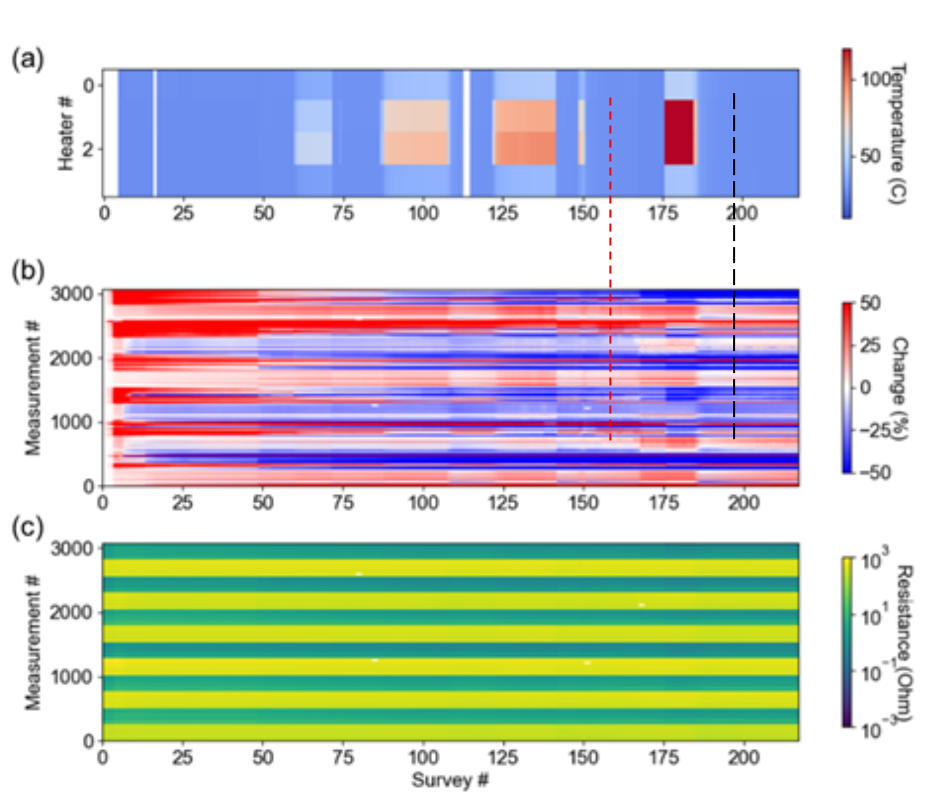

Figure 40. Resistance and temperature across all ERT surveys. (a) Temperature, (b) change in resistivity, and (c) raw resistance (Rutqvist et al., 2023).

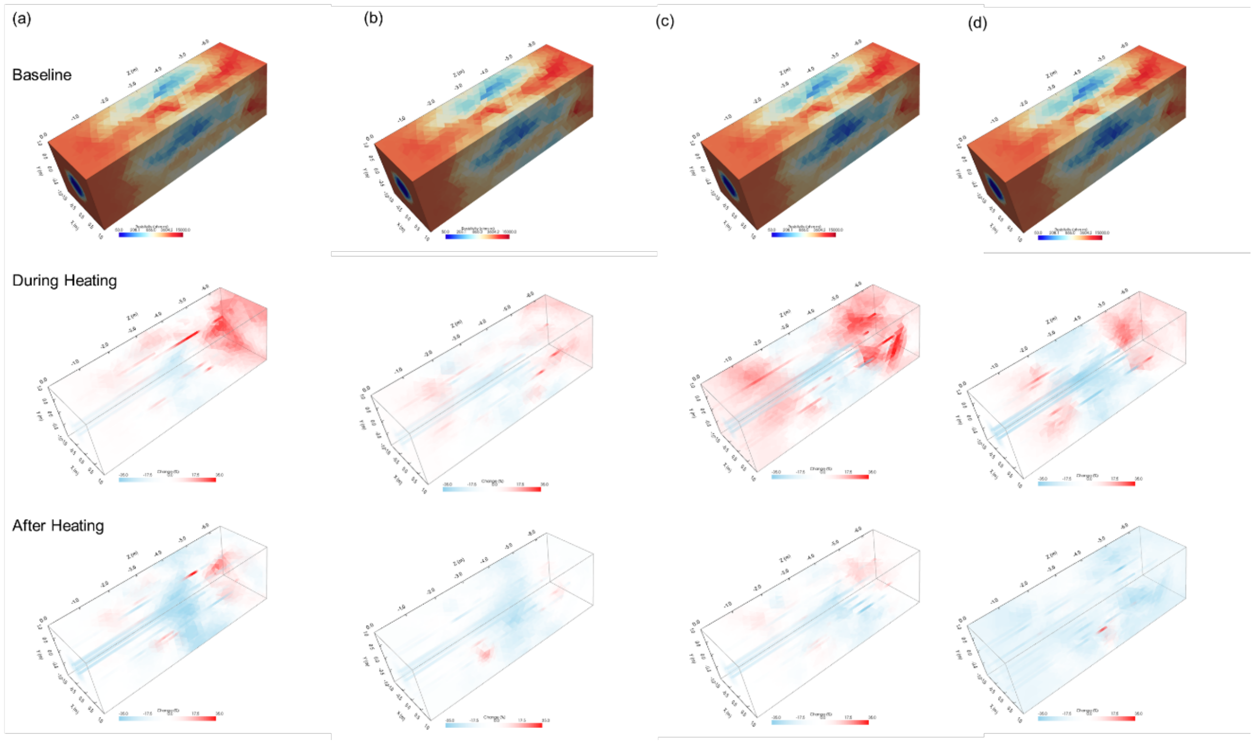

Figure 41. Baseline resistivity (top) and resistivity changes during or after heating phases. (a) BATS 2a, (b) BATS 2b, (c) BATS 2c, and (d) BATS 2d (Rutqvist et al., 2023).

Figure 41 shows the results of inversion differenced to illustrate the changes in resistivity associated with heating and subsequent cooling during each of the four heating phases. This figure illustrates the baseline resistivity (top row) and resistivity changes (lower rows) during the four primary BATS 2 heating events (each heating event is a column). To highlight the specific changes in each heating event, the resistivity model before each heating phase is shown as a baseline. Even though the four heating events were quite different in magnitude of temperature change, the results in Figure 41 show similarities, suggesting that it may not have a significant impact on subsequent processes. The four heating events display similar resistivity trend features. The resistivity decreases in the central part, particularly in the area close to the heater (~3.5m), while the resistivity increases in the edge areas. Resistivity is known to change with temperature and brine content. To determine the leading cause of this change in resistivity will require additional analysis.

Additional data, background, and analysis of the ERT data are presented in Rutqvist et al. (2023).

4.6 Fiber Optic (F) Data

A near-continuous data recording was maintained over the course of nine months during the BATS 2 test. The raw data collected are plotted Figure 42. The point where the fiber first meets grout in the wall of the drift is located at approximately 2 meters along the fiber (large strain anomaly), while the heater location is at about 4.5 to 5 meters along the fiber (large temperature anomaly associated with heating events). The variation in entrance location can be attributed to the differing lengths of optical fiber outside the borehole.

The raw temperature and strain measurements obtained by the distributed fiber optic sensing shows a correlation between the deeper strain anomaly (the shallow anomaly being near the drift face where strain associated with room closure is maximum) and the location of increased temperature. Both the strain and temperature data indicate deformation when the heater was operated three times—in September 2022 (BATS 2b), October 2022 (BATS 2c), and May 2023 (BATS 2d). The simultaneous occurrences of maximum strain and maximum temperature changes at the depth associated with the heater suggest that maximum deformation is due to heating, rather than creep closure of the drift.

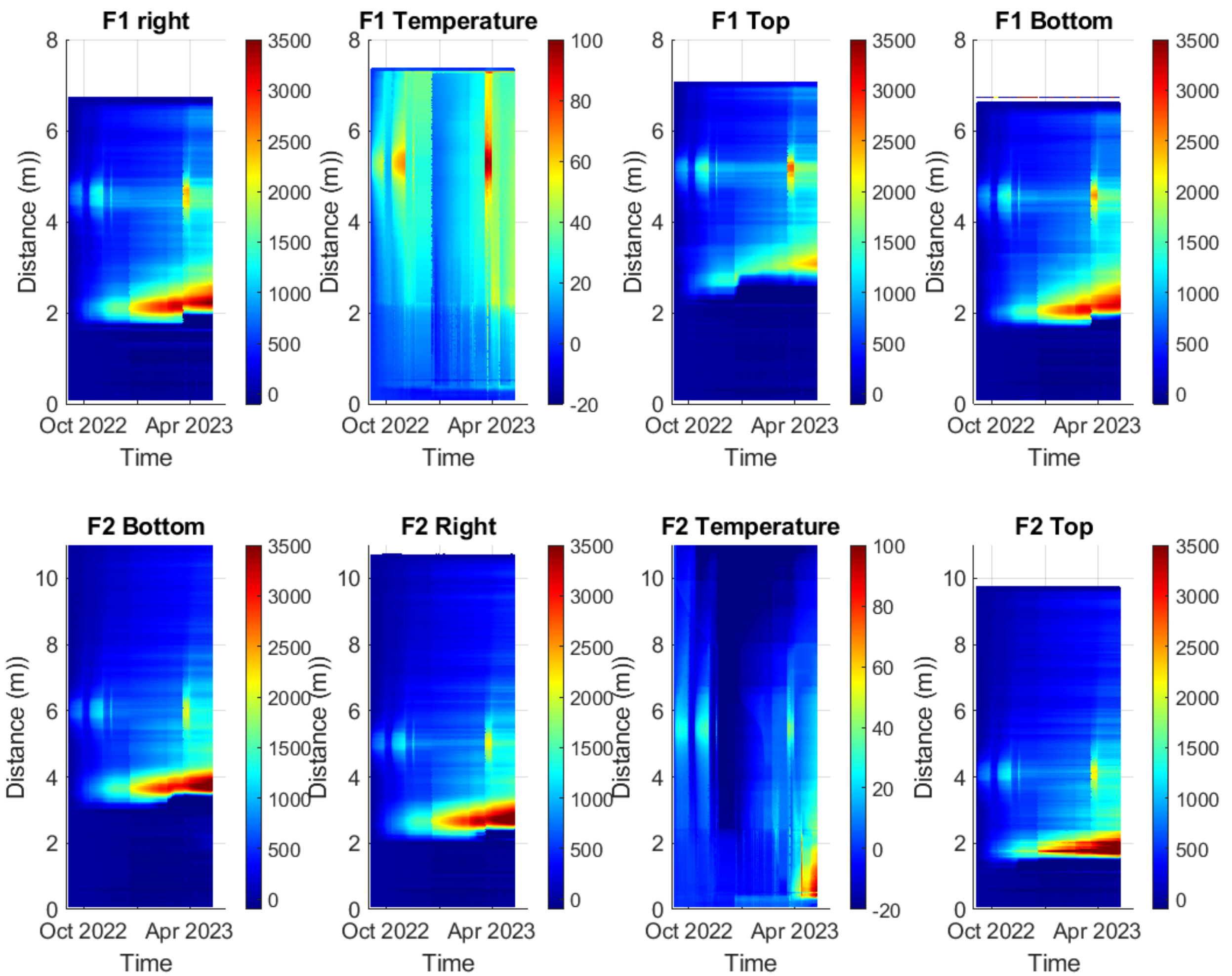

Figure 42. Raw fiber optic strain (DSS, microstrain) and temperature (DTS, ºC) data (Rutqvist et al., 2023).

More analysis, including adjusted and calibrated fiber optic data, are presented in Rutqvist et al. (2023).

4.7 Liquid Sample Borehole (SM) Data

4.7.1 SM: Air temperature and RH time series

Figure 43 shows the temperature and RH associated with the behind-the packer interval in the SM and SL boreholes. The right panel shows the air temperature behind the packer rising during the heating portion of the test (red and green curves), while the left panel shows the RH rising during heating in the heated SL borehole (but initially not the heated SM borehole). RH near 75% is indicative of equilibrium between moist air and halite.

The rise in RH behind the packer during heating is likely due to liquid brine being present in the seal borehole, but not the sample borehole (because of repeated removal of any standing brine for geochemical sampling). The upward spikes (~1%) in the RH data are in response to power outages. The RH sensor requires a warm-up time each time after the power is disconnected. The downward spikes (1-2%) in the RH data in the SM borehole are associated with sampling attempts. A vacuum pump is connected to the 0.635 cm [0.25 in] tubing to extract any brine standing at the back of the borehole. When air and water are removed from the borehole for sampling, less humid drift air must flow in to replace it.

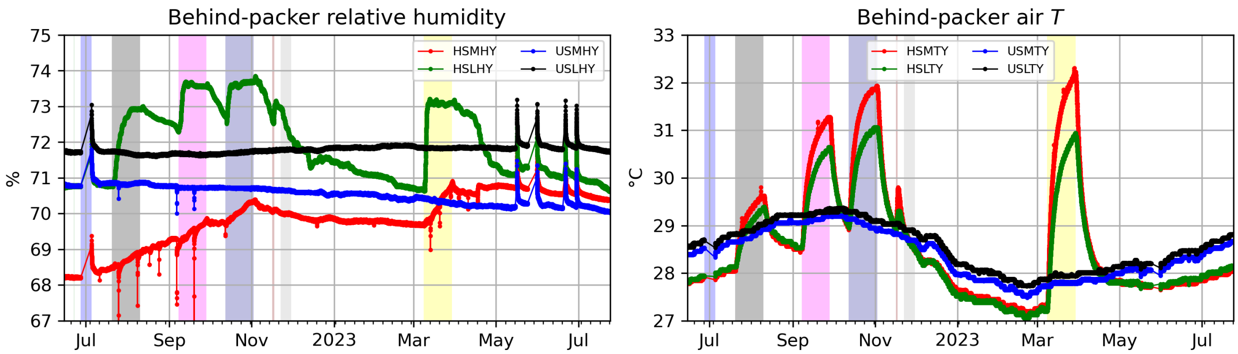

Figure 43. Relative humidity (left) and air temperature (right) for SM and SL boreholes.

4.7.2 SM: Liquid brine samples

Volumes of brine sampled during BATS 2 are listed Table A-7 for all boreholes. Brine production volumes through time for the heated SM borehole are plotted in Figure 44 (see RH and air temperature in this borehole as red lines in Figure 43). Geochemical data associated with SM samples are listed in Table A-9 and plotted in Figure 45 and Figure 46. The heated SM borehole was drilled 9 February 2022 (Table A-1), and the mechanical packer (as opposed to sewer plug) was installed 13 April 2022 (Table A-6, marked by vertical dashed line in SM brine figures).

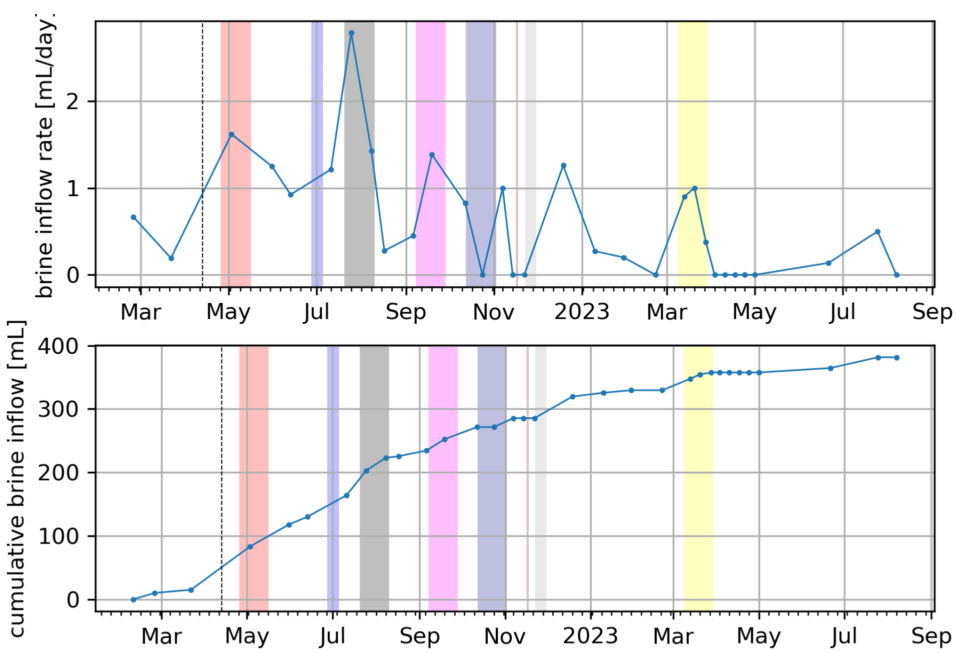

Figure 44. Brine production in heated SM borehole through time.

The highest averaged rate of brine production in the SM borehole was observed during heating event BATS 2a. The second highest rate of brine production was just after installing the permanent inflatable packer. The third highest rate of brine production was during heating event BATS 2b.

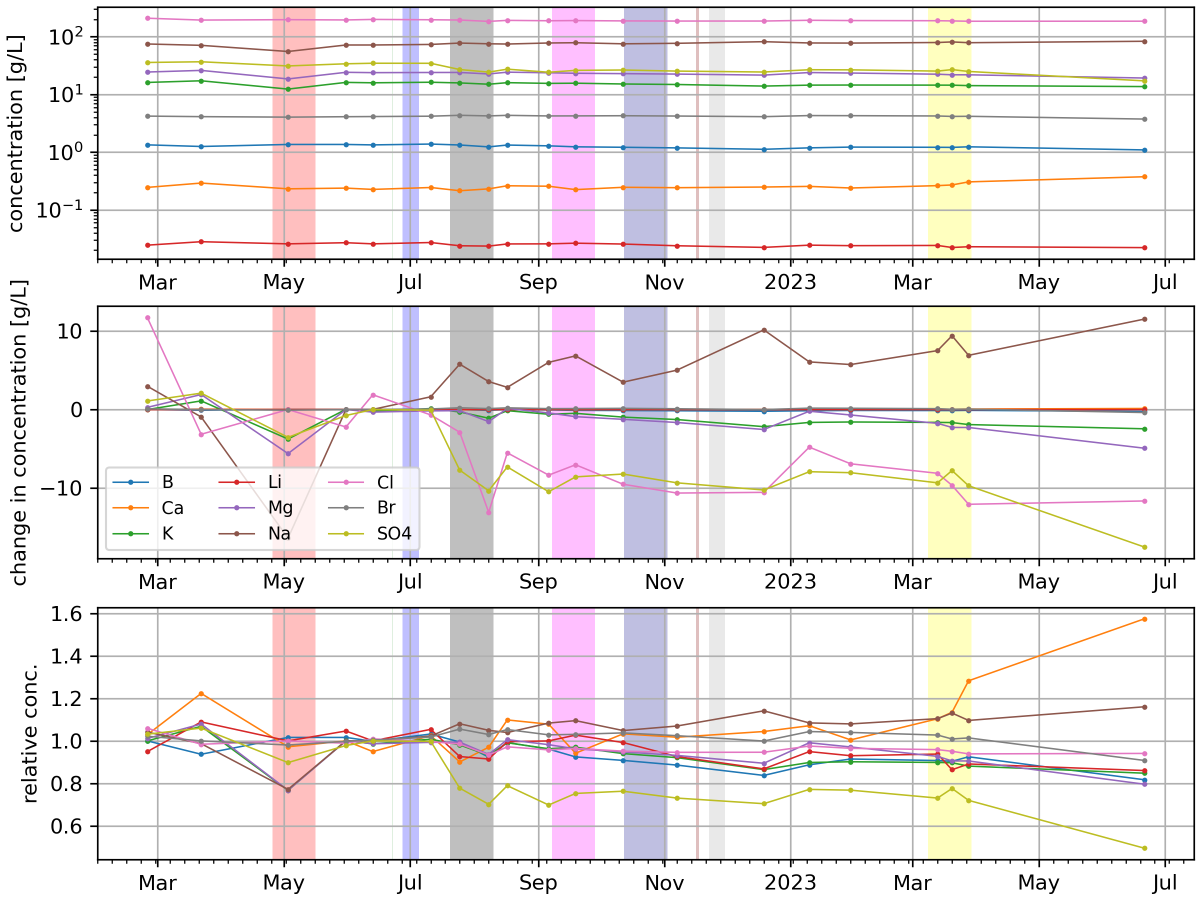

Figure 45. Brine chemistry data through time in heated SM borehole. (top) observed concentrations, (middle) change in concentrations, and (bottom) relative change in concentration.

Figure 45 shows the wide range of dissolved species tracked in BATS brine samples. The top panel shows over three orders of magnitude between lithium and chloride. The middle panel shows differences in species through time (compared to the median of the first 5 samples), which is mostly dominated by the higher-concentration species (i.e., sodium and chloride), which start deviating before the BATS 2a heater test. The bottom panel shows the relative changes in concentrations (divided by the median of the first 5 samples), which is mostly dominated by changes in more minor species (i.e., calcium), which change most after the BATS 2d heater test. Sulphate appears significant in both the middle and bottom panels. Kuhlman et al. (2018) performed laboratory evaporation experiments and numerical modeling to understand evaporation in a closed system, but the borehole is an open system – more brine flows into the borehole during the tests, while the brine concentrates due to heating.

Figure 46 shows ratios of Na/Cl and K/Mg ion concentrations through time at the SM borehole (see Table A-9 for data in g/L). Molar ratios (computed from value converted from g/L to moles/L through the molar weight) are plotted because they are less sensitive to dilution issues during sample collection (i.e., contamination by a small amount of clean rinse water between sampling events) or during laboratory processing (i.e., during dilution of samples to 100 or 1,000 times, based on requirements of the analytical instrument).

The Na/Cl data show a steady increase with time (the third sample in May 2022 is suspect for cross-contamination during sampling). The K/Mg data show a dip after BATS 2c, followed by an increase to higher than the initial level.

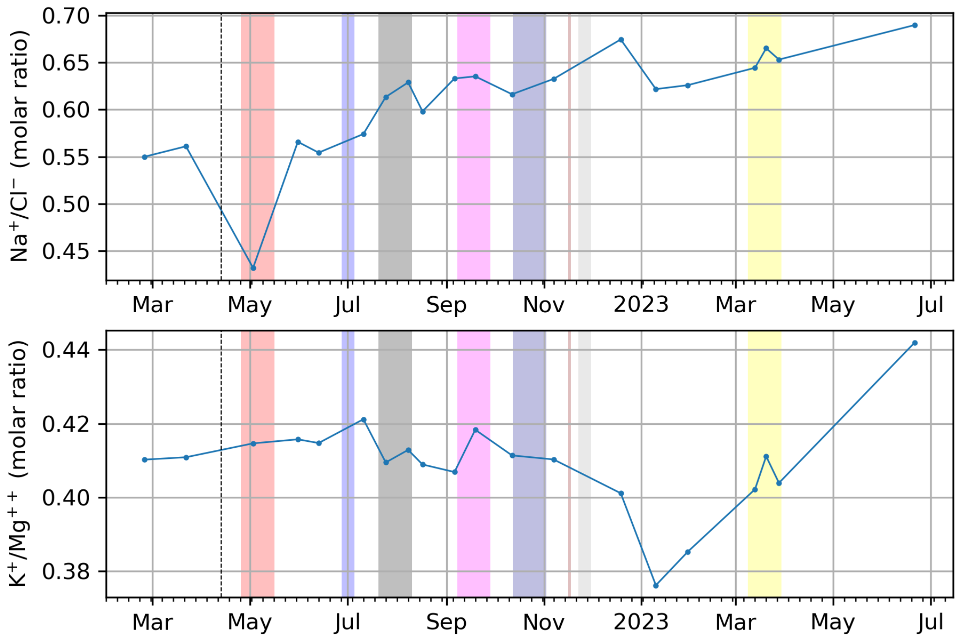

Figure 46. Ratios of ions in heated SM borehole brine samples through time.

To place these values and changes in context, these SM sample data are plotted in Figure 47 against other BATS 1 and BATS 2 samples collected, as well as historical Map Unit 0 (MU-0, where BATS 2 is completed), Marker Bed 139 (MB-139, approximately 1 to 2 m below where BATS 2 is completed), and fluid inclusion data. See Roberts et al. (1999) for a detailed description of WIPP in-repository stratigraphy.

The two samples that show the lowest K/Mg ratio (early 2023) appear more like the BATS 1 data collected previously (see two red dots in Figure 47 that are located inside the pink “BATS 1” box). This change in brine chemistry also occurs within a few months after the marked increase in gas permeability (faster declines in argon gas pressure behind the packer, reported in Figure 29) observed in the heated D borehole. One possible explanation is that fractures created during heating and cooling during the BATS 2c and aborted BATS 2d test in November 2022 created pathways that connected to the horizon associated with BATS 1 (i.e., MU-3), which then allowed brine to drain down towards the heated D and SM boreholes over the course of the following months (although the rate of brine production in the SM borehole did not change significantly during this time, Figure 44). This migration of brine might have reduced the permeability of newly opened fractures to gas (possibly even contributing to the “concave down” behavior observed in the heated D borehole pressure response; see Figure 30) and could have changed the brine chemistry observed in the heated SM borehole. Another possible explanation for the changes in brine chemistry could be the changes in temperature, related to the temperature-dependent solubility of the salt.

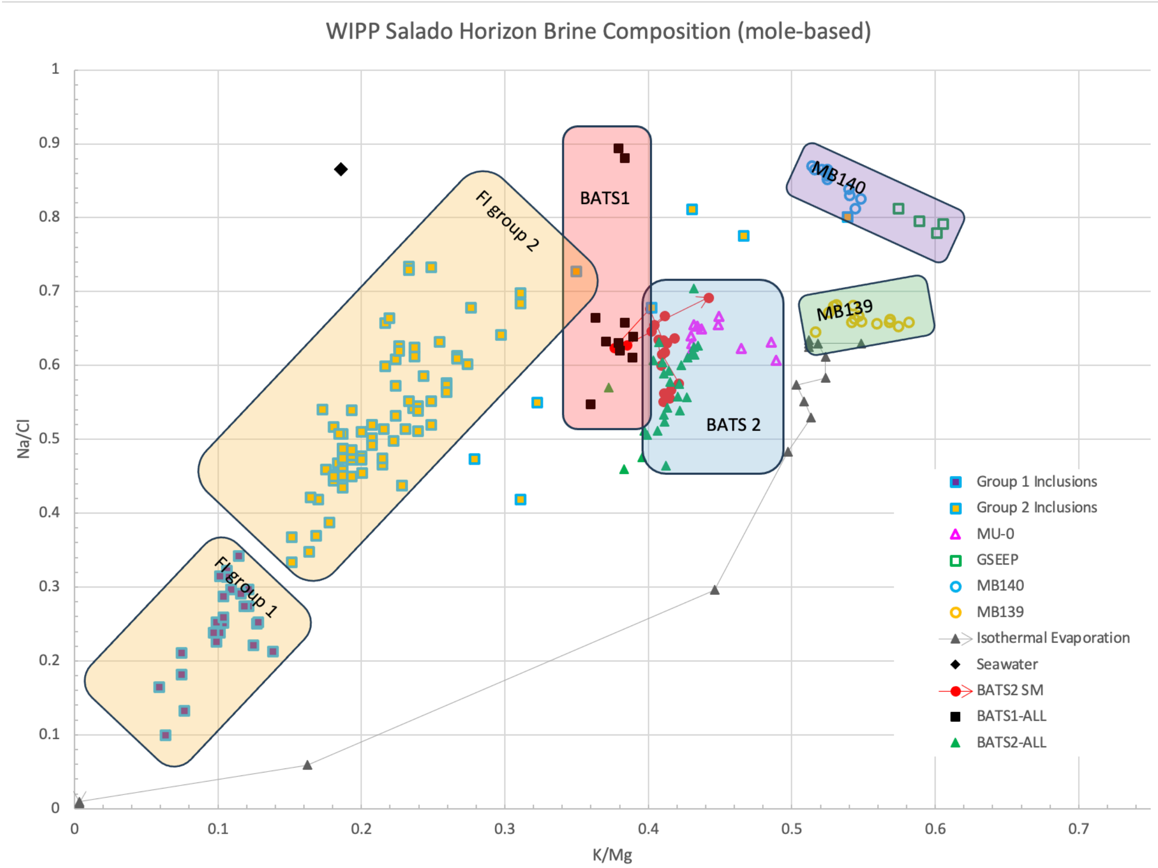

Figure 47. BATS SM brine chemistry timeseries (red circles) plotted with historic fluid inclusions, BATS 1, and WIPP historic brine MU-0, MB-139, and MB-140 (Krumhansl et al., 1990). Sample data converted from g/L in Appendix to moles/L before computing ratios.

4.8 Seal Borehole Data

The new BATS 2 seals were emplaced as part of the BATS 2 construction, while the unheated seals from BATS 1 are still in place and will remain in place longer, with over-coring of both sets of seals occurring at a future date (possibly during preparations for BATS 3).

4.8.1 SL: Air temperature and RH time series

Figure 43 shows the air temperature and relative humidity data associated with the SL boreholes. Unlike the SM boreholes, the relative humidity behind the packer rises in the SL borehole in response to heating. This could likely be due to standing brine in the borehole being removed from the SM borehole by vacuum pump, while brine in the SL borehole would remain, and would tend to saturate parts the emplaced seals with time.

4.8.2 SL: Strain and temperature time series

The lab-constructed seals were instrumented with embedded strain gauges to observe strain in the salt once the borehole has closed in and made contact on the laboratory-fabricated cement plugs. The vibrating-wire GEOKON strain gauges installed in seals as part of BATS 1 in the unheated seal have failed and are no longer reporting valid values. The VPG strain gauges in the unheated seal are still working (blue line in Figure 48), and the data show a change in slope in December 2022. This is interpreted to mean the borehole has crept shut against the unheated seal, so now the sample is showing a higher strain rate under the now-increase stress in the seal. This strain gauge was installed as part of

BATS 1 in 2019 and is embedded in the salt concrete portion (see detailed description in Kuhlman et al., 2020) of the unheated SL composite seal. It has taken roughly three years for the borehole to close in on the salt concrete seal. Similar VPG strain gauges in the sorel and salt concrete seals in the heated SL boreholes (red and green lines in Figure 48) show clear straining in response to heating events. In May 2023, after BATS 2d, the VPG gauge in the heated sorel cement seal saw a similar increase in strain rate, followed by another jump at the end of June 2023. It has taken roughly one year for the borehole to close in on the BATS 2 heated sorel seal.

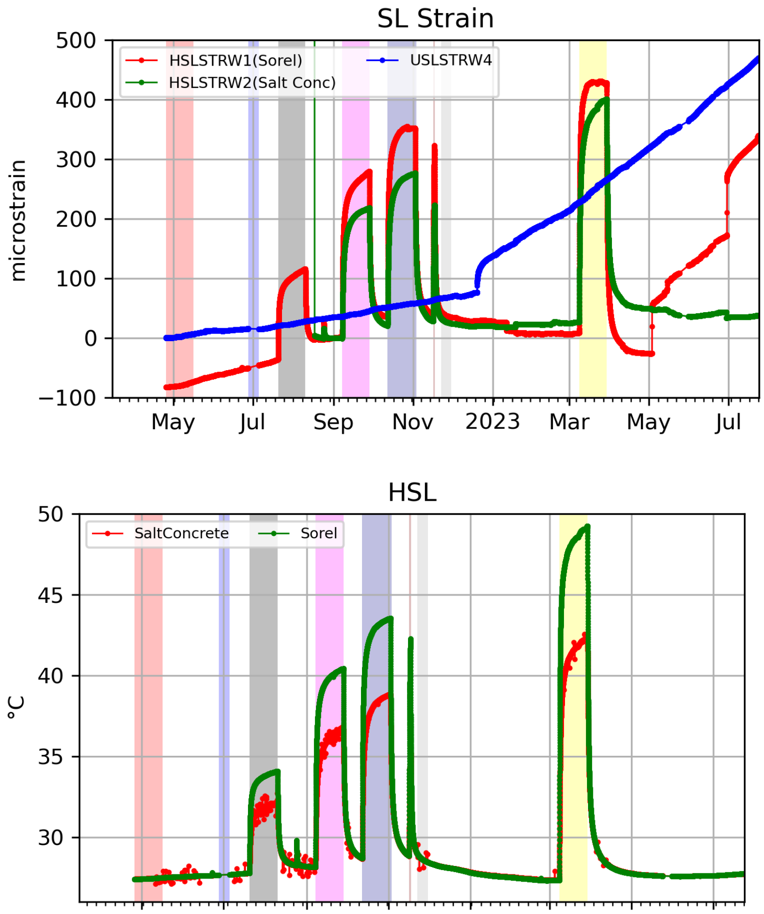

Figure 48. Strain (top) and temperature (bottom) inside cement plugs in SL borehole.

In heater event BATS 2d, the Sorel plug experienced a change in temperature of approximately 22 ºC (green curve in bottom of Figure 48), and a change in strain of approximately 425 microstrains (red curve in top of Figure 48). This translates to a coefficient of volume expansion of 19 microstrains/ºC, or a coefficient of linear expansion of 6.4 microstrains/ºC, which agrees reasonably with the value of 5.18 microstrains/ºC in the literature for 5-1-8 Sorel cement below 180 ºC (Pavlíkov et al., 2020). The coefficient of thermal expansion of halite is approximately twice as high, at 13 microstrains/ºC (Wang & Reeber, 1996).

4.9 In-Drift Time Series

Weather station measurements were made in the N-940 drift. Figure 49 shows 10-minute average air temperature, RH, barometric pressure, and air speed near the datalogger enclosures. Drift air temperature increased during the observation period, associated with summer weather. The RH generally rises from spring into summer, associated with changing seasons on the surface, since air from the surface is ventilated through the mine. Large changes in ventilation air speeds are likely due to changes in routing of ventilation in the WIPP underground, which are due to ventilation needs and proximity of other activities in WIPP (e.g., mining or rock bolting). Lower ventilation air speeds occur at night when fewer personnel are underground at WIPP. Barometric pressure fluctuations generally stay between 960 and 970 mbar, with higher-amplitude fluctuations in winter and spring.

The air temperature in the drift fluctuated approximately 3.5 ºC through a 12-month period, but there are spikes of higher temperatures observed when the mine ventilation is low, possibly due to heat generated by the instrumentation and computers in the N-940 drift at BATS.

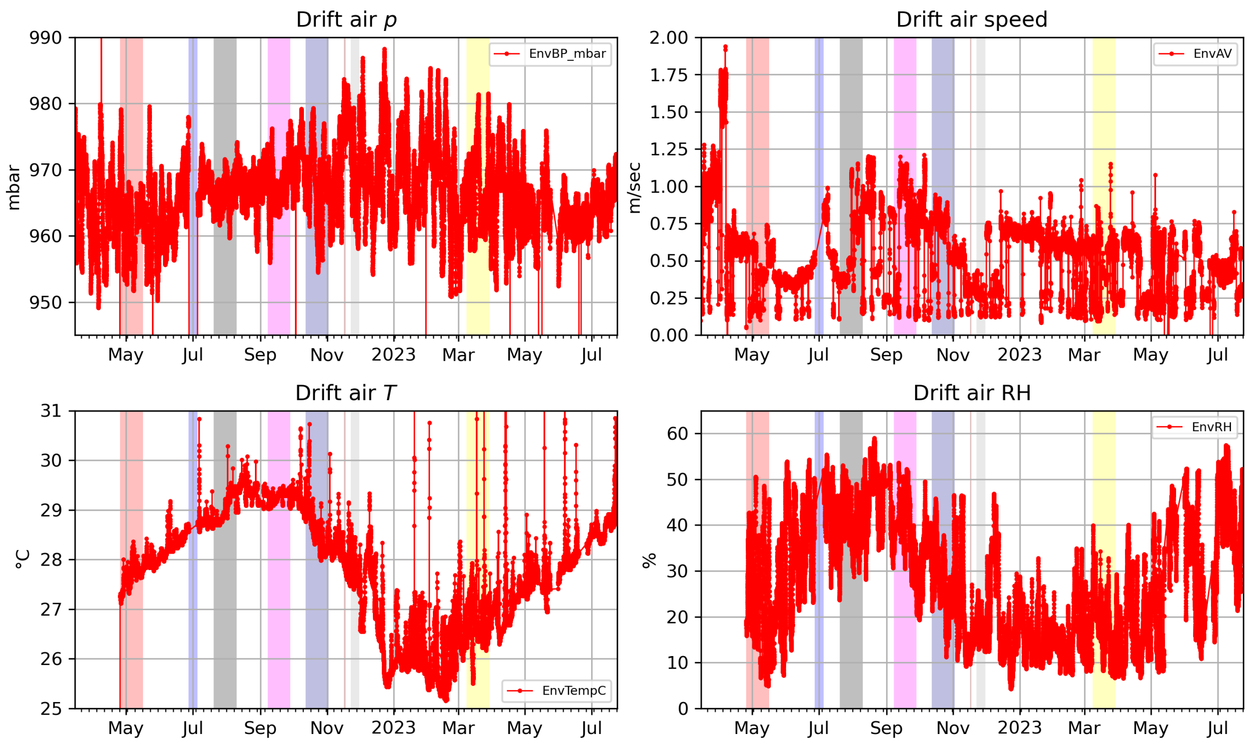

Figure 49. In-drift barometric pressure (top left), air speed (top right), air temperature (bottom left), and RH (bottom right) during BATS 2.

5. Summary

This report presents the observations from the Brine Availability Test in Salt (BATS) field test in the underground at the Waste Isolation Pilot Plant (WIPP). We presented the motivation and technical background for creating coupled process field experiments in salt, along with summarizing data collected from the first four heating phases of BATS 2 (heating events a-d). Brine is important to radioactive waste disposal safety as brine leads to corrosion of waste packages and waste forms, is the primary offsite transport vector, can resist final elimination of excavation porosity by creep closure, and presents a high chlorine concentration environment enabling reduced risk of in-package nuclear criticality. The main goals of the BATS field test are to collect data that lead to better understanding and possible confirmation of model predictions related to brine availability in bedded salt and to train a new generation of scientists and technicians on the use of underground research labs in the US for radioactive waste disposal.

The report describes the first four heating events of BATS 2. Eight of the boreholes have instrumentation grouted into them (T1, T2, E1, E2, E3, E4, F1 and F2), while four of the remaining boreholes are isolated with inflatable or mechanical packers (HP, D, SM, SL). The four AE boreholes are not grouted or sealed with packers. BATS 2a was conducted in July and August of 2022, with BATS 2b and BATS 2c following short cool-down periods in September and October 2022. Some equipment related delays (related to the gas analyzer, ERT, and Picarro) pushed BATS 2d to March 2023.

In each array, electrical resistivity electrodes in the four E boreholes are used to interrogate changes in apparent resistivity through time due to brine migration and temperature variation. The ERT system has shown a sensitivity to the migration and distribution of brine during and after heating. The four AE boreholes contain decentralized piezoelectric transducers for monitoring the timing and locating the source of AE in the salt. The two T boreholes, along with temperature measurements in most of the other boreholes, are used to monitoring the spatial and temporal variability of temperature around the heater. Aside from a few interactions between the ERT system and the thermocouples (which led to premature failure of most of the thermocouples in the unheated ERT boreholes), the sealed Type-K thermocouples being used have proven to be generally robust in the salt environment. The ERT boreholes in BATS 2 use RTDs to reduce the noise previously observed during ERT testing each night, but the RTDs still experience some noise. The SL borehole includes a laboratory-created composite seal (salt concrete and sorel cement), instrumented with strain gauges behind a mechanical packer. The D borehole is pressurized with argon, which is used to test the changing gas permeability of the system (i.e., pressure decay), and monitor breakthrough of gas to the gas analyzer in the HP borehole after BATS 2d. The central HP borehole contains a 1250-Watt heater used to heat a 71-cm interval of the borehole, while moisture is removed with flowing dry nitrogen for in-drift analyses of gas and water isotope composition.

The AE system saw significant activity at the beginning and end of each heating cycle. The ERT system showed systematic changes in resistivity around the heater associated with each heating event. The Picarro CRDS showed changes in water isotopes, possibly related to the change in the relative contribution of fluid inclusions to the overall brine. Both the unheated and heated seals showed evidence for creep closure of the salt and loading of the plug with increased stress. By BATS 2c, the gas permeability had markedly increased, as monitored by gas pressure decline rates in the heated D borehole. A “concave down” pressure response was observed in late 2022, and changes in brine chemistry were observed in the SM borehole. The data are presented in this report with some analyses, but it will take some time to fully understand the coupled thermal, hydrological, mechanical, and chemical processes going on in the BATS 2 array.

The overall theme in BATS 2 is seeing multiple lines of evidence that an accumulation of damage occurs in the salt associated with both heating and cooling to different temperatures. The BATS tests included:

- thermal (changes in temperature due to a range of heat setpoints; ranging from lower to higher temperatures than the BATS 1 test in early 2020);

- hydrological (water production associated with heating and cooling in the HP borehole and gas tracer tests between D and HP boreholes using argon);
- mechanical (closure observations in HP and change in strain rate in the SL boreholes, supplemented by observations of the timing and location of damage through acoustic emissions);
- chemical (water isotope observations through time in HP borehole gas stream and brine chemistry observations through samples made across time in the SM borehole); and
- indirect geophysical responses (electrical resistivity tomography changes due to heating and distributed fiber optic strain and temperature measurements showing effects of both heating and drift closure).

Each of these responses were characteristic of a system changing through damage and brine migration. The focus of BATS is “brine availability”, which is related to the occurrence of brine, and the evolution of the flow networks that bring gas and brine to boreholes and excavations.

The large response of brine inflow after the end of the BATS 1 test (Jan-Mar 2020) was notably not observed to the same degree in BATS 2a through BATS 2d. The difference in the response of the system between these tests is a point which will be investigated further in future work.

6. Next Stages

Additional heater tests are planned for the remainder of 2023 and into 2024, building on some of the lessons learned during FY23. To alleviate problems associated with overwhelming the water vapor collection system, we have purchased a new nitrogen regulator that allows multiple bottles of UHP N_2 gas to be connected to the inflow system in parallel. This will allow higher flowrates of gas to be set at the beginning of a heated period, while minimizing the risk of running out of gas over a weekend. We intend to re-run a test like BATS 2d at higher gas flowrates. We also intend to run a test with more gradually increasing start-up and decreasing shut-down heating rates. Current heater tests are essentially a step change on or off. We also want to run a cyclic heater test (this was intended at the end of BATS 1, but there were issues with the heater controller used in that test that didn't allow it to be programmed this way). The new heater controller should allow arbitrary heater power profiles, including gradual ramping up or down over hours or days, or even a smooth sinusoidal heating distribution.

Any future heater tests will continue to use gas permeability tests conducted in the heated D borehole to confirm when changes in apparent gas permeability occur, associated with damage imparted from heating or changes in brine saturation due.

In FY24, we intend to update the BATS 5-year plan (Kuhlman et al., 2021a), which includes plans for BATS 3. This next phase which will involve a series of smaller tests that are not centered around a single borehole. Hopefully this approach will reduce scheduling issues and test interference issues. We hope to continue to develop and test hypotheses associated with brine availability and migration in the excavation damaged zone salt.

BATS 1 provided some key information about the changes in permeability with temperature and damage associated with heating the salt. BATS 2 has further explored the evolution of damage in salt with new instrumentation at a at range of heater temperatures. The BATS series of tests aim to further illuminate the key mechanisms and couplings that govern thermal-hydrological-mechanical-chemical processes and how they relate to key fluid and solid changes (e.g., boiling point of brine or the dewatering point of certain minerals) that would be driven by the emplacement of heat-generating waste into a salt repository.

7. References

Beauheim, R.L. & R.M. Roberts, 2002. Hydrology and hydraulic properties of a bedded evaporite formation, *Journal of Hydrology, 259*(1–4):66–68.

Boukhalfa, H., E. Guiltinan, T. Rahn, D. Weaver, B. Dozier, S. Otto, P.H. Stauffer, M. Mills, K. Kuhlman, E. Matteo, C. Herrick, M. Nemer, J. Heath, Y. Xiong, C. Lopez, J. Rutqvist, Y. Wu & M. Hu, 2019. *2019 LANL Experiments and Simulations in Support of Salt R&D*, (34 p.) M3SF-19LA010303014, LA-UR-19–29830, Los Alamos, NM: Los Alamos National Laboratory.

Davies, C. & F. Bernier [Eds.], 2005. *Impact of the Excavation Disturbed or Damaged Zone (EDZ) on the Performance of Radioactive Waste Geological Repositories*, (359 p.) EUR 21028 EN, Brussels, Belgium: European Commission.

Guiltinan, E.J., K.L. Kuhlman, J. Rutqvist, M. Hu, H. Boukhalfa, M. Mills, S. Otto, D.J. Weaver, B. Dozier & P.H. Stauffer, 2020. Temperature response and brine availability to heated boreholes in bedded salt, *Vadose Zone Journal, 19*(1):e20019.

Guiltinan, E., H. Boukhalfa, C. Campe, J. Davis, D. Eldridge, O. Marina, H. Miller, S. Otto, T. Rahn, A. Stansberry, P.H. Stauffer, K.L. Kuhlman, M. Mills, R. Jayne, E. Matteo, C. Herrick, M. Nemer, J. Heath, Y. Xiong, C. Choens, M. Paul, J. Rutqvist, Y. Wu, H. Tounsi& M. Hu, 2023. *2023 LANL Contributions to the BATS Test in WIPP*, (67 p.) LA-UR-23–29483. Los Alamos, NM: Los Alamos National Laboratory.

Jordan, A.B., H. Boukhalfa, F.A. Caporuscio; B.A. Robinson & P.H. Stauffer, 2015. Hydrous mineral dehydration around heat-generating nuclear waste in bedded salt formations, *Environmental Science & Technology*, 5:1–13.

Kuhlman, K.L., 2019. *Processes in Salt Repositories*, (41 p.) SAND19–6441R, Albuquerque, NM: Sandia National Laboratories. https://doi.org/10.2172/1559569

Kuhlman, K.L. & B. Malama, 2013. *Brine Flow in Heated Geologic Salt*, (128 p.) SAND2013–1944, Carlsbad, NM: Sandia National Laboratories. https://doi.org/10.2172/1095129

Kuhlman, K.L. & S.D. Sevougian, 2013. *Establishing the Technical Basis for Disposal of Heat-Generating Waste in Salt*, (100 p.) SAND2013–6212P, FCRD-UFD-2013–000233. Albuquerque, NM: Sandia National Laboratories.

Kuhlman, K.L., M.M. Mills & E.N. Matteo, 2017. *Consensus on Intermediate Scale Salt Field Test Design*, (95 p.) SAND2017–3179R, Albuquerque, NM: Sandia National Laboratories. https://doi.org/10.2172/1365470

Kuhlman, K.L., C.M. Lopez, M.M. Mills, J.M. Rimsza & D.C. Sassani, 2018. *Evaluation of Spent Nuclear Fuel Disposition in Salt (FY18)*, (83 p.) M2SF-18SN010303031, SAND2018–11355R, Albuquerque, NM: Sandia National Laboratories. https://doi.org/10.2172/1481605

Kuhlman, K., M. Mills, R. Jayne, E. Matteo, C. Herrick, M. Nemer, J. Heath, Y. Xiong, C. Choens, P. Stauffer, H. Boukhalfa, E. Guiltinan, T. Rahn, D. Weaver, B. Dozier, S. Otto, J. Rutqvist, Y. Wu, M. Hu, S. Uhlemann & J. Wang, 2020. *FY20 Update on Brine Availability Test in Salt*, (107 p.) SAND2020–9034R. Albuquerque, NM: Sandia National Laboratories. https://doi.org/10.2172/1657890

Kuhlman, K.L., S. Otto, P. Stauffer & Y. Wu, 2021a. *Brine Availability Test in Salt (BATS) Extended Plan for Experiments at the Waste Isolation Pilot Plant (WIPP)*, (25 p.) SAND2021–3497R. Albuquerque, NM: Sandia National Laboratories. https://doi.org/10.2172/1773028

Kuhlman, K., M. Mills, R. Jayne, E. Matteo, C. Herrick, M. Nemer, J. Heath, Y. Xiong, C. Choens, M. Paul, P. Stauffer, H. Boukhalfa, E. Guiltinan, T. Rahn, D. Weaver, S. Otto, J. Davis, J. Rutqvist,

Y. Wu, M. Hu, S. Uhlemann & J. Wang, 2021b. *Brine Availability Test in Salt (BATS) FY21 Update*, (64 p.) SAND2021–10962R. Albuquerque, NM: Sandia National Laboratories. https://doi.org/10.2172/1821547

Kuhlman, K., M. Mills, R. Jayne, E. Matteo, C. Herrick, M. Nemer, Y. Xiong, C. Choens, M. Paul, C. Downs, D. Fontes, B. Kernen, P. Stauffer, H. Boukhalfa, E. Guiltinan, T. Rahn, S. Otto, J. Davis, M. Carrasco Jr., J. Mata, J. Rutqvist, Y. Wu, H. Tounsi, M. Hu, S. Uhlemann & J. Wang, 2022. *Brine Availability Test in Salt (BATS) FY22 Update*, (82 p.) SAND2022–12142R. Albuquerque, NM: Sandia National Laboratories.

Kuhlman, K., E.N. Matteo, M.M. Mills, R.S. Jayne, J.B. Coulibaly, B. Reedlunn & J. Bean, 2023. *Salt International Collaborations FY23 Update*, (22 p.) SAND2023-07447R. Albuquerque, NM: Sandia National Laboratories.

Olivella, S., S. Castagna, E.E. Alonso & A. Lloret, 2011. Porosity variation in saline media induced by temperature gradients: experimental evidences and modelling. *Transport in Porous Media, 90*:763–777.

Pavlíková, M., A. Pivák & Z. Pavlík, 2020. "High temperature dilatometric measurements of MOC" in *Thermophysics 25th International Meeting*, Smolenice, Slovokía, 7-9 September 2020.

Roberts, R.M., R.L. Beauhiem & P.S. Domski, 1999. *Hydraulic Testing of Salado Formation Evaporites at the Waste Isolation Pilot Plant Site: Final Report,* (288 p.) SAND98–2537, Albuquerque, NM: Sandia National Laboratories.

Roedder, E., 1984. The fluids in salt. *American Mineralogist, 69*(5–6):413–439.

Rutqvist, J., M. Hu, H. Tounsi, Y. Wu, C. Steefel, S. Uhlemann, J. Wang, H. Chen & B. Gilbert, 2023. *Salt Coupled THMC Processes Research Activities at LBNL: FY23 Progress* (146 p.) M3SF-23LB010303032, Berkeley, CA: Lawrence Berkeley National Laboratory.

Sandia National Laboratories (SNL), Los Alamos National Laboratory (LANL) & Lawrence Berkeley National Laboratory (LBNL), 2020. *Project Plan: Salt in situ Heater Test*, (20 p.) SAND2020–1251R.

Stauffer, P.H., A.B. Jordan, D.J. Weaver, F.A. Caporuscio, J.A. Ten Cate, H. Boukhalfa, B.A. Robinson, D.C. Sassani, K.L. Kuhlman, E.L. Hardin, S.D. Sevougian, R.J. MacKinnon, Y. Wu, T.A. Daley, B.M. Freifeld, P.J. Cook, J. Rutqvist & J.T. Birkholzer, 2015. *Test Proposal Document for Phased Field Thermal Testing in Salt,* (104 p.) LA-UR-15–23154, FCRD-UFD-2015–000077. Los Alamos, NM: Los Alamos National Laboratory.

Wang, K. & R.R. Reeber, 1996. Thermal expansion of alkali halides at high pressure: NaCl as an example. *Physics and Chemistry of Minerals, 23*:354–360.

A-1. Appendix: Tabular Data

Additional data, summarized or exemplified in figures in the main text, are presented here in tabular form.

Table A-1. Sequence of BATS 2 borehole drilling and coring.

Borehole ID	Planned Depth [ft]	Drill Bit Size [in]	Actual Depth [ft]	Drilling Start Date	Drilling End Date	Days Drilling
E4	19.0	2.13	19.0	10/27/21	10/27/21	0.5
AE1	11.0	2.13	10.99	10/27/21	10/27/21	0.5
E3	19.0	2.13	19.0	01/18/22	01/18/22	0.25
AE3	11.0	2.13	11.0	01/18/22	01/18/22	0.25
F1	18.0	2.13	18.0	01/18/22	01/18/22	0.25
E2	19.0	2.13	19.0	01/18/22	01/18/22	0.25
AE2	11.0	2.13	11.0	01/19/22	01/19/22	0.25
T1	18.0	2.13	18.0	01/20/22	01/20/22	0.25
HP (cored)	12.0	4.83	12.54	01/27/22	02/01/22	3.0
T2	18.0	2.13	18.0	02/09/22	02/09/22	0.25
F2	30.0	2.13	30.0	02/09/22	02/09/22	0.25
AE4	11.0	2.13	11.01	02/15/22	02/15/22	0.25
SM	15.0	2.13	15.0	02/09/22	02/09/22	0.25
D	15.0	2.13	15.04	02/15/22	02/15/22	0.25
SL (cored)	11.5	4.83	11.55	02/16/22	02/17/22	2.0
E1	19.0	2.13	19.01	02/18/22	02/18/22	0.25

Table A-2. Proposed and as-built coordinates for BATS 2 boreholes. Center of HP borehole at drift face is (0,0,0) of both planned and as-built coordinate systems. +X is west along N-940, +Y is south into the wall, and +Z is vertically up.

			Planned Drift Face (Y=0)		As-built Drift Face (assume Y=0)		As-Built Back of Borehole (assume straight borehole)		
	Diameter (cm)	Length (m)	X (m)	Z (m)	X (m)	Z (m)	X (m)	Y (m)	Z (m)
AE1	5.33	3.3498	0.292	0.704	0.307	0.706	0.298	3.350	0.704
AE2	5.33	3.3528	0.704	-0.292	0.709	-0.287	0.704	3.353	-0.296
AE3	5.33	3.3528	-0.292	-0.504	-0.293	-0.496	-0.298	3.353	-0.508
AE4	5.33	3.3558	-0.704	0.293	-0.694	0.299	-0.712	3.356	0.293
D	5.33	4.5842	0.000	0.188	0.021	0.202	0.012	4.584	0.203
E1	5.33	5.7942	0.704	0.293	0.716	0.302	0.764	5.794	0.302
E2	5.33	5.7912	0.292	-0.504	0.300	-0.493	0.288	5.791	-0.524
E3	5.33	5.7912	-0.704	-0.292	-0.688	-0.276	-0.685	5.791	-0.294
E4	5.33	5.7912	-0.292	0.704	-0.282	0.717	-0.269	5.791	0.733
F1	5.33	5.4864	0.000	-0.188	0.010	-0.191	0.018	5.486	-0.270
F2	5.33	9.1440	-0.292	0.000	-0.277	0.011	-0.274	9.144	-0.018
HP	12.19	3.8222	0.000	0.000	0.000	0.000	0.012	3.822	-0.052
SL	12.19	3.5204	0.188	0.293	0.203	0.302	0.200	3.520	0.310
SM	5.33	4.5720	0.188	0.000	0.199	0.006	0.181	4.572	-0.017
T1	5.33	5.4864	-0.975	0.000	-0.961	0.006	-0.975	5.486	-0.031
T2	5.33	5.4864	-0.671	0.000	-0.658	0.011	-0.690	5.486	0.031

Table A-3. Temperature measurement names and locations.

Borehole ID	Name	Depth [m]	Instrument
E1	HE1RTD1	1.52	RTD
E1	HE1RTD2	2.51	RTD
E1	HE1RTD3	2.97	RTD
E1	HE1RTD4	3.43	RTD
E1	HE1RTD5	5.79	RTD
E2	HE2RTD1	1.52	RTD
E2	HE2RTD2	2.51	RTD
E2	HE2RTD3	2.97	RTD
E2	HE2RTD4	3.43	RTD
E2	HE2RTD5	5.79	RTD
E3	HE3RTD1	1.52	RTD
E3	HE3RTD2	2.51	RTD
E3	HE3RTD3	2.97	RTD
E3	HE3RTD4	3.43	RTD
E3	HE3RTD5	5.79	RTD
E4	HE4RTD1	1.52	RTD
E4	HE4RTD2	2.51	RTD
E4	HE4RTD3	2.97	RTD
E4	HE4RTD4	3.43	RTD
E4	HE4RTD5	5.79	RTD
SL	HSLTY	1.20	TRH Probe
SM	HSMTY	1.50	TRH Probe
AE1	HAE1TC1	2.44	Type K TC
AE1	HAE1TC2	2.97	Type K TC
AE1	HAE1TC3	3.35	Type K TC
AE2	HAE2TC1	2.44	Type K TC
AE2	HAE2TC2	2.97	Type K TC
AE2	HAE2TC3	3.35	Type K TC
AE3	HAE3TC1	2.44	Type K TC
AE3	HAE3TC2	2.97	Type K TC
AE3	HAE3TC3	3.35	Type K TC
AE4	HAE4TC1	2.44	Type K TC
AE4	HAE4TC2	2.97	Type K TC
AE4	HAE4TC3	3.35	Type K TC
F1	HF1TC1	2.51	Type K TC
F1	HF1TC2	2.97	Type K TC
F1	HF1TC3	3.43	Type K TC
F1	HF1TC4	4.57	Type K TC
F2	HF2TC1	1.52	Type K TC

Borehole ID	Name	Depth [m]	Instrument
F2	HF2TC2	2.51	Type K TC
F2	HF2TC3	2.97	Type K TC
F2	HF2TC4	3.43	Type K TC
F2	HF2TC5	4.57	Type K TC
F2	HF2TC6	6.86	Type K TC
F2	HF2TC7	9.14	Type K TC
HP	HHPTC1	2.47	Type K TC
HP	HHPTC2	2.81	Type K TC
HP	HHPTC3	2.81	Type K TC
HP	HHPTC4	3.12	Type K TC
HP	HHPTC5	3.12	Type K TC
HP	HHPTC6	3.48	Type K TC
SL	HSL Salt Conc	3.25	Type K TC
SL	HSL Sorel	3.25	Type K TC
T1	T1TC1	0.30	Type K TC
T1	T1TC2	0.61	Type K TC
T1	T1TC3	0.91	Type K TC
T1	T1TC4	1.22	Type K TC
T1	T1TC5	1.52	Type K TC
T1	T1TC6	1.83	Type K TC
T1	T1TC7	2.13	Type K TC
T1	T1TC8	2.51	Type K TC
T1	T1TC9	2.74	Type K TC
T1	T1TC10	2.97	Type K TC
T1	T1TC11	3.43	Type K TC
T1	T1TC12	3.66	Type K TC
T1	T1TC13	3.96	Type K TC
T1	T1TC14	4.27	Type K TC
T1	T1TC15	4.57	Type K TC
T1	T1TC16	4.88	Type K TC
T1	T1TC17	5.18	Type K TC
T1	T1TC18	5.49	Type K TC
T2	T2TC1	0.30	Type K TC
T2	T2TC2	0.61	Type K TC
T2	T2TC3	0.91	Type K TC
T2	T2TC4	1.22	Type K TC
T2	T2TC5	1.52	Type K TC
T2	T2TC6	1.83	Type K TC
T2	T2TC7	2.13	Type K TC
T2	T2TC8	2.51	Type K TC
T2	T2TC9	2.74	Type K TC

Borehole ID	Name	Depth [m]	Instrument
T2	T2TC10	2.97	Type K TC
T2	T2TC11	3.43	Type K TC
T2	T2TC12	3.66	Type K TC
T2	T2TC13	3.96	Type K TC
T2	T2TC14	4.27	Type K TC
T2	T2TC15	4.57	Type K TC
T2	T2TC16	4.88	Type K TC
T2	T2TC17	5.18	Type K TC
T2	T2TC18	5.49	Type K TC

Table A-4. As-built thermocouple and RTD coordinates. +X is west along N-940; +Y is south into the drift wall; +Z is up. Origin is center of HP borehole at drift face. Assumes sensors in center of a straight borehole.

Borehole	Sensor ID	Sensor depth [m]	Sensor X [m]	Sensor Y [m]	Sensor Z [m]	Distance to heater midpoint [m]
AE1	HAE1TC1	2.438	0.301	2.438	0.705	0.963
AE1	HAE1TC2	2.972	0.299	2.972	0.705	0.799
AE1	HAE1TC3	3.353	0.298	3.353	0.704	0.884
AE2	HAE2TC1	2.438	0.705	2.438	-0.294	0.914
AE2	HAE2TC2	2.972	0.705	2.972	-0.295	0.74
AE2	HAE2TC3	3.353	0.704	3.353	-0.296	0.831
AE3	HAE3TC1	2.438	-0.297	2.438	-0.505	0.773
AE3	HAE3TC2	2.972	-0.298	2.972	-0.506	0.558
AE3	HAE3TC3	3.353	-0.298	3.353	-0.508	0.675
AE4	HAE4TC1	2.438	-0.707	2.438	0.294	0.956
AE4	HAE4TC2	2.972	-0.71	2.972	0.293	0.793
AE4	HAE4TC3	3.353	-0.712	3.353	0.293	0.88
E1	HE1RTD1	1.524	0.729	1.524	0.302	1.655
E1	HE1RTD2	2.515	0.737	2.515	0.302	0.926
E1	HE1RTD3	2.972	0.741	2.972	0.302	0.807
E1	HE1RTD4	3.429	0.744	3.429	0.302	0.929
E1	HE1RTD5	5.791	0.764	5.791	0.302	2.936
E2	HE2RTD1	1.524	0.296	1.524	-0.501	1.549
E2	HE2RTD2	2.515	0.294	2.515	-0.506	0.714
E2	HE2RTD3	2.972	0.294	2.972	-0.509	0.548
E2	HE2RTD4	3.429	0.293	3.429	-0.511	0.713
E2	HE2RTD5	5.791	0.288	5.791	-0.524	2.871
E3	HE3RTD1	1.524	-0.687	1.524	-0.281	1.628
E3	HE3RTD2	2.515	-0.687	2.515	-0.284	0.87
E3	HE3RTD3	2.972	-0.687	2.972	-0.285	0.738
E3	HE3RTD4	3.429	-0.686	3.429	-0.286	0.867
E3	HE3RTD5	5.791	-0.685	5.791	-0.294	2.912
E4	HE4RTD1	1.524	-0.279	1.524	0.721	1.664
E4	HE4RTD2	2.515	-0.276	2.515	0.724	0.937
E4	HE4RTD3	2.972	-0.275	2.972	0.725	0.817
E4	HE4RTD4	3.429	-0.274	3.429	0.726	0.935
E4	HE4RTD5	5.791	-0.269	5.791	0.733	2.934
F1	HF1TC1	2.515	0.013	2.514	-0.227	0.497
F1	HF1TC2	2.972	0.014	2.971	-0.234	0.193
F1	HF1TC3	3.429	0.015	3.429	-0.24	0.496
F1	HF1TC4	4.572	0.016	4.572	-0.257	1.611
F2	HF2TC1	1.524	-0.277	1.524	0.006	1.48
F2	HF2TC2	2.515	-0.276	2.515	0.003	0.544
F2	HF2TC3	2.972	-0.276	2.972	0.002	0.289
F2	HF2TC4	3.429	-0.276	3.429	0	0.538
F2	HF2TC5	4.572	-0.276	4.572	-0.003	1.623
F2	HF2TC6	6.858	-0.275	6.858	-0.01	3.893
F2	HF2TC7	9.144	-0.274	9.144	-0.018	6.176
HP	HHPTC1	2.467	0.008	2.467	-0.034	0.508
HP	HHPTC2	2.812	0.009	2.812	-0.038	0.163
HP	HHPTC3	2.813	0.009	2.813	-0.038	0.162
HP	HHPTC4	3.117	0.01	3.116	-0.042	0.141
HP	HHPTC5	3.117	0.01	3.116	-0.042	0.141
HP	HHPTC6	3.476	0.011	3.476	-0.047	0.501
SL	HSLTY	1.204	0.202	1.204	0.305	1.815
SL	HSL SConc	3.246	0.2	3.246	0.309	0.481
SL	HSL Sorel	3.246	0.2	3.246	0.309	0.481

Borehole	Sensor ID	Sensor depth [m]	Sensor X [m]	Sensor Y [m]	Sensor Z [m]	Distance to heater midpoint [m]
SM	HSMTY	1.503	0.193	1.503	-0.001	1.484
T1	T1TC1	0.305	-0.962	0.305	0.004	2.842
T1	T1TC2	0.61	-0.963	0.61	0.002	2.558
T1	T1TC3	0.914	-0.963	0.914	0	2.279
T1	T1TC4	1.219	-0.964	1.219	-0.002	2.008
T1	T1TC5	1.524	-0.965	1.524	-0.004	1.748
T1	T1TC6	1.829	-0.966	1.829	-0.006	1.506
T1	T1TC7	2.134	-0.967	2.134	-0.008	1.289
T1	T1TC8	2.515	-0.968	2.515	-0.011	1.081
T1	T1TC9	2.743	-0.968	2.743	-0.012	1.005
T1	T1TC10	2.972	-0.969	2.972	-0.014	0.979
T1	T1TC11	3.429	-0.97	3.429	-0.017	1.08
T1	T1TC12	3.658	-0.971	3.658	-0.019	1.195
T1	T1TC13	3.962	-0.971	3.962	-0.021	1.392
T1	T1TC14	4.267	-0.972	4.267	-0.023	1.623
T1	T1TC15	4.572	-0.973	4.572	-0.025	1.875
T1	T1TC16	4.877	-0.974	4.877	-0.027	2.141
T1	T1TC17	5.182	-0.975	5.181	-0.029	2.416
T1	T1TC18	5.486	-0.975	5.486	-0.031	2.698
T2	T2TC1	0.305	-0.66	0.305	0.012	2.753
T2	T2TC2	0.61	-0.661	0.61	0.013	2.459
T2	T2TC3	0.914	-0.663	0.914	0.014	2.168
T2	T2TC4	1.219	-0.665	1.219	0.016	1.882
T2	T2TC5	1.524	-0.667	1.524	0.017	1.602
T2	T2TC6	1.829	-0.669	1.829	0.018	1.333
T2	T2TC7	2.134	-0.67	2.134	0.019	1.084
T2	T2TC8	2.515	-0.673	2.515	0.02	0.825
T2	T2TC9	2.743	-0.674	2.743	0.021	0.725
T2	T2TC10	2.972	-0.675	2.972	0.022	0.688
T2	T2TC11	3.429	-0.678	3.429	0.024	0.827
T2	T2TC12	3.658	-0.679	3.658	0.025	0.972
T2	T2TC13	3.962	-0.681	3.962	0.026	1.207
T2	T2TC14	4.267	-0.683	4.267	0.027	1.468
T2	T2TC15	4.572	-0.685	4.572	0.028	1.743
T2	T2TC16	4.877	-0.687	4.877	0.029	2.026
T2	T2TC17	5.182	-0.688	5.182	0.03	2.315
T2	T2TC18	5.486	-0.69	5.486	0.031	2.608

Table A-5. Acoustic emission sensor coordinates. Same coordinate system as thermocouples and RTDs. Assumes boreholes are straight and sensors pressed against borehole wall, pointing towards HP borehole.

borehole	Sensor ID	Sensor depth [m]	Sensor X [m]	Sensor Y [m]	Sensor Z [m]	Distance to heater midpoint [m]
AE1	1	0.087	0.288	3.262	0.68	0.824
AE1	2	0.696	0.29	2.654	0.68	0.837
AE1	17	1.002	0.29	2.348	0.68	0.996
AE1	3	1.305	0.291	2.045	0.68	1.21
AE1	4	1.861	0.293	1.489	0.681	1.676
AE2	5	0.088	0.68	3.265	-0.286	0.77
AE2	6	0.694	0.68	2.659	-0.284	0.78
AE2	18	0.995	0.681	2.357	-0.283	0.944
AE2	7	1.307	0.681	2.045	-0.282	1.172
AE2	8	1.919	0.682	1.433	-0.281	1.699
AE3	9	0.085	-0.285	3.268	-0.484	0.608
AE3	10	0.699	-0.284	2.654	-0.482	0.62
AE3	11	1.31	-0.283	2.043	-0.48	1.071
AE3	12	1.921	-0.282	1.432	-0.478	1.63
AE4	13	0.083	-0.687	3.273	0.283	0.823
AE4	14	0.696	-0.683	2.66	0.284	0.828
AE4	15	1.306	-0.68	2.05	0.285	1.199
AE4	16	1.917	-0.677	1.439	0.286	1.714

Table A-6. TCO BATS2 major events (SN is serial number).

Date	Activity Category	Description
27-Oct-2021	BATS 2 Drilling & Coring	Drilling started for BATS 2 heated array.
1-Nov-2021	BATS 2 Brine Sampling	Brine samples collected from BATS 2 AE1 and E4 boreholes.
2-Feb-2022	BATS 2 Brine Sampling	Brine samples collected from BATS 2 AE1, AE3, E2, E3, E4, F1, and T1 boreholes.
18-Feb-2022	BATS 2 Drilling & Coring	Drilling completed for BATS 2 heated array.
24-Feb-2022	BATS 2 Brine Sampling	Brine samples collected from BATS 2 AE4, D, F2, SM, E2, and E3 boreholes.
28-Feb-2022	BATS 2 Drilling & Coring	All BATS 2 boreholes blown out with air and cleaned.
1-Mar-2022	BATS 2 Video Logging	Video logging of BATS 2 E1, E2, E3, E4, F1, F2, T1, and T2 boreholes.
3-Mar-2022	BATS 2 Permeability Testing	Permeability testing of BATS 2 SL borehole.
3-Mar-2022	BATS 2 Instrumentation Installation	Installation of the D inflatable packer in the BATS 2 D borehole.
7-Mar-2022	BATS 2 Permeability Testing	Permeability testing of BATS 2 HP borehole.
7-Mar-2022	BATS 2 Instrumentation Installation	Data collection started for datalogger SN 7071 file named BATS2_Array_Unheated_Gas_SN7071.
7-Mar-2022	BATS 2 Instrumentation Installation	Data collection started for datalogger SN 7072 file named BATS2_Array_Unheated_Temperature_SN7072.
8-Mar-2022	BATS 2 Brine Sampling	Brine samples collected from BATS 2 AE2, AE3, AE4, D, E1, E2, E3, E4, F1, F2, HP, SL, SM, T1, AND T2 boreholes.
14-Mar-2022	BATS 2 Video Logging	Video logging of BATS 2 AE1, AE2, AE3, AE4, D, HP, SL, and SM boreholes.
15-Mar-2022	BATS 2 Grouting Instrument Arrays	Instrument arrays grouted in BATS 2 T1, T2, and E1 boreholes.
21-Mar-2022	BATS 2 Grouting Instrument Arrays	Instrument arrays grouted in BATS 2 E2, E3, and E4 boreholes.
22-Mar-2022	BATS 2 Brine Sampling	Brine samples collected from BATS 2 AE2, AE3, AE4, D, F1, F2, HP, SL, AND SM boreholes.
23-Mar-2022	BATS 2 Instrumentation Installation	Data collection started for datalogger SN 29189 file named BATS2_ERT_RTDs_SN29189.
28-Mar-2022	BATS 2 Grouting Instrument Arrays	Instrument arrays grouted in BATS 2 F1 and F2 boreholes.
5-Apr-2022	BATS 2 Instrumentation Installation	Installation of the SL cement plug in the BATS 2 SL borehole.
5-Apr-2022	BATS 2 Instrumentation Installation	Data collection started for datalogger SN 19480 file named BATS2_Heated_Temperature_SN19480.
13-Apr-2022	BATS 2 Instrumentation Installation	Installation of the SM mechanical packer in the BATS 2 SM borehole.
14-Apr-2022	BATS 2 Instrumentation Installation	Installation of the HP packer assembly in the BATS 2 HP borehole.
25-Apr-2022	BATS 2 Instrumentation Installation	The Picarro and Gas Analyzer were started for gas flow measurements and data collection.
25-Apr-2022	BATS 2 Instrumentation Installation	Circulation plumbing completed and circulation flow started to heated and unheated arrays.
25-Apr-2022	BATS 2 Instrumentation Installation	Data collection started for datalogger SN 7069 file named BATS2_Array_D_Borehole_Inflation_SN7069.
25-Apr-2022	BATS 2 Instrumentation Installation	Data collection started for datalogger SN 16312 file named BATS2_Heated_Gas_SN16312.
25-Apr-2022	BATS 2 Instrumentation Installation	Data collection started for datalogger SN 7075 file named BATS2_LVDT_SG_TRH_SN7075.
25-Apr-2022	BATS 2 Instrumentation Installation	Data collection started for datalogger SN 29190 file named BATS2_Power_Controller_SN29190.
3-May-2022	BATS 2 Brine Sampling	Brine sample collected from SM borehole.
9-May-2022	BATS 2 Power Outage	Planned power outage, power restored 5/10/2022.
25-May-2022	BATS 2 Permeability Testing	Permeability testing of BATS 2 D borehole - nitrogen gas.
31-May-2022	BATS 2 Brine Sampling	Brine sample collected from SM borehole.
9-Jun-2022	BATS 2 Power Outage	Planned power outage, power restored 6/13/2022.
13-Jun-2022	BATS 2 Brine Sampling	Brine sample collected from SM borehole.
22-Jun-2022	BATS 2 Instrumentation Installation	Power controller testing and troubleshooting. Power controller issues resolved, and the power controller is ready to use for heating.

Date	Activity Category	Description
27-Jun-2022	BATS 2 Power Outage	Planned power outage, power restored 7/5/2022.
11-Jul-2022	BATS 2 Brine Sampling	Brine sample collected from SM borehole.
11-Jul-2022	BATS 2 Instrumentation Installation	Power controller settings re-configured.
18-Jul-2022	BATS 2 Permeability Testing	Permeability testing of BATS 2 D borehole - nitrogen gas. Test ended and nitrogen vented from the borehole.
18-Jul-2022	BATS 2 Permeability Testing	Permeability testing of BATS 2 D borehole - argon gas. The argon gas will also act as a tracer for the gas analyzer.
20-Jul-2022	BATS 2a Heating Event	The BATS 2 HP borehole heater was set to a 90 °C set point for 3 weeks of scheduled heating.
25-Jul-2022	BATS 2 Brine Sampling	Brine sample collected from SM borehole.
25-Jul-2022	BATS 2 Instrumentation Installation	Datalogger SN 29190 (power controller) was re-configured to capture additional power controller data.
29-Aug-2022	BATS 2 Power Outage	Planned Power Outage, power restored 9/6/2023
6-Sep-2022	BATS 2 Brine Sampling	Brine sample collected from SM borehole. 9 ml sample clear to cloudy in color
7-Sep-2022	BATS 2b Heating Event	The BATS 2 HP borehole heater was set to a 115 °C set point for 3 weeks of scheduled heating.
19-Sep-2022	BATS 2 Brine Sampling	Brine sample collected from SM borehole. 18 ml sample light brown in color
3-Oct-2022	BATS 2 Picarro Issues	Instrument not working as expected, no measurements were being made by the Picarro from 10/3/22 to 11/2/22
5-Oct-2022	BATS 2 Power Outage	Unexpected Power Outage from 10:24 to 11:20
12-Oct-2022	BATS 2 Brine Sampling	Brine sample collected from SM borehole. 19 ml sample light brown in color
12-Oct-2022	BATS 2c Heating Event	The BATS 2 HP borehole heater was set to a 130 °C set point for 3 weeks of scheduled heating.
24-Oct-2022	BATS 2 Brine Sampling	Brine sample collection attempted from SM borehole.
3-Nov-2022	BATS 2 Picarro Issues	Replacement Picarro installed.
7-Nov-2022	BATS 2 Brine Sampling	Brine sample collected from SM borehole. 14 ml sample
7-Nov-2022	BATS 2 ERT Issues	ERT file sizes started decreasing in size. Periodically the ERT is not finishing data runs. Issues persist through 12/5/22
14-Nov-2022	BATS 2 Brine Sampling	Brine sample collection attempted from SM borehole.
14-Nov-2022	BATS 2 Power Outage	Unexpected Power Outage from 07:43 to 09:08
16-Nov-2022	BATS 2d Heating Event	The BATS 2 HP borehole heater was set to a 140 °C set point, but test aborted after ~1.5 days
21-Nov-2022	BATS 2 gas analyzer issues	Gas analyzer is no longer recording data in P vs T mode
22-Nov-2022	BATS 2 Brine Sampling	Brine sample collection attempted from SM borehole.
22-Nov-2022	BATS 2 HP packer	packer removed from HP borehole to check heater, blister in packer rubber prevents re-insertion of packer.
30-Nov-2022	BATS 2 HP packer	packer blister bled using syringe, packer re-inserted into heated HP borehole and re-inflated
5-Dec-2022	BATS 2 ERT Issues	The ERT problem is related to the internal battery. The battery is low. The ERT was turned off to try to re-charge the battery.
7-Dec-2022	BATS 2 ERT Issues	The ERT was re-started. The small file size issue continued and the internal battery was low. Issue persisted through 12/14/22
7-Dec-2022	BATS 2 Gas Analyzer Issues	Gas analyzer is returning errors about RGA head
14-Dec-2022	BATS 2 ERT Issues	The ERT was removed from service and a replacement ERT will be installed in February.
14-Dec-2022	BATS 2 Gas Analyzer Issues	Gas analyzer is removed from service
19-Dec-2022	BATS 2 Brine Sampling	Brine sample collected from SM borehole. 34 ml sample
9-Jan-2023	BATS 2 Power Outage	Unexpected Power Outage from 19:20 to 20:06
10-Jan-2023	BATS 2 Brine Sampling	Brine sample collected from SM borehole. 6 ml sample light brown in color
18-Jan-2023	BATS 2 Gas Analyzer Issues	Repaired gas analyzer is re-connected and started in P vs T mode
20-Jan-2023	BATS 2 Power Outage	Unexpected Power Outage from 00:49 to 08:55
30-Jan-2023	BATS 2 Brine Sampling	Brine sample collected from SM borehole. 4 ml sample clear to colorless
21-Feb-2023	BATS 2 Brine Sampling	Brine sample collection attempted from SM borehole.
27-Feb-2023	BATS 2 ERT Issues	The replacement ERT was installed and ERT data collection resumed.
8-Mar-2023	BATS 2d Heating Event	The BATS 2 HP borehole heater was set to a 140 °C set point for 3 weeks of scheduled heating.

Date	Activity Category	Description
13-Mar-2023	BATS 2 Brine Sampling	Brine sample collected from SM borehole. 18 ml sample light brown in color
16-Mar-2023	BATS 2 Power Outage	Unexpected Power Outage, power restored 3/20/23
20-Mar-2023	BATS 2 Brine Sampling	Brine sample collected from SM borehole. 7 ml sample clear to colorless
28-Mar-2023	BATS 2 Brine Sampling	Brine sample collected from SM borehole. 3 ml sample clear to colorless
1-Apr-2023	BATS 2 Picarro Issues	Instrument has intermittent errors and is repeatedly not operating as expected. Errors continue through 7/2/23
3-Apr-2023	BATS 2 Brine Sampling	Brine sample collection attempted from SM borehole.
10-Apr-2023	BATS 2 Brine Sampling	Brine sample collection attempted from SM borehole.
10-Apr-2023	BATS 2 Power Outage	Unexpected Power Outage, power restored 4/17/23
17-Apr-2023	BATS 2 Brine Sampling	Brine sample collection attempted from SM borehole.
24-Apr-2023	BATS 2 Brine Sampling	Brine sample collection attempted from SM borehole.
1-May-2023	BATS 2 Brine Sampling	Brine sample collection attempted from SM borehole.
1-May-2023	BATS 2 Power Outage	Unexpected Power Outage, power restored 5/8/23
8-May-2023	BATS 2 Power Outage	Planned Power Outage, power restored 11:05
8-May-2023	BATS 2 Power Outage	Unexpected Power Outage, power restored 5/9/23
10-May-2023	BATS 2 ERT Issues	The ERT stopped working due to low internal battery voltage. The ERT was re-started.
12-May-2023	BATS 2 Power Outage	Unexpected Power Outage, power restored 5/16/23
16-May-2023	BATS 2 Power Outage	Multiple unexpected Power Outages during the day
17-May-2023	BATS 2 ERT Issues	The ERT stopped working due to low internal battery voltage. The ERT was turned off. A replacement ERT is installed in July.
23-May-2023	BATS 2 Power Outage	Unexpected Power Outage, power restored 5/24/23
19-Jun-2023	BATS 2 Power Outage	Planned Power Outage, power restored 6/21/23
21-Jun-2023	BATS 2 Brine Sampling	Brine sample collected from SM borehole. 7 ml sample light brown in color
22-Jun-2023	BATS 2 Power Outage	Unexpected Power Outage from 23:20 to 23:30
2-Jul-2023	BATS 2 Picarro Issues	Picarro is no longer working. All troubleshooting and attempted fixes did not resolve instrument issues. Picarro removed from service.
10-Jul-2023	BATS 2 ERT Issues	The replacement ERT was installed and ERT data collection resumed.
24-Jul-2023	BATS 2 Power Outage	Planned Power Outage at 08:45
25-Jul-2023	BATS 2 Brine Sampling	Brine sample collected from SM borehole. 17 ml sample light brown in color
7-Aug-2023	BATS 2 Brine Sampling	Brine sample collection attempted from SM borehole.
7-Aug-2023	BATS 2 Power Outage	Planned Power Outage at 08:45

Table A-7. BATS 2 brine production and sample collection log.

Date	ID	Volume Collected, mL	Notes
11/01/21	AE1	5	Vacuum pump: 2 sample bottles used for collection.
11/01/21	E4	3	Vacuum pump: 2 sample bottles used for collection. More brine in the borehole that the tubing and pump could not collect.
02/02/22	AE1	3	Brine squeezed from sponge directly into sample vials.
02/02/22	AE2	1.5	No sample retrieved from sponge due to insufficient brine volume. Sponge saved in plastic bag.
02/02/22	AE3	8	Brine squeezed from sponge directly into sample vials.
02/02/22	E2	20	Brine squeezed from sponge directly into sample vials.
02/02/22	E3	12	Brine squeezed from sponge directly into sample vials.
02/02/22	E4	1.5	Brine squeezed from sponge directly into sample vials.
02/02/22	F1	12	Brine squeezed from sponge directly into sample vials.
02/02/22	T1	8	Brine squeezed from sponge directly into sample vials.
02/02/22	T1	8	Brine squeezed from sponge directly into sample vials.
02/24/22	AE4	10	Brine squeezed from sponge directly into sample vials. Liquid is brown - most likely due to salt drill cuttings.
02/24/22	D	10	Brine squeezed from sponge directly into sample vials. Liquid is brown - most likely due to salt drill cuttings.
02/24/22	E1	1	Sample volume is too small for getting brine into sample vial. Sponge with brine was saved and bagged.
02/24/22	E2	10	Brine squeezed from sponge directly into sample vials. Liquid is cloudy - most likely due to salt drill cuttings.
02/24/22	E3	12	Brine squeezed from sponge directly into sample vials. Liquid is cloudy - most likely due to salt drill cuttings.
02/24/22	F2	8	Brine squeezed from sponge directly into sample vials. Liquid is brown - most likely due to salt drill cuttings.
02/24/22	SM	10	Brine squeezed from sponge directly into sample vials. Liquid is brown in color - most likely due to salt cuttings in the borehole from drilling.
02/24/22	T2	2	Sample volume is too small for getting brine into sample vial. Sponge with brine was saved and bagged.
03/22/22	AE1	1	Not enough sample for transfer to vial.
03/22/22	AE2	5	Brine squeezed from sponge directly into sample vials. Cloudy in color.
03/22/22	AE3	8	Brine squeezed from sponge directly into sample vials. Brown in color.
03/22/22	AE4	8	Brine squeezed from sponge directly into sample vials. Brown in color.
03/22/22	D	10	Brine squeezed from sponge directly into sample vials. Brown in color.
03/22/22	F1	8	Brine squeezed from sponge directly into sample vials. Light brown in color.
03/22/22	F2	8	Brine squeezed from sponge directly into sample vials. Brown in color.
03/22/22	HP	2	Brine squeezed from sponge directly into sample vials. Brown in color. Only 1 or 2 drops transferred to vial.
03/22/22	SL	3	Brine squeezed from sponge directly into sample vials. Brown in color.
03/22/22	SM	5	Brine squeezed from sponge directly into sample vials. Brown in color.
05/03/22	SM	68	Brine sampled behind mechanical packer (installed 4/13/22), collected with vacuum pump.
05/31/22	SM	35	Light brown brine sample collected with vacuum pump.
06/13/22	SM	12	Brine sample collected with vacuum pump.
07/11/22	SM	34	Light brown brine sample collected with vacuum pump.
07/25/22	SM	39	Light brown to clear brine sample collected with vacuum pump.
08/08/22	SM	20	Brine sample collected with vacuum pump.
08/17/22	SM	2.5	Light brown brine sample collected with vacuum pump.

Date	ID	Volume Collected, mL	Notes
9/6/2022	SM	9	Clear to cloudy sample collected with vacuum pump
9/19/2022	SM	18	Light brown sample collected with vacuum pump
10/12/2022	SM	19	Light brown sample collected with vacuum pump
10/24/2022	SM	0	Vacuum pump, no sample collected
11/7/2022	SM	14	Sample collected with vacuum pump
11/14/2022	SM	0	Vacuum pump, no sample collected
11/22/2022	SM	0	Vacuum pump, no sample collected
12/19/2022	SM	34	Sample collected with vacuum pump
1/10/2023	SM	6	Light brown sample collected with vacuum pump
1/30/2023	SM	4	Clear to colorless sample collected with vacuum pump
2/21/2023	SM	0	Vacuum pump, no sample collected
3/13/2023	SM	18	Light brown sample collected with vacuum pump
3/20/2023	SM	7	Clear to colorless sample collected with vacuum pump
3/28/2023	SM	3	Clear to colorless sample collected with vacuum pump
4/3/2023	SM	0	Vacuum pump, no sample collected
4/10/2023	SM	0	Vacuum pump, no sample collected
4/17/2023	SM	0	Vacuum pump, no sample collected
4/24/2023	SM	0	Vacuum pump, no sample collected
5/1/2023	SM	0	Vacuum pump, no sample collected
6/21/2023	SM	7	Light brown sample collected with vacuum pump
7/25/2023	SM	17	acuum pump
8/7/2023	SM	0	Vacuum pump, no sample collected

Volumes from sponge collection are estimated without graduated cylinder.

Table A-8. BATS 2 brine ionic species composition data, values in g/L. Blue samples collected with vacuum pump; orange samples collected with sponge. SM samples after 2/22/22 in next table.

Borehole	Species	11/01/21	11/01/21	02/02/22	02/24/22	03/08/22	03/22/22
AE1	B	1.547	1.483	1.548			
	Ca	0.274	0.266	0.28			
	K	14.016	13.586	14.422			
	Li	0.041	0.04	0.042			
	Mg	21.379	20.609	24.083			
	Na	65.671	64.039	71.873			
	Cl	160.372	163.551	194.362			
	Br	3.707	3.536	3.793			
	SO_4	19.138	19.182	21.168			
AE3	B			1.599			1.758
	Ca			0.294			0.297
	K			15.602			17.844
	Li			0.042			0.046
	Mg			24.037			27.802
	Na			75.768			68.141
	Cl			192.408			207.766
	Br			3.684			3.612
	SO_4			21.080			24.766
AE4	B				1.648	1.821	1.712

Borehole	Species	11/01/21	11/01/21	02/02/22	02/24/22	03/08/22	03/22/22
	Ca				0.329	0.295	0.309
	K				15.659	17.686	17.116
	Li				0.043	0.046	0.045
	Mg				23.457	27.045	25.301
	Na				74.687	65.048	71.463
	Cl				199.343	196.154	197.673
	Br				3.731	4.213	3.560
	SO_4				21.282	24.452	22.575
D	B				1.669		1.715
	Ca				0.31		0.296
	K				16.319		17.124
	Li				0.044		0.045
	Mg				24.697		25.753
	Na				74.583		69.628
	Cl				195.406		197.765
	Br				3.811		3.493
	NO_3						5.418
	SO_4				21.422		22.345
E1	B					1.955	
	Ca					0.324	
	K					19.433	
	Li					0.048	
	Mg					28.629	
	Na					66.935	
	Cl					191.473	
	Br					4.097	
	SO_4					24.256	
E2	B			1.642	1.671	1.964	
	Ca			0.318	0.326	0.283	
	K			15.715	16.667	19.437	
	Li			0.043	0.043	0.048	
	Mg			23.596	24.01	29.3	
	Na			74.086	79.805	61.446	
	Cl			192.731	196.874	203.890	
	Br			3.800	3.908	3.722	
	SO_4			21.191	21.258	26.292	
E3	B			1.666	1.655	1.637	
	Ca			0.322	0.315	0.33	
	K			16.642	16.164	15.933	
	Li			0.044	0.043	0.043	
	Mg			24.055	23.122	23.179	
	Na			77.711	78.6	76.814	
	Cl			194.674	193.399	194.004	
	Br			3.586	3.758	3.342	
	SO_4			20.784	20.750	20.470	
E4	B	0.439	0.421				
	Ca	0.029	0.025				
	K	0.244	0.285				
	Li	0.023	0.023				
	Mg	0.14	0.131				
	Na	0.116	0.168				
	Cl	5.072	5.026				
	SO_4	2.110					
F1	B			1.639		1.826	1.93
	Ca			0.313		0.317	0.283
	K			16.183		18.119	18.583
	Li			0.043		0.046	0.048
	Mg			23.778		27.421	29.068

Borehole	Species	11/01/21	11/01/21	02/02/22	02/24/22	03/08/22	03/22/22
	Na			75.495		68.445	64.949
	Cl			194.048		197.788	195.659
	Br			3.965		3.550	3.679
	NO_3						4.541
	SO_4			20.907		23.597	24.488
	B				1.632		1.727
	Ca				0.301		0.313
	K				15.863		16.903
	Li				0.043		0.044
F2	Mg				22.812		24.345
	Na				75.909		75.298
	Cl				190.590		164.928
	Br				3.623		3.216
	SO_4				19.127		18.713
	B					1.81	
	Ca					0.298	
	K					18.592	
	Li					0.047	
HP	Mg					29.206	
	Na					63.484	
	Cl					205.887	
	Br					3.702	
	SO_4					3.702	
	B					1.896	
	Ca					0.288	
	K					19.127	
	Li					0.048	
SL	Mg					31.019	
	Na					61.374	
	Cl					205.776	
	Br					3.761	
	SO_4					26.457	
	B				1.582		1.684
	Ca				0.317		0.343
	K				16.155		17.262
	Li				0.043		0.044
	Mg				24.482		26.118
SM	Na				74.918		70.999
	Cl				204.994		189.717
	Br				3.783		3.390
	NO_3						
	SO_4				22.334		21.576
	B			1.642		1.903	
	Ca			0.317		0.315	
	K			15.856		18.812	
	Li			0.042		0.047	
T1	Mg			23.086		28.419	
	Na			76.059		65.459	
	Cl			210.791		192.670	
	Br			3.820		3.782	
	SO_4			21.468		24.260	
	B					1.778	
	Ca					0.313	
	K					17.347	
T2	Li					0.045	
	Mg					25.593	
	Na					69.118	
	Cl					185.574	

Borehole	Species	11/01/21	11/01/21	02/02/22	02/24/22	03/08/22	03/22/22
	Br					3.292	
	SO_4					21.983	

Table A-9. BATS 2 brine ionic species composition data for heated SM borehole, values in g/L.

	B	Ca	K	Li	Mg	Na	Cl	Br	SO_4
2/24/22	1.339	0.245	16.16	0.025	24.48	74.92	209.4	4.217	35.85
3/22/22	1.255	0.292	17.26	0.028	26.12	71.00	194.6	4.127	36.85
5/31/22	1.361	0.238	16.18	0.027	24.20	71.94	195.5	4.117	34.00
6/13/22	1.337	0.226	15.93	0.026	23.88	71.96	199.6	4.143	34.76
7/11/22	1.383	0.244	16.28	0.027	24.03	73.58	197.0	4.202	34.68
7/25/22	1.332	0.215	15.85	0.024	24.06	77.74	194.8	4.356	27.03
8/8/22	1.236	0.231	15.05	0.024	22.66	75.52	184.6	4.251	24.39
8/17/22	1.329	0.262	16.01	0.026	24.34	74.78	192.2	4.347	27.44
9/6/22	1.287	0.257	15.56	0.026	23.77	77.97	189.3	4.244	24.27
9/19/22	1.238	0.225	15.67	0.027	23.29	78.80	190.7	4.254	26.17
10/12/22	1.216	0.246	15.19	0.026	22.95	75.44	188.2	4.282	26.53
11/7/22	1.187	0.243	14.88	0.024	22.55	76.97	187.1	4.228	25.41
12/19/22	1.122	0.249	13.97	0.022	21.65	82.11	187.1	4.124	24.49
1/10/23	1.189	0.255	14.51	0.025	23.99	78.03	192.9	4.308	26.83
1/30/23	1.225	0.240	14.57	0.024	23.51	77.69	190.8	4.291	26.70
3/13/23	1.215	0.263	14.52	0.024	22.44	79.47	189.6	4.240	25.41
3/20/23	1.211	0.271	14.50	0.022	21.92	81.36	188.0	4.164	26.98
3/28/23	1.239	0.306	14.24	0.023	21.91	78.87	185.6	4.185	25.03
6/21/23	1.094	0.375	13.70	0.022	19.27	83.49	186.0	3.747	17.21

Table A-10. Desiccant water production data for heated array.

Date Time Start	Date Time End	ΔTime [day]	ΔH_2O mass [g]	Rate of change H_2O [g/day]	Upstream gas mass flow rate [std mL/min]
4/25/22 13:22	4/26/22 12:46	0.9750	14.17	14.53	500
4/26/22 12:46	4/27/22 10:00	0.8847	13.03	14.73	500
4/27/22 10:10	4/29/22 00:15	1.5868	25.08	15.81	500
5/02/22 08:40	5/03/22 12:04	1.1417	16.80	14.72	500
5/03/22 12:04	5/04/22 07:53	0.8257	4.91	5.95	200
5/04/22 07:53	5/05/22 07:43	0.9931	6.00	6.04	200
5/05/22 07:48	5/09/22 08:10	4.0153	22.91	5.71	200
5/10/22 07:55	5/11/22 09:15	1.0556	5.07	4.80	200
5/11/22 09:15	5/16/22 08:30	4.9688	12.60	2.54	200
5/16/22 08:30	5/18/22 09:51	2.0563	2.23	1.08	75
5/18/22 09:51	5/23/22 08:14	4.9326	5.96	1.21	75
5/23/22 08:14	5/24/22 13:51	1.2340	1.47	1.19	75
5/24/22 13:51	5/25/22 07:45	0.7458	0.80	1.07	75
5/25/22 07:45	5/31/22 08:03	6.0125	6.11	1.02	75
5/31/22 08:03	6/02/22 09:06	2.0437	2.53	1.24	75
6/02/22 09:06	6/06/22 07:54	3.9500	3.38	0.86	75
6/06/22 07:54	6/09/22 08:33	3.0271	2.97	0.98	75
6/09/22 08:33	6/13/22 08:00	3.9771	3.40	0.85	75
6/13/22 08:00	6/15/22 07:55	1.9965	1.73	0.87	75
6/15/22 07:55	6/22/22 08:11	7.0111	5.98	0.85	75
6/22/22 08:11	6/27/22 08:00	4.9924	3.99	0.80	75
7/05/22 09:45	7/07/22 08:24	1.9437	3.66	1.88	75
7/07/22 08:24	7/11/22 07:55	3.9799	5.75	1.44	75
7/11/22 07:55	7/18/22 08:14	7.0132	7.72	1.10	75
7/18/22 08:14	7/20/22 07:56	1.9875	1.64	0.83	75
7/20/22 07:56	7/25/22 08:02	5.0042	6.21	1.24	75
7/25/22 08:02	7/26/22 11:32	1.1458	1.37	1.20	75
7/26/22 11:32	8/01/22 07:54	5.8486	7.06	1.21	75
8/01/22 07:54	8/04/22 10:34	3.1111	3.02	0.97	75
4/25/22 13:22	4/26/22 12:46	0.9750	14.17	14.53	500
8/4/22 10:34	8/8/22 07:56	3.8903	3.32	0.85	75
8/8/22 07:56	8/10/22 07:47	1.9938	1.84	0.92	75
8/10/22 07:55	8/15/22 07:45	4.9931	6.34	1.27	75
8/15/22 07:45	8/16/22 10:42	1.1229	1.74	1.55	75
8/16/22 10:42	8/17/22 07:34	0.8694	1.34	1.5412	75
8/17/22 07:34	8/22/22 07:45	5.0076	8.1	1.6175	75
8/22/22 07:45	8/24/22 07:25	1.9861	2.87	1.445	75
8/24/22 07:25	8/29/22 07:39	5.0097	7.08	1.4133	75
8/29/22 07:39	9/6/22 08:45	8.0458	10.83	1.346	75
9/6/22 08:45	9/7/22 14:55	1.2569	1.79	1.4241	75
9/7/22 14:55	9/12/22 08:57	4.7514	9.52	2.0036	75
9/12/22 08:57	9/19/22 08:30	6.9812	13.18	1.8879	75
9/19/22 08:30	9/22/22 09:36	3.0458	5.1	1.6744	75
9/22/22 09:36	9/26/22 07:38	3.9181	5.79	1.4778	75
9/26/22 07:38	9/28/22 08:20	2.0292	2.86	1.4094	75
9/28/22 08:20	10/3/22 07:48	4.9778	7.84	1.575	75
10/3/22 07:48	10/5/22 08:08	2.0139	3.75	1.8621	75
10/5/22 08:08	10/12/22 09:54	7.0736	14.47	2.0456	75
10/12/22 09:54	10/17/22 07:31	4.9007	14.86	3.0322	75
10/17/22 07:31	10/19/22 07:55	2.0167	6.29	3.119	75
10/19/22 07:55	10/24/22 07:33	4.9847	16.22	3.2539	75
10/24/22 07:33	11/1/22 08:40	8.0465	26.04	3.2362	75
11/1/22 08:40	11/2/22 11:46	1.1292	4.01	3.5513	75

Date Time Start	Date Time End	ΔTime [day]	ΔH_2O mass [g]	Rate of change H_2O [g/day]	Upstream gas mass flow rate [std mL/min]
11/2/22 11:46	11/3/22 07:54	0.8389	2.64	3.1470	75
11/3/22 07:54	11/7/22 07:50	3.9972	10.45	2.6143	75
11/7/22 07:50	11/9/22 08:44	2.0375	4.64	2.2773	75
11/9/22 08:44	11/14/22 10:00	5.0528	10.71	2.1196	75
11/14/22 10:00	11/16/22 07:37	1.9007	3.87	2.0361	75
11/16/22 07:37	11/21/22 08:10	5.0229	13.15	2.6180	75
11/21/22 08:10	11/22/22 07:47	0.9840	2.16	2.1951	75
11/22/22 07:47	11/28/22 10:00	6.0924	0.34	0.0558	0
11/28/22 10:00	11/30/22 08:07	1.9215	0.03	0.0156	0
11/30/22 08:07	12/5/22 08:46	5.0271	14.44	2.8724	100
12/5/22 08:46	12/7/22 08:59	2.0090	6.1	3.0363	100
12/7/22 08:59	12/11/22 20:20	4.4729	13.03	2.9131	100
12/12/22 10:10	12/13/22 08:40	0.9375	2.63	2.8053	100
12/13/22 08:40	12/14/22 08:55	1.0104	2.64	2.6128	100
12/14/22 08:55	12/15/22 11:13	1.0958	3.06	2.7924	100
12/15/22 11:13	12/16/22 08:18	0.8785	2.47	2.8117	100
12/16/22 08:18	12/19/22 07:25	2.9632	8.4	2.8348	100
12/19/22 07:25	12/21/22 08:10	2.0313	5.63	2.7717	100
12/21/22 08:10	1/4/23 08:55	14.0313	39.43	2.8102	100
1/6/23 09:05	1/10/23 08:30	3.9757	10.86	2.7316	100
1/10/23 08:30	1/17/23 07:54	6.9750	19.35	2.7742	100
1/17/23 07:54	1/18/23 09:00	1.0458	2.89	2.7633	100
1/18/23 09:00	1/23/23 08:50	4.9931	13.87	2.7779	100
1/23/23 08:50	1/30/23 09:40	7.0347	19.43	2.7620	100
1/30/23 09:40	2/6/23 08:15	6.9410	19.59	2.8224	100
2/6/23 08:15	2/8/23 08:29	2.0097	5.75	2.8611	100
2/8/23 08:29	2/9/23 07:53	0.9750	2.71	2.7795	100
2/9/23 07:53	2/13/23 07:40	3.9910	10.71	2.6836	100
2/13/23 07:40	2/15/23 07:45	2.0035	5.6	2.7951	100
2/15/23 07:45	2/21/23 08:05	6.0139	17.04	2.8334	100
2/21/23 08:05	2/22/23 08:40	1.0243	3.03	2.9581	100
2/22/23 08:40	2/27/23 08:04	4.9750	14.01	2.8161	100
2/27/23 08:04	3/6/23 07:35	6.9799	19.55	2.8009	100
3/6/23 07:35	3/8/23 07:37	2.0014	5.67	2.8330	100
3/8/23 07:37	3/13/23 07:44	5.0049	19.22	3.8403	100
3/13/23 07:44	3/15/23 08:33	2.0340	7.57	3.7217	100
3/15/23 08:48	3/20/23 07:47	4.9576	18.78	3.7881	100
3/20/23 07:47	3/22/23 07:50	2.0021	8.02	4.0058	100
3/22/23 07:50	3/23/23 12:00	1.1736	9.13	7.7794	200
3/23/23 12:00	3/28/23 08:35	4.8576	57.05	11.7444	300
3/28/23 08:35	3/29/23 09:19	1.0306	16.94	16.4377	400
3/29/23 09:19	4/3/23 08:45	4.9764	45.41	9.1251	400
4/3/23 08:45	4/4/23 08:35	0.9931	2.51	2.5276	150
4/4/23 08:35	4/5/23 07:37	0.9597	3	3.1259	150
4/5/23 07:37	4/10/23 08:27	5.0347	12.56	2.4947	100
4/10/23 08:27	4/12/23 07:38	1.9660	4.98	2.5331	100
4/12/23 07:38	4/17/23 07:55	5.0118	12.55	2.5041	100
4/17/23 07:55	4/19/23 08:40	2.0313	5.26	2.5895	100
4/19/23 08:40	4/24/23 08:05	4.9757	13.08	2.6288	100
4/24/23 08:05	4/26/23 07:55	1.9931	5.43	2.7245	100
4/26/23 07:55	5/1/23 09:18	5.0576	13.9	2.7483	100
5/1/23 09:18	5/8/23 08:45	6.9771	18.81	2.6960	100
5/8/23 08:45	5/10/23 08:03	1.9708	5.25	2.6638	100
5/10/23 08:03	5/13/23 03:37	2.8153	7.87	2.7955	100
5/16/23 12:48	5/17/23 08:50	0.8347	2.28	2.7314	100

Date Time Start	Date Time End	ΔTime [day]	ΔH_2O mass [g]	Rate of change H_2O [g/day]	Upstream gas mass flow rate [std mL/min]
5/17/23 08:50	5/22/23 08:21	4.9799	13.74	2.7591	100
5/22/23 08:21	5/31/23 07:57	8.9833	1.57	0.1748	100
5/31/23 07:57	6/5/23 08:30	5.0229	14.63	2.9127	100
6/5/23 08:30	6/6/23 09:00	1.0208	3.13	3.0661	100
6/6/23 09:00	6/7/23 10:27	1.0604	3.69	3.4798	100
6/7/23 10:27	6/12/23 07:59	4.8972	14.29	2.9180	100
6/12/23 08:07	6/14/23 08:24	2.0118	6.1	3.0321	100
6/14/23 08:24	6/19/23 07:44	4.9722	14.42	2.9001	100
6/19/23 07:44	6/21/23 08:00	2.0111	0.5	0.2486	0
6/21/23 08:00	6/26/23 08:03	5.0021	7.53	1.5054	100
6/26/23 08:13	6/27/23 07:40	0.9771	2.77	2.8350	100
6/27/23 07:40	6/29/23 08:35	2.0382	6.06	2.9732	100
6/29/23 08:35	7/3/23 07:43	3.9639	12.79	3.2266	100
7/3/23 07:43	7/5/23 09:09	2.0597	6.37	3.0927	100
7/5/23 09:09	7/10/23 08:37	4.9778	15.98	3.2103	100
7/10/23 08:37	7/12/23 07:58	1.9729	6.35	3.2186	100
7/12/23 07:58	7/24/23 07:25	11.9771	37.77	3.1535	100
7/24/23 07:25	7/25/23 07:45	1.0139	2.49	2.4559	100
7/25/23 07:45	7/31/23 08:07	6.0153	18.33	3.0472	100
7/31/23 08:07	8/2/23 07:26	1.9715	5.66	2.8709	100
8/2/23 07:26	8/7/23 07:40	5.0097	14.86	2.9662	100

Table A-11. Desiccant water production data for unheated array.

Date Time Start	Date Time End	ΔTime [day]	ΔH_2O mass [g]	Rate of change H_2O mass [g/day]	Upstream gas mass flow rate [std mL/min]
4/25/22 13:18	4/26/22 12:46	0.9778	11.07	11.3216	500
4/26/22 12:46	4/27/22 10:00	0.8847	9.7	10.9639	500
4/27/22 10:10	5/2/22 08:30	4.9306	14.61	2.9632	500
5/2/22 08:30	5/3/22 12:04	1.1486	0.57	0.4963	50
5/3/22 12:04	5/4/22 07:53	0.8257	0.44	0.5329	50
5/4/22 07:53	5/5/22 07:43	0.9931	0.68	0.6848	50
5/5/22 07:43	5/9/22 08:10	4.0188	2.44	0.6072	50
5/10/22 07:55	5/11/22 09:22	1.0604	0.6	0.5658	50
5/11/22 09:22	5/16/22 08:30	4.9639	2.67	0.5379	50
5/16/22 08:36	5/18/22 09:52	2.0528	0.83	0.4043	50
5/18/22 09:52	5/23/22 08:15	4.9326	1.93	0.3913	50
5/23/22 08:15	5/24/22 13:51	1.2333	0.58	0.4703	50
5/24/22 13:51	5/25/22 07:48	0.7479	0.31	0.4145	50
5/25/22 07:48	5/31/22 08:04	6.0111	1.89	0.3144	25
5/31/22 08:04	6/2/22 09:08	2.0444	0.78	0.3815	25
6/2/22 09:08	6/6/22 08:00	3.9528	1.25	0.3162	25
6/6/22 08:00	6/9/22 08:33	3.0229	1.2	0.397	25
6/9/22 08:33	6/13/22 08:00	3.9771	1.36	0.342	25
6/13/22 08:00	6/15/22 07:55	1.9965	0.66	0.3306	25
6/15/22 07:55	6/22/22 08:30	7.0243	2.58	0.3673	25
6/22/22 08:30	6/27/22 08:00	4.9792	1.75	0.3515	25
7/5/22 09:45	7/7/22 08:30	1.9479	1.1	0.5647	25
7/7/22 08:30	7/11/22 07:55	3.9757	1.79	0.4502	25
7/11/22 07:55	7/18/22 08:18	7.016	2.74	0.3905	25
7/18/22 08:18	7/20/22 07:58	1.9861	0.81	0.4078	25
7/20/22 07:58	7/25/22 08:09	5.0076	2.21	0.4413	25
7/25/22 08:09	7/26/22 11:32	1.141	0.45	0.3944	25
7/26/22 11:32	8/1/22 07:55	5.8493	2.46	0.4206	25
8/1/22 07:55	8/4/22 10:34	3.1104	1.29	0.4147	25
8/4/22 10:34	8/8/22 08:15	3.9035	1.62	0.42	25
8/8/22 08:15	8/10/22 07:47	1.9806	0.9	0.45	25
8/10/22 07:47	8/15/22 07:45	4.9986	2.07	0.41	25
8/15/22 07:45	8/16/22 10:42	1.1229	0.49	0.44	25
8/16/22 10:42	8/17/22 07:34	0.8694	0.41	0.4716	25
8/17/22 07:34	8/22/22 07:40	5.0042	4.48	0.8953	25
8/22/22 07:40	8/24/22 07:28	1.9917	0.81	0.4067	25
8/24/22 07:28	8/29/22 07:28	5	2.02	0.404	25
8/29/22 07:28	9/6/22 08:45	8.0535	3.3	0.4098	25
9/6/22 08:45	9/7/22 14:55	1.2569	0.66	0.5251	25
9/7/22 14:55	9/12/22 08:40	4.7396	2.2	0.4642	25
9/12/22 08:40	9/19/22 08:30	6.9931	3.12	0.4462	25
9/19/22 08:30	9/22/22 09:27	3.0396	1.19	0.3915	25
9/22/22 09:27	9/26/22 07:30	3.9187	1.7	0.4338	25
9/26/22 07:30	9/28/22 08:20	2.0347	0.94	0.462	25
9/28/22 08:20	10/3/22 07:48	4.9778	1.99	0.3998	25
10/3/22 07:48	10/5/22 08:05	2.0118	0.39	0.1939	25
10/5/22 08:05	10/12/22 09:54	7.0757	3.6	0.5088	25
10/12/22 09:54	10/17/22 07:31	4.9007	1.99	0.4061	25
10/17/22 07:31	10/19/22 07:58	2.0187	0.68	0.3368	25
10/19/22 07:58	10/24/22 07:33	4.9826	2.48	0.4977	25
10/24/22 07:33	11/1/22 08:40	8.0465	3.75	0.4660	25
11/1/22 08:40	11/2/22 11:46	1.1292	0.57	0.5048	25
11/2/22 11:46	11/3/22 07:54	0.8389	0.09	0.1073	25
11/3/22 07:54	11/7/22 07:50	3.9972	1.95	0.4878	25

Date Time Start	Date Time End	ΔTime [day]	ΔH_2O mass [g]	Rate of change H_2O mass [g/day]	Upstream gas mass flow rate [std mL/min]
11/7/22 07:50	11/9/22 08:44	2.0375	0.95	0.4663	25
11/9/22 08:44	11/14/22 10:00	5.0528	2.04	0.4037	25
11/14/22 10:00	11/16/22 07:37	1.9007	0.59	0.3104	25
11/16/22 07:37	11/21/22 08:10	5.0229	2.16	0.4300	25
11/21/22 08:10	11/22/22 07:47	0.9840	0.36	0.3658	25
11/22/22 07:47	11/28/22 10:00	6.0924	2.55	0.4186	25
11/28/22 10:00	11/30/22 08:07	1.9215	0.74	0.3851	25
11/30/22 08:07	12/5/22 08:46	5.0271	2.2	0.4376	25
12/5/22 08:46	12/7/22 08:59	2.0090	0.97	0.4828	25
12/7/22 08:59	12/12/22 10:10	5.0493	2.29	0.4535	25
12/12/22 10:10	12/13/22 08:40	0.9375	0.41	0.4373	25
12/13/22 08:40	12/14/22 08:55	1.0104	0.27	0.2672	25
12/14/22 08:55	12/15/22 11:13	1.0958	0.35	0.3194	25
12/15/22 11:13	12/16/22 08:18	0.8785	0.35	0.3984	25
12/16/22 08:18	12/19/22 07:25	2.9632	1.18	0.3982	25
12/19/22 07:25	12/21/22 08:10	2.0313	0.69	0.3397	25
12/21/22 08:10	1/4/23 08:55	14.0313	6.26	0.4461	25
1/4/23 08:55	1/10/23 08:30	5.9826	2.37	0.3961	25
1/10/23 08:30	1/17/23 07:54	6.9750	2.83	0.4057	25
1/17/23 07:54	1/18/23 08:50	1.0389	0.55	0.5294	25
1/18/23 08:50	1/23/23 08:50	5.0000	2.15	0.4300	25
1/23/23 08:50	1/30/23 09:40	7.0347	2.93	0.4165	25
1/30/23 09:40	2/6/23 08:15	6.9410	3.43	0.4942	25
2/6/23 08:15	2/8/23 08:29	2.0097	0.96	0.4777	25
2/8/23 08:29	2/9/23 07:53	0.9750	0.32	0.3282	25
2/9/23 07:53	2/13/23 07:45	3.9944	1.79	0.4481	25
2/13/23 07:45	2/15/23 07:49	2.0028	0.87	0.4344	25
2/15/23 07:49	2/21/23 08:08	6.0132	3.16	0.5255	25
2/21/23 08:08	2/22/23 08:40	1.0222	0.52	0.5087	25
2/22/23 08:40	2/27/23 08:04	4.9750	2.35	0.4724	25
2/27/23 08:04	3/6/23 07:35	6.9799	3.34	0.4785	25
3/6/23 07:35	3/8/23 07:37	2.0014	0.91	0.4547	25
3/8/23 07:37	3/13/23 07:44	5.0049	2.71	0.5415	25
3/13/23 07:44	3/15/23 08:33	2.0340	1.03	0.5064	25
3/15/23 08:33	3/20/23 07:47	4.9681	2.45	0.4932	25
3/20/23 07:47	3/22/23 07:50	2.0021	1.31	0.6543	25
3/22/23 07:50	3/23/23 12:00	1.1736	1.01	0.8606	25
3/23/23 12:00	3/28/23 08:35	4.8576	7.64	1.5728	50
3/28/23 08:35	3/29/23 09:19	1.0306	2.03	1.9698	50
3/29/23 09:19	4/3/23 08:45	4.9764	6.6	1.3263	50
4/3/23 08:45	4/4/23 08:35	0.9931	0.86	0.8660	50
4/4/23 08:38	4/5/23 07:45	0.9632	0.63	0.6541	50
4/5/23 07:45	4/10/23 08:32	5.0326	2.6	0.5166	25
4/10/23 08:32	4/12/23 07:43	1.9660	0.85	0.4324	25
4/12/23 07:43	4/17/23 08:02	5.0132	2.32	0.4628	25
4/17/23 08:02	4/19/23 08:45	2.0299	0.99	0.4877	25
4/19/23 08:45	4/24/23 08:09	4.9750	2.27	0.4563	25
4/24/23 08:09	4/26/23 08:00	1.9938	0.95	0.4765	25
4/26/23 08:00	5/1/23 09:22	5.0569	2.52	0.4983	25
5/1/23 09:22	5/8/23 08:55	6.9813	3.17	0.4541	25
5/8/23 08:55	5/10/23 08:06	1.9660	0.88	0.4476	25
5/10/23 08:06	5/13/23 09:00	3.0375	1.53	0.5037	25
5/16/23 12:48	5/17/23 08:53	0.8368	0.3	0.3585	25
5/17/23 08:53	5/22/23 08:21	4.9778	1.58	0.3174	25
5/22/23 08:21	5/31/23 07:57	8.9833	6.03	0.6712	25

Date Time Start	Date Time End	ΔTime [day]	ΔH_2O mass [g]	Rate of change H_2O mass [g/day]	Upstream gas mass flow rate [std mL/min]
5/31/23 07:57	6/5/23 08:34	5.0257	2.62	0.5213	25
6/5/23 08:34	6/6/23 09:03	1.0201	0.6	0.5882	25
6/6/23 09:03	6/7/23 10:31	1.0611	0.61	0.5749	25
6/7/23 10:31	6/12/23 07:59	4.8944	2.31	0.4720	25
6/12/23 08:07	6/14/23 08:24	2.0118	1.08	0.5368	25
6/14/23 08:24	6/19/23 07:44	4.9722	2.39	0.4807	25
6/19/23 07:44	6/21/23 08:00	2.0111	0.06	0.0298	0
6/21/23 08:00	6/24/23 06:10	2.9236	1.59	0.5438	25
6/26/23 08:15	6/27/23 07:42	0.9771	0.4	0.4094	25
6/27/23 07:42	6/29/23 08:37	2.0382	1.04	0.5103	25
6/29/23 08:37	7/3/23 07:43	3.9625	2.57	0.6486	25
7/3/23 07:43	7/5/23 08:58	2.0521	1.12	0.5458	25
7/5/23 09:09	7/10/23 08:41	4.9806	3.01	0.6044	25
7/10/23 08:41	7/12/23 08:09	1.9778	1.13	0.5713	25
7/12/23 08:09	7/24/23 07:31	11.9736	6.44	0.5378	25
7/24/23 07:31	7/25/23 07:47	1.0111	0.46	0.4549	25
7/25/23 07:47	7/31/23 08:07	6.0139	3.1	0.5155	25
7/31/23 08:07	8/2/23 07:26	1.9715	1.02	0.5174	25
8/2/23 07:26	8/7/23 07:40	5.0097	2.56	0.5110	25

APPENDIX E

NFCSC DOCUMENT COVER SHEET[1]

Name/Title of Deliverable/Milestone/Revision No. ___Brine Availability Test in Salt (BATS) FY23 Update

Work Package Title and Number: Salt Disposal R&D – SNL

Work Package WBS Number: SF-23SN01030305

Responsible Work Package Manager: Kris Kuhlman__ Kris Kuhlman ___(26 Aug 2023). (Name/Signature)

Date Submitted

Quality Rigor Level for Deliverable/Milestone[2]	☐ QRL-1 ☐ Nuclear Data	☐ QRL-2	☒ QRL-3	☐ QRL-4 Lab QA Program[3]

This deliverable was prepared in accordance with Sandia National Laboratories *(Participant/National Laboratory Name)* QA program which meets the requirements of

☒ DOE Order 414.1 ☐ NQA-1 ☐ Other

This Deliverable was subjected to:

☒ Technical Review	☐ Peer Review
Technical Review (TR)	**Peer Review (PR)**
Review Documentation Provided	**Review Documentation Provided**
☐ Signed TR Report or,	☐ Signed PR Report or,
☐ Signed TR Concurrence Sheet or,	☐ Signed PR Concurrence Sheet or,
☒ Signature of TR Reviewer(s) below	☐ Signature of PR Reviewer(s) below

Name and Signature of Reviewers

Jason Heath Jason Heath 26 Aug 2023

NOTE 1: *Appendix E should be filled out and submitted with the deliverable. Or, if the PICS:NE system permits, completely enter all applicable information in the PICS:NE Deliverable Form. The requirement is to ensure that all applicable information is entered either in the PICS:NE system or by using the NFCSC Document Cover Sheet.*

- *In some cases there may be a milestone where an item is being fabricated, maintenance is being performed on a facility, or a document is being issued through a formal document control process where it specifically calls out a formal review of the document. In these cases, documentation (e.g., inspection report, maintenance request, work planning package documentation or the documented review of the issued document through the document control process) of the completion of the activity, along with the Document Cover Sheet, is sufficient to demonstrate achieving the milestone.*

NOTE 2: *If QRL 1, 2, or 3 is not assigned, then the QRL 4 box must be checked, and the work is understood to be performed using laboratory QA requirements. This includes any deliverable developed in conformance with the respective National Laboratory / Participant, DOE or NNSA-approved QA Program.*

NOTE 3: *If the lab has an NQA-1 program and the work to be conducted requires an NQA-1 program, then the QRL-1 box must be checked in the work Package and on the Appendix E cover sheet and the work must be performed in accordance with the Lab's NQA-1 program. The QRL-4 box should not be checked.*